e^+e^- INTERACTIONS AT HIGH ENERGIES

Sau Lan WU

Department of Physics
University of Wisconsin, Madison, Wisconsin, 53706 U.S.A.*
and

Deutsches Elektronen-Synchrotron, DESY, Hamburg, Germany

Introduction

In this review I shall attempt to cover the new experimental results on high energy e^+e^- colliding beam physics since the Berkeley Conference of last year. The data have been obtained mostly from PEP and PETRA, together with some contribution from CESR and TRISTAN.

PETRA started operation in 1978 and stopped in 1986. Although most of the data were taken at the center-of-mass energies 34 and 35 GeV, it reached a maximum of 46.8 GeV. PEP started operation in 1980 and is now in the middle of an upgrading program. It has run mostly at 29 GeV. PEP and PETRA together have accumulated an impressive abundance of information on e^+e^- interactions in the center-of-mass energy range of 14 GeV to 46.8 GeV. TRISTAN is the newest member of the family of high-energy e^+e^- colliding beam accelerators. It started operation in November 1986 at 50 GeV and is running at 52 GeV at present. The topics to be covered here are:

1. R and α_S

2. Electroweak Interference

3. Search for New Particles
4. Measurements of B-hadron lifetime

The subjects on jets and jet fragmentation are covered in this conference by W. Hoffmann, the τ-lepton physics by D. Hitlin and two photon physics by J.-E. Olsson.

Section 1   R and α_S

So far as the determination of the quark-gluon coupling constant α_S is concerned, there has been significant progress in two directions since the 1986 Berkeley Conference [1.1]. First, the CELLO collaboration [1.2] has carried out a beautiful piece of work on the determination of α_S and also $sin^2\theta_W$ [1.3] from the measurements of R, where θ_W is the Weinberg angle and R is defined as the ratio

$$R = \frac{\text{total cross section for e}^+\text{e}^- \rightarrow \text{ hadrons}}{\text{total cross section for e}^+\text{e}^- \rightarrow \mu^+\mu^-} \tag{1.1}$$

at the same energy. More precisely, the denominator is *not* the actual total cross section for $e^+e^- \rightarrow \mu^+\mu^-$, but rather the theoretical total cross section in the lowest-order QED without weak interactions, i.e., without the Z^o diagram. This theoretical total cross section is

$$\sigma(e^+e^- \rightarrow \mu^+\mu^-) = \frac{2\pi\alpha^2}{3s}\beta\,(3 - \beta^2), \tag{1.2}$$

where β is the velocity of the produced muons, and the mass of the electron has been neglected. α is the fine-structure constant and s is the square of the center-of-mass energy.

Secondly, there are new measurements from the CELLO [1.4], MARK II [1.5], MARK J [1.6] and TASSO [1.7] collaborations on α_S using the energy-energy correlation asymmetry [1.8]. These recent results are in much better agreement with each other.

1.1 Running coupling constant

In the CELLO [1.2] determination of α_S and $sin^2\theta_W$ from R, experimental data over a wide energy range, from $\sqrt{s} = 9.45$ GeV to 52 GeV, are used for a simultaneous fit. In this procedure, the way α_S depends on s is assumed to be given by second order QCD [1.9]:

$$\alpha_S(s) = \frac{12\pi}{(33 - 2N_f)\ell n(\frac{s}{\Lambda^2})}[1 - 6\frac{153 - 19N_f}{(33 - 2N_f)^2}\frac{\ell n[\ell n(\frac{s}{\Lambda^2})]}{\ell n(\frac{s}{\Lambda^2})}] \qquad (1.3)$$

where N_f is the number of quark flavors that can be pair-produced at the energy under consideration and Λ is a shorthand for $\Lambda_{\overline{MS}}$, the QCD scale parameter in the modified minimal-subtraction scheme.

An alternative formula for this running quark-gluon coupling constant is used for example by the JADE collaboration [1.10]:

$$\alpha_S(s) = \frac{12\pi}{(33 - 2\,N_f)\ell n\left(\frac{s}{\Lambda'^2}\right) + \frac{6(153 - 19\,N_f)}{33 - 2N_f}\,\ell n[\ell n(\frac{s}{\Lambda'^2})]} \qquad (1.4)$$

where Λ' is used to avoid confusion. Although equation (1.3) is more generally used, equations (1.3) and (1.4) are equivalent so far as second order QCD is concerned.

Since these two formulae are not identical and have caused some confusion, it is the purpose here to carry out a numerical comparison. In Figure 1.1, we have taken $N_f = 5$ and

$$\alpha_S(s) = 0.11 - 0.18 \qquad \text{for } \sqrt{s} = 34 \text{ GeV}$$

in steps of 0.01, and show the dependence of α_S on $\sqrt{s}$. In the range plotted, the results from (1.3) and (1.4) differ by less than 0.1%. Therefore, so far as the variation of $\alpha_S(s)$ where s is concerned, these two formulae can be considered to be identical.

The situation is quite different in connection with the value of the QCD parameter. In Figure 1.2 we plot the ratio Λ'/Λ as a function of Λ which gives the same value of α_S at 34 GeV. It is seen that Λ' is consistently smaller than Λ by more than 10%. This ratio varies from 0.887 to 0.877 for $\alpha_S(s)$ at $\sqrt{s} = 34$ GeV from 0.11 to 0.18. Therefore, care must be taken in comparing various determinations of $\Lambda_{\overline{MS}}$.

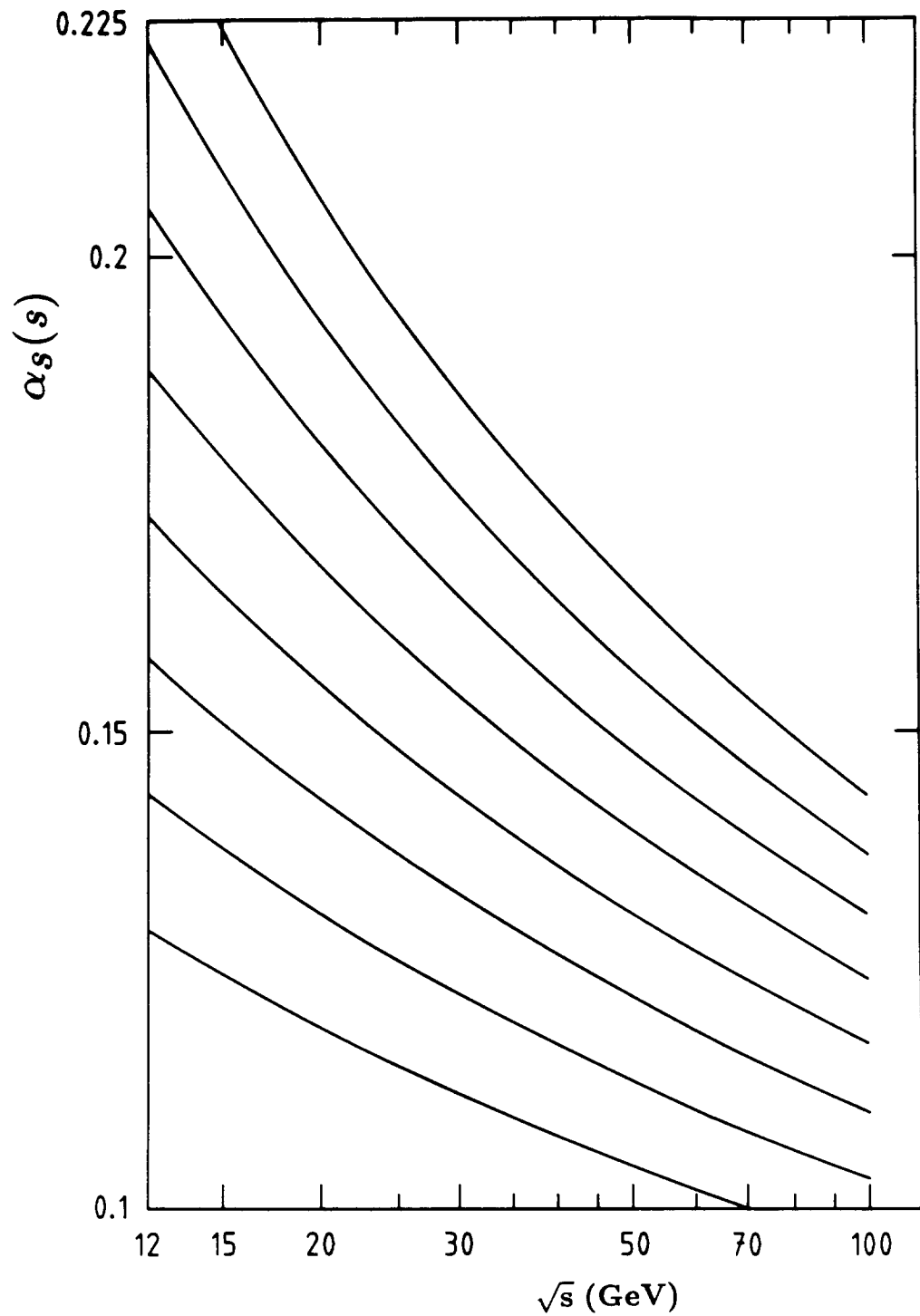In this report, we always use the formula (1.3).

.

FIGURE 1.1

The running quark-gluon coupling constant $\alpha_S(s)$. Here $N_f = 5$, and $\alpha_S(s) = 0.11 - 0.18$ for $\sqrt{s} = 34$ GeV in steps of 0.01.
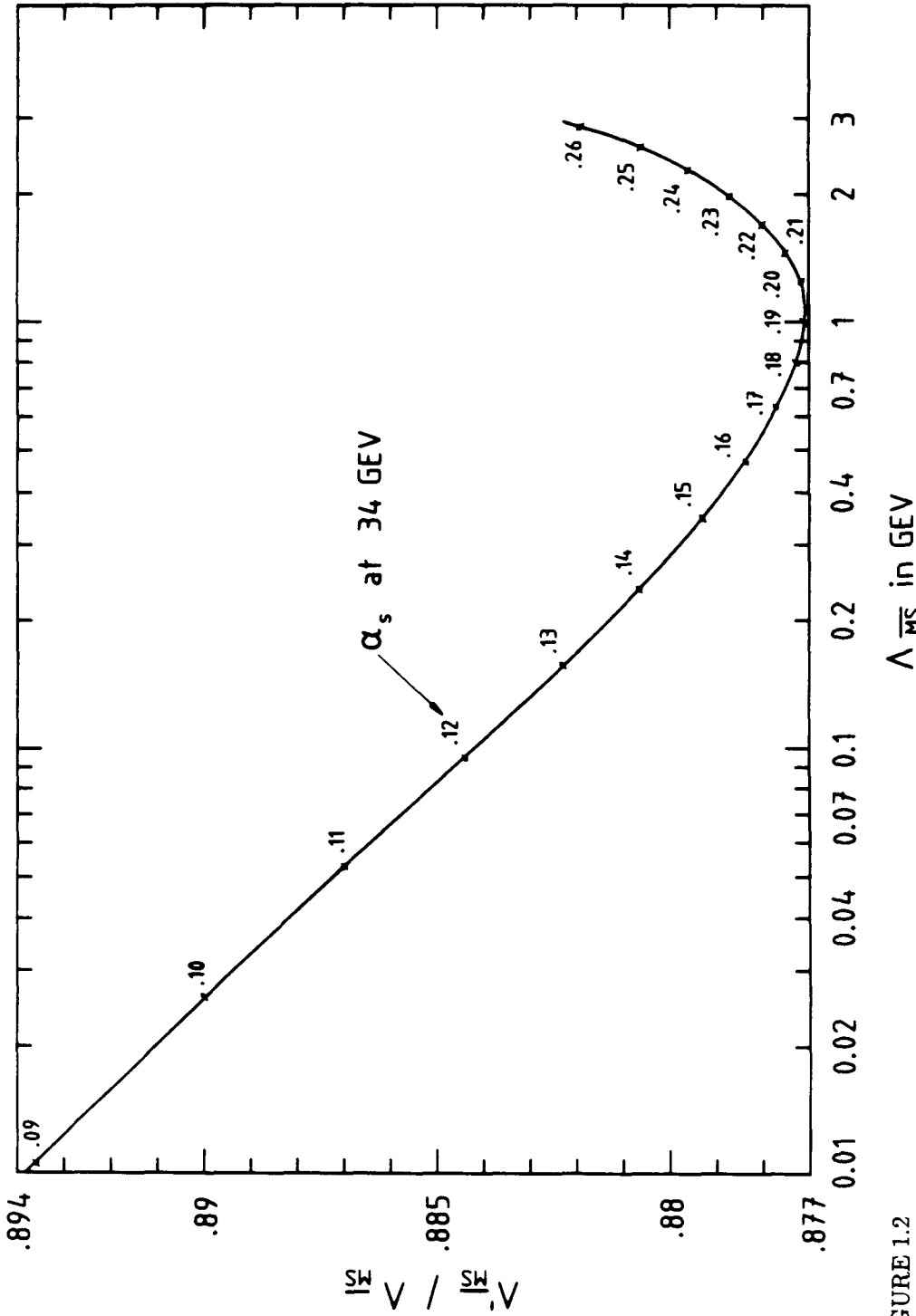
FIGURE 1.2

Ratio of two determinations of the QCD scale parameter in the modified minimum-subtraction scheme, both in second order. $\Lambda_{\overline{MS}}$ and $\Lambda'_{\overline{MS}}$ are determined according to eqs. (1.3) and (1.4) respectively.

1.2 Determination of α_S and $sin^2\theta_W$ from R

In the quark parton model, the value of R, as defined by equation (1.1), is given by

$$R = 3 \sum_f Q_f^2,$$

where the factor of 3 is due to the quark color, Q_f is the electric quark charge in units of the positron charge, and the sum runs over the quark flavors which can be produced at the relevant centre-of-mass energy.

In second order QCD, R is corrected by [1.11]

$$R = (3 \sum_f Q_f^2)[1 + \frac{\alpha_S(s)}{\pi} + (1.986 - 0.115 \, N_f) \, (\frac{\alpha_S(s)}{\pi})^2] \qquad (1.5)$$

where the size of the α_S term is about 5% and the α_S^2 term about 0.4%.

At the highest PETRA and TRISTAN energies Z^o exchange and, to a lesser extent, the interference between γ and Z^o exchanges become important. The prediction of the standard model, including quark mass effects, can be written as [1.12]:

$$R = 3 \sum_f [(\frac{\beta}{2}(3-\beta^2)(1+C_1^V(\frac{\alpha_S(s)}{\pi}+C_2^V(\frac{\alpha_S(s)}{\pi})^2)C_{VV}+\beta^3(1+C_1^A\frac{\alpha_S(s)}{\pi}+C_2^A(\frac{\alpha_S(s)}{\pi})^2)C_{AA}]$$

$$(1.6)$$

with

$$C_{VV} = Q_f^2 - 2Q_f v_e v_f Re(\chi(s)) + (v_e^2 + a_e^2)v_f^2|\chi(s)|^2$$

$$C_{AA} = (v_e^2 + a_e^2)a_f^2|\chi(s)|^2.$$

Here v and a stand for the vector and axial vector couplings of the electron and the quarks:

$$v_e = -1 + 4sin^2\theta_W \qquad\qquad a_e = -1$$

$$v_f = +1 - \tfrac{8}{3}sin^2\theta_W, \qquad\qquad a_f = +1 \quad \text{for } f = u,c$$

$$v_f = -1 + \tfrac{4}{3}sin^2\theta_W, \qquad\qquad a_f = -1 \quad \text{for } f = d,s,b$$

and

$$\chi(s) = \frac{G_F}{8\sqrt{2}\pi\alpha} \, \frac{s \, m_Z^2}{s - m_Z^2 + im_Z\Gamma_Z} \qquad (1.7)$$

with m_Z and Γ_Z being the mass and the width of the Z^o. In (1.6), C_1^V and C_1^A are complicated functions of β, and the dependence of C_2^V and C_2^A on β apparently has not yet been calculated.

Equations (1.3) and (1.5) to (1.7) allow the simultaneous determination of α_s and $sin^2\theta_W$ from the R values.

Earlier work on determination of α_s from R was carried out by JADE [1.13], MARK J [1.14] and TASSO [1.15]. In the recent work of CELLO [1.2] they used the R values [1.16] from CELLO, CESR, DORIS, PEP and PETRA and also the following new ones contributed to this conference:

$$R = 3.5 \pm 0.07 \pm 0.12 \qquad \text{at } \sqrt{s} = 9.46 \text{ GeV}$$

from the Crystal Ball collaboration [1.17] at DORIS and

$$R = 4.34 \pm 0.27 \qquad \text{at } \sqrt{s} = 51.7 \text{ GeV}$$

from the AMY, TOPAZ and VENUS collaborations [1.18] at TRISTAN. This last value is obtained by averaging their data at 50 and 52 GeV from all these experiments.

The parameters α_s (or $\Lambda_{\overline{MS}}$) and $sin^2\theta_W$ are determined by fitting equations (1.3) and (1.5) to (1.7) to the data. Over 60 R values from different experiments and different $\sqrt{s}$ points are used. The question to be asked is: How does one handle the normalization errors when one combines data from different experiments? This problem is solved by CELLO as follows [1.2]:

CELLO defines an $n \times n$ error matrix V_{ij} for n measurements. The diagonal elements are given for each measurement by the sum of the squares of the statistical error σ_{stat}, point to point systematic error σ_{ptp}, and common normalization error σ_{norm}. The correlation between data points i and j is contained in the off-diagonal matrix element V_{ij}, which is taken to be the product of σ^i_{norm} and σ^j_{norm} of the two normalization errors. The expression to be minimized is then:

$$\chi^2 = \Delta^T V^{-1} \Delta$$

Here Δ is the vector of the n residuals $R_i - R_{fit}$. In this method all data points are handled in a symmetric way. With this matrix one fits the two physical parameters $\Lambda_{\overline{MS}}$ and $sin^2\theta_W$.

From the fit to the data of CESR, DORIS, PEP, PETRA and TRISTAN as mentioned above, CELLO [1.2] obtains

$$\alpha_S(34^2\text{GeV}^2) = 0.138 \pm 0.023$$

$$\Lambda_{\overline{MS}} = 0.222^{+0.251}_{-0.153} \text{ GeV}$$

$$sin^2\theta_W = 0.243 \pm 0.020$$

The data and their statistical and total systematic errors as well as the fit are shown in Figure 1.3. As mentioned above, the variation of α_S as a function of s was taken into account, and $s = 34^2\text{GeV}^2$ has been chosen as reference. $m_Z = 92.3$ GeV/c^2 and $\Gamma_Z = 2.5$ GeV/c^2 have been used in the fit but the results for the fitted parameters are insensitive to these values. The fitted value of the weak mixing angle $sin^2\theta_W$ is in good agreement with the world average of 0.23, which has been determined in neutrino scattering [1.19] and the masses of the weak gauge bosons [1.20]. If one imposes $sin^2\theta_W = 0.23$, one gets for the strong coupling constant

$$\alpha_S(34^2\text{GeV}^2) = 0.145 \pm 0.020$$

$$\Lambda_{\overline{MS}} = 0.286^{+0.245}_{-0.168} \text{ GeV}$$

with the statistical and the systematic errors combined in quadrature.

1.3 Determination of α_S from the Asymmetry in Energy-Energy Correlation

Asymmetry in energy-energy correlation [1.8] (EEC) has been a popular way to determine the quark-gluon coupling constant α_S. The energy-energy correlation is an energy weighted angular correlation defined by [1.5]

$$EEC(\chi) = \frac{1}{N_{events}} \sum^{N_{events}} \sum_i \sum_j \frac{E_i E_j}{s} \delta(\chi - \chi_{ij}) \qquad (1.8)$$

where i and j run over all particles (charged and neutral) in the event, and χ_{ij} is the angle between particles i and j. The energy-energy correlation asymmetry (EECA) is simply

$$A(\chi) = EEC(180^o - \chi) - EEC(\chi). \qquad (1.9)$$

Two-jet events from $e^+e^- \rightarrow q\bar{q}$ contribute to the EEC predominantly near $\chi = 0^o$ and $\chi = 180^o$, but events with hard gluon radiations populate the EEC at intermediate angles
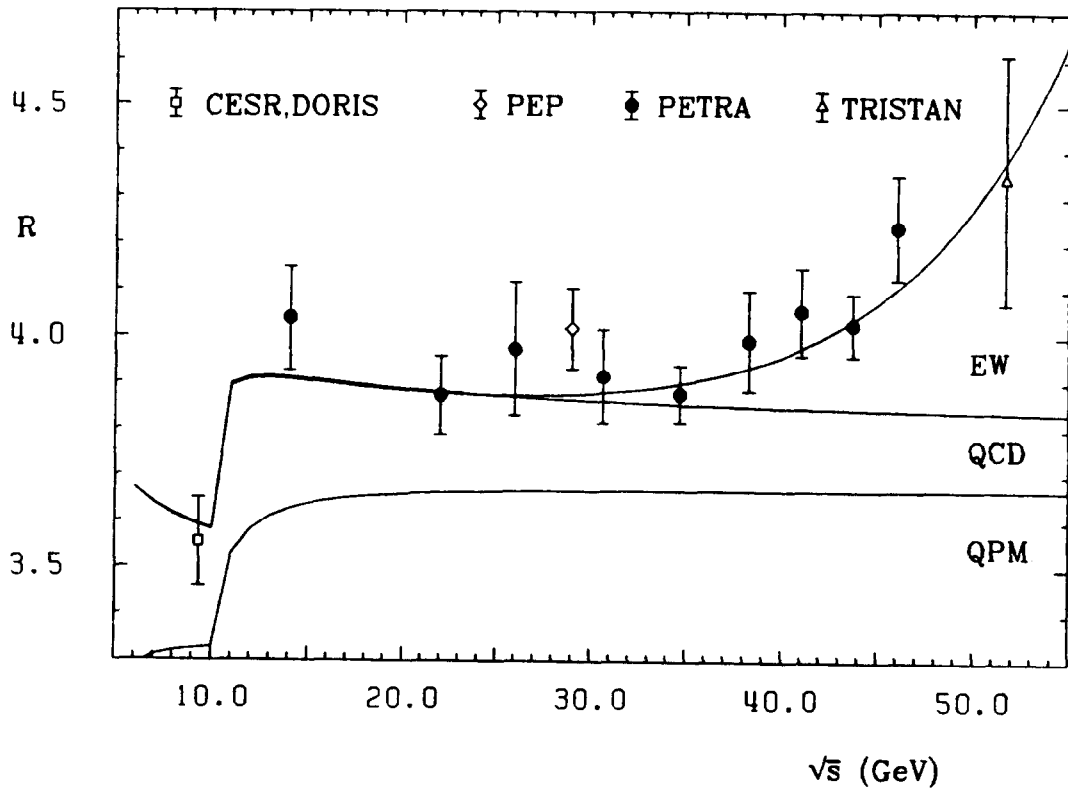
FIGURE 1.3

Averaged R values as function of $\sqrt{s}$. The errors include statistical and correlated normalization errors. The top curve represents the best fit.

as well. For this reason, the dependence of the EEC on χ is sensitive to α_S. An advantage of using the EECA to determine α_S is that many of the effects of fragmentation and experimental error contribute symmetrically to the EEC, and cancel in the EECA. However, this expected advantage of being less fragmentation dependent is not fully realized because it turns out that the EECA is sensitive to how the gluon is imbedded in the fragmentation scheme.

Figure 1.4 gives a summary of the values of α_S obtained by various experimental collaborations at PEP and PETRA on the basis of the EECA. The older results, up to 1986, are shown on the left hand side, and taken from a figure of Naroska [1.10]. The new 1987 results from CELLO [1.4], MARK II [1.5], and TASSO [1.7] are shown on the right hand side. With the exception of one TASSO point where the independent fragmentation model [1.21] is used, all the new results are based on the Lund fragmentation model [1.22].

As seen from Figure 1.4, the main difference between the new results and the old results is that, for the new results based on the Lund fragmentation, the agreement between the different experiments is excellent. Note that the different experimental collaborations use second-order QCD calculations from different groups:

ERT (Ellis, Ross and Terrano [1.23]; 1981),

GKS (Gutbrod, Kramer and Schierholz [1.24]; 1984),

AB (Ali and Barreiro [1.25]; 1982),

GS (Gottschalk and Shatz [1.26]; 1985)

The agreements between the new results using the Lund model of fragmentation indicate that the second order QCD calculations of ERT, GKS, AB and GS agree. Furthermore the parameters of fragmentation models have been better tuned recently due to more thorough work by the PEP and PETRA experimental groups. The better values of parameters are responsible for reducing significantly the disagreement in α_S values using the independent fragmentation model versus the Lund model.

We concentrate on the last four data points shown in Figure 1.3 by CELLO [1.4], MARK II [1.5], and TASSO [1.7], all using the Lund fragmentation model. The experimental results are shown in more detail in Table 1.1, where the third column gives the
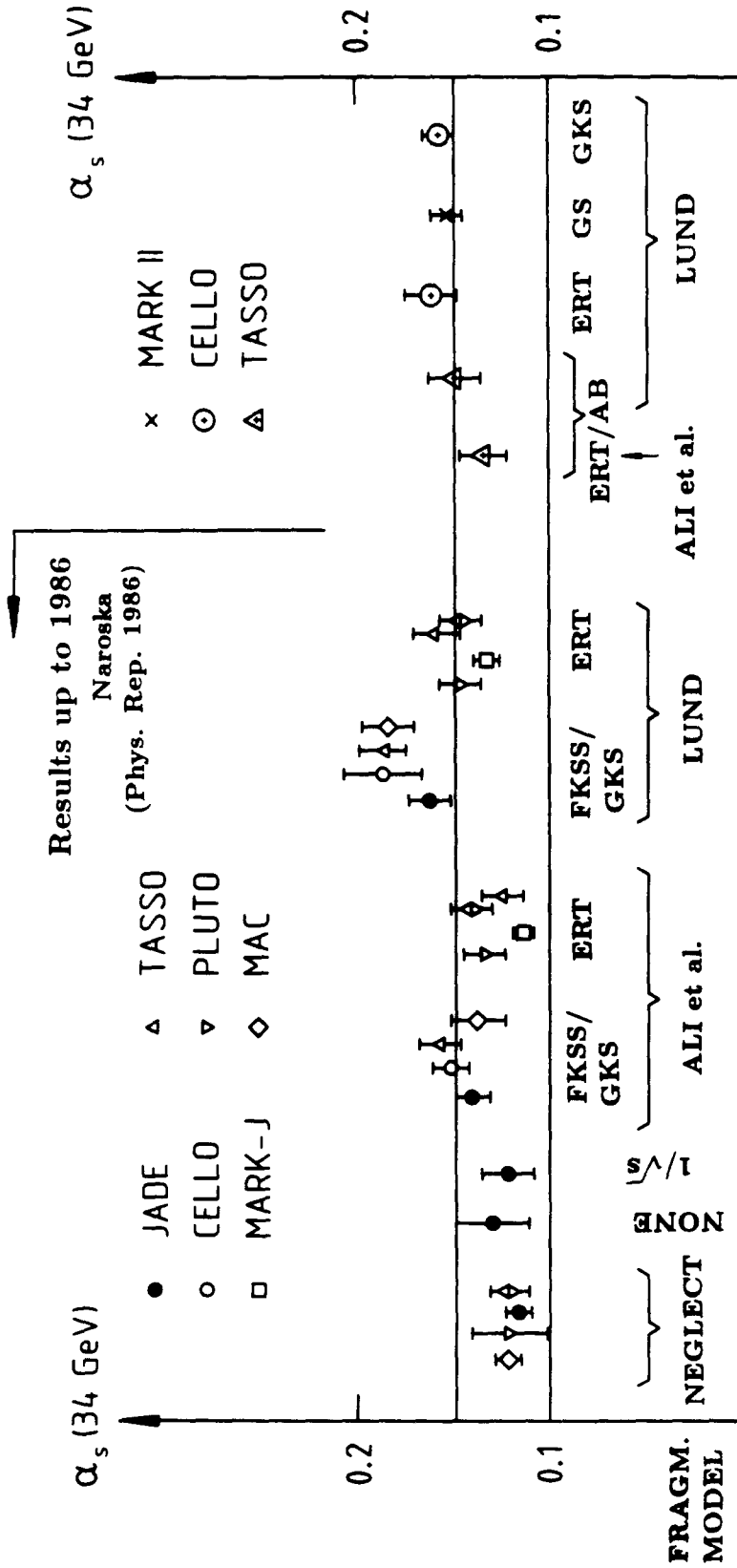
FIGURE 1.4

α_s determined from the asymmetry of the energy-energy correlation to $O(\alpha_s^2)$ by e^+e^- experiments. Below the data is indicated which QCD matrix element is used and how fragmentation is treated. The five data points on the right are the new ones since the 1986 Berkeley Conference.

values of α_S as obtained by the various collaborations. Unlike the situation in section 1.2 on the determination of α_S from R, equation (1.3), which gives the dependence of α_S on s, is not used. However, in order to have a meaningful comparison and an average, equation (1.3) is used to transform these values in the third column to a common energy of $\sqrt{s} = 34$ GeV, shown in the last column. These four values in this last column are then averaged with the statistical and the systematic errors combined in quadrature. The result is

$$\alpha_S(34^2 \text{ GeV}) = 0.156 \pm 0.005$$

$$\Lambda_{\overline{MS}} = (0.42 \pm 0.06) \text{ GeV}$$

We emphasize that this error of ± 0.005 does not include uncertainties due to the fragmentation model. This small error is, however, not due to the averaging of four pieces of experimental data. The reason is instead that the CELLO result at 35 GeV, where most of the PETRA data is taken, has a very small error (see Table 1.1). It is difficult to give an accurate estimate of the possible error due to fragmentation.

1.4 Discussion

It may be interesting to contrast these two very different ways of determining the quark-gluon coupling constant α_S. The main advantage of the first method, a fit to the many measured values of R, is that it is insensitive to the jet fragmentation models. Furthermore, the second-order QCD contribution to R is known and small. The main disadvantage of this method, as seen from equation (1.5), is that R does not depend sensitively on α_S. For example, a 10% change in α_S leads to a change in R of less than $\frac{1}{2}\%$.

For the second method of the EECA, the advantage and disadvantage are reversed. Inspite of the cancellation of many of the effects of fragmentation in the EECA, the result still shows sensitivity to the fragmentation model used. On the other hand, if we ignore this uncertainty due to the fragmentation model, then the resulting determination of α_S can be quite accurate.

Table 1.1

Recent determination of the α_S from EECA using Lund Fragmentation Model

Collaboration	$\sqrt{s}$ in GeV	$\alpha_S(s)$	$\alpha_S(34^2 \text{ GeV}^2)$
MARK II [1.5]	29	$0.158 \pm 0.003 \pm 0.008$	$0.153 \pm 0.003 \pm 0.007$
CELLO [1.4]	44	$0.154 \pm 0.006 \pm 0.010$	$0.161 \pm 0.007 \pm 0.011$
CELLO [1.4]	35	$0.157 \pm 0.004 \pm 0.005$	$0.158 \pm 0.004 \pm 0.005$
TASSO [1.7]	44	$0.143 \pm 0.005 \pm 0.012$	$0.150 \pm 0.005 \pm 0.013$
MARKJ [1.6]	35	$0.129 \pm 0.004 \pm 0.012$	
MARK J [1.6]	44	$0.108 \pm 0.007 \pm 0.010$	
Average			0.156 ± 0.005

The results of MARK J are not used in the average [1.27].

Table 2.1

Values of v_f and a_f in the standard model

f	e^-, μ^-, τ^-	ν_e, ν_μ, ν_τ	d, s, b	u, c, t
Q_f	-1	0	$-\frac{1}{3}$	$\frac{2}{3}$
v_f	$-1 + 4sin^2\theta_W$	1	$-1 + \frac{4}{3}sin^2\theta_W$	$1 - \frac{8}{3}sin^2\theta_W$
a_f	-1	1	-1	1

Section 2   Electroweak Interference

2.1   Introduction

In the standard model [2.1], the process

$$e^-e^+ \to f\bar{f}$$

can proceed not only through one-photon annihilation (Figure 2.1a) but also through one-Z^o annihilation (Figure 2.1b) where f can be any fundamental fermion in the three families, including the yet unobserved top quark t. The couplings of the fermion f, including the electron e, to the photon and the Z^o are explicitly shown in Figure 2.1. While the coupling to γ involves as usual only the vector current, that to the Z^o is a weak coupling and has both a vector and an axial vector part [2.1]. The interference between the axial vector coupling to Z^o and the vector coupling to both γ and Z^o is responsible for the forward-backward asymmetry. The values of the vector coupling v_f and the axial vector coupling a_f as defined in Figure 2.1 for various fermions are given in Table 2.1 in terms of the Weinberg angle θ_W. Since the Weinberg angle is fairly accurately known from other experiments, the standard model gives unambiguous predictions for this forward-backward asymmetry. Thus a measurement of this asymmetry gives a direct test of the standard model.

On the basis of the two diagrams of Figure 2.1, the differential cross section for $e^-e^+ \to f\bar{f}$ is, in the standard model with the quark mass neglected [2.2]

$$\frac{d\sigma(e^-e^+ \to f\bar{f})}{d\cos\theta} = \frac{\pi\alpha^2}{2s}\{Q_f^2(1+\cos^2\theta) - \frac{2Q_f gs(s/m_Z^2 - 1)[v_e v_f(1+\cos^2\theta) + 2a_e a_f\cos\theta]}{(s/m_Z^2 - 1)^2 + \Gamma_Z^2/m_Z^2}$$

$$+ \frac{s^2 g^2[(v_e^2 + a_e^2)(v_f^2 + a_f^2)(1+\cos^2\theta) + 8v_e a_e v_f a_f\cos\theta]}{(s/m_Z^2 - 1)^2 + \Gamma_Z^2/m_Z^2}\} \tag{2.1}$$

where m_Z and Γ_Z are the mass and width of Z^o, Q_f is the fermion charge in units of e and

$$g = \frac{\sqrt{2}G_F}{4e^2} = \frac{\sqrt{2}G_F}{16\pi\alpha} \tag{2.2}$$

in terms of the Fermi weak coupling constant G_F. Integration over θ gives in particular:

$$R_f = Q_f^2 - \frac{2Q_f gs(s/m_Z^2 - 1)v_e v_f - s^2 g^2(v_e^2 + a_e^2)(v_f^2 + a_f^2)}{(s/m_Z^2 - 1)^2 + \Gamma_Z^2/m_Z^2} \tag{2.3}$$
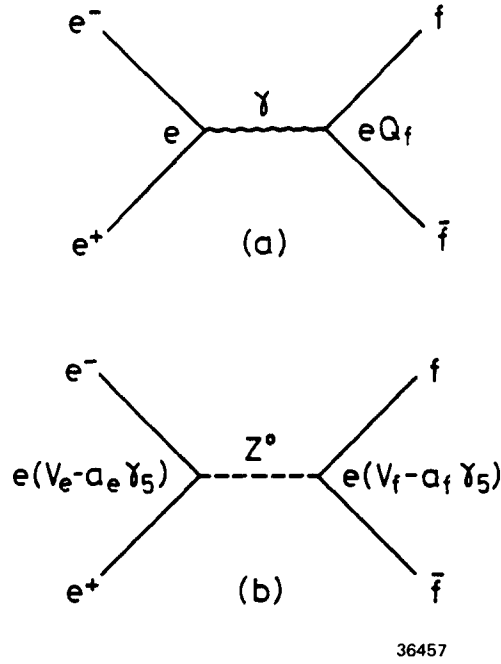
FIGURE 2.1

The process $e^+e^- \rightarrow f\bar{f}$ in the standard model.

These formulae are not valid for Bhabha scattering. As they stand, (2.1) and (2.3) are valid for μ and τ. They are also valid for the quarks provided that the right-hand sides are multiplied by the color factor 3.

The asymmetry $A(\theta)$, as a function of θ, is defined by

$$A_f(\theta) = \frac{d\sigma(e^-e^+ \rightarrow f\bar{f})/d\cos\theta|_\theta - d\sigma(e^-e^+ \rightarrow f\bar{f})/d\cos\theta|_{\pi-\theta}}{d\sigma(e^-e^+ \rightarrow f\bar{f})/d\cos\theta|_\theta + d\sigma(e^-e^+ \rightarrow f\bar{f})/d\cos\theta|_{\pi-\theta}} \qquad (2.4)$$

It therefore follows from (2.1) that the angular dependence of $A(\theta)$ is very simply

$$A_f(\theta) = A_f(0)\frac{2\cos\theta}{1 + \cos^2\theta} \qquad (2.5)$$

and $A_f(0)$, the asymmetry at $\theta = 0$, is explicitly

$$A_f(0) = \frac{-2Q_f gs(s/m_Z^2 - 1)a_e a_f + 4s^2 g^2 v_e a_e v_f a_f}{Q_f^2[(s/m_Z^2 - 1)^2 + \Gamma_Z^2/m_Z^2] - 2Q_f gs(s/m_Z^2 - 1)v_e v_f + s^2 g^2 (v_e^2 + a_e^2)(v_f^2 + a_f^2)} \qquad (2.6)$$
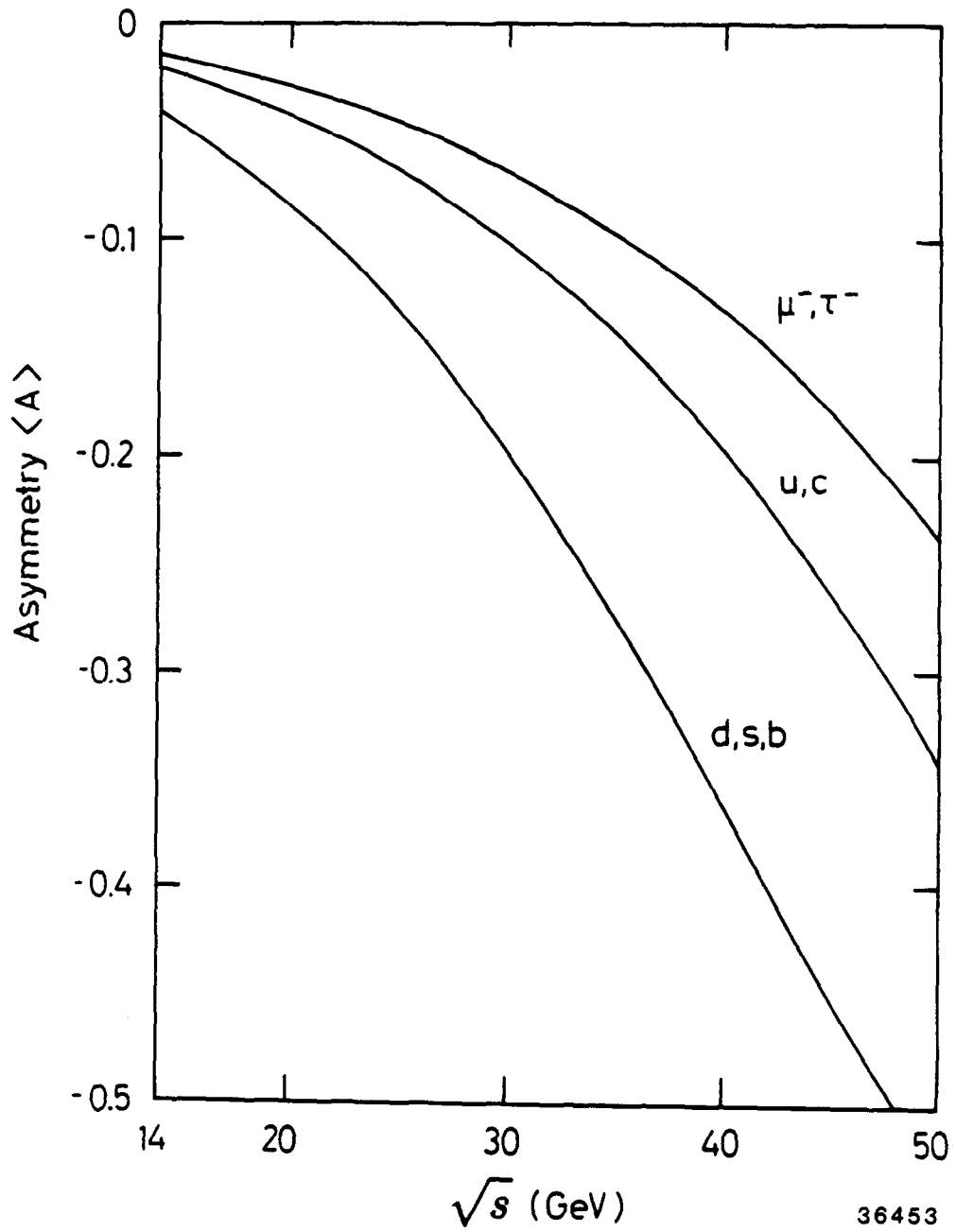
FIGURE 2.2

Average asymmetry on the basis of the standard model.

If the acceptance is 4π, then by (2.5) the average asymmetry is

$$\langle A_f \rangle = \frac{\sigma(\theta < \pi/2) - \sigma(\theta > \pi/2)}{\sigma(\theta < \pi/2) + \sigma(\theta > \pi/2)} = \frac{3}{4} A_f(0) \qquad (2.7)$$

The formulas (2.5), (2.6) and (2.7) are valid for all fundamental fermions, both leptons and quarks, with the exception of the electron.

Using the measured Weinberg angle of $sin^2\theta_W = 0.228$, this average asymmetry $\langle A_f \rangle$ of (2.7) is plotted in Figure 2.2, in the PEP and PETRA energy range for the various fermions. Note that, for these fermions, the total cross section is more sensitive to v than to a, while the forward-backward asymmetry is more sensitive to a than to v.

2.2 Radiative correction

In the on-shell parametrization the QED radiative corrections to the Z^o exchange happen to cancel approximately the one loop corrections to the Z^0 propagator at PEP and PETRA energies [2.3], at least within the accuracies of the experimental results. Therefore, to correct the measured value of the charge asymmetry it is sufficient to apply only the pure α^3 QED corrections to the one photon exchange graph. This approximation is sometimes called the "reduced QED" correction. The α^3 terms of QED corrections comes from (i) diagrams in Figure 2.3, (ii) interference of diagrams in Figure 2.4 with diagrams in Figure 2.1(a). The size of this "reduced QED" correction of order α^3 is about 2% [2.4] at PEP and PETRA energies. At these energies diagrams of QED radiative corrections due to Z^o exchange shown in Figure 2.5 (contribute to about +0.7% [2.4] for the μ-pair asymmetry) cancels approximately the diagram in Figure 2.6 of the one loop corrections due to Z^o propagator (−0.7%).

2.3 Electroweak Interference in the Lepton Sector

2.3.1. Electroweak Interference in $e^+e^- \rightarrow \mu^+\mu^-$

In 1986, PETRA had accumulated more luminosity at $\sqrt{s} = 35$ GeV than it did at $\sqrt{s} = 34.5$ GeV in 1980-1982. Therefore the μ-pair asymmetry measurement at $\sqrt{s} \sim 34$ to 35 GeV has improved accuracy. The angular distributions from CELLO [2.5], JADE [2.6], MARK J [2.7] and TASSO [2.8] for $\sqrt{s} \sim 34$ to 35 GeV are shown in Figure 2.7(a) to (d). The results, compiled by Naroska [2.4], are given in Table 2.2 for the μ-pair asymmetry
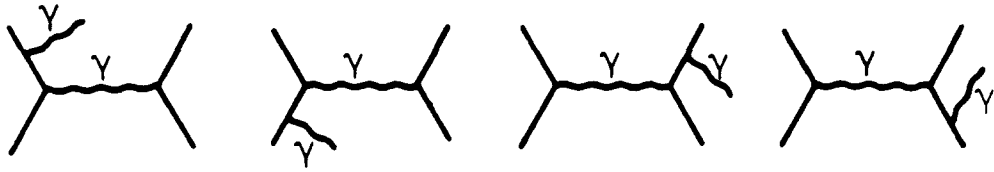
FIGURE 2.3

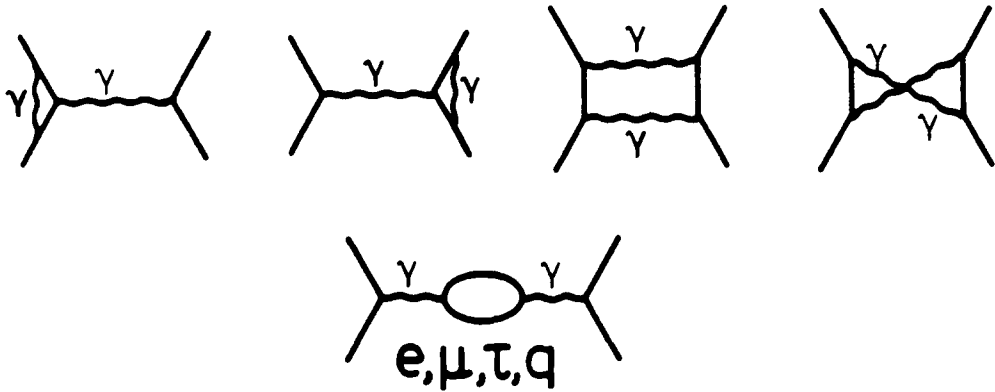Feynman diagrams for $e^+e^- \rightarrow \ell^+\ell^- \gamma$ via virtual photon.

FIGURE 2.4

Feynman diagrams for vertex and self-energy corrections to $e^+e^- \rightarrow \ell^+\ell^-$ via virtual photon.
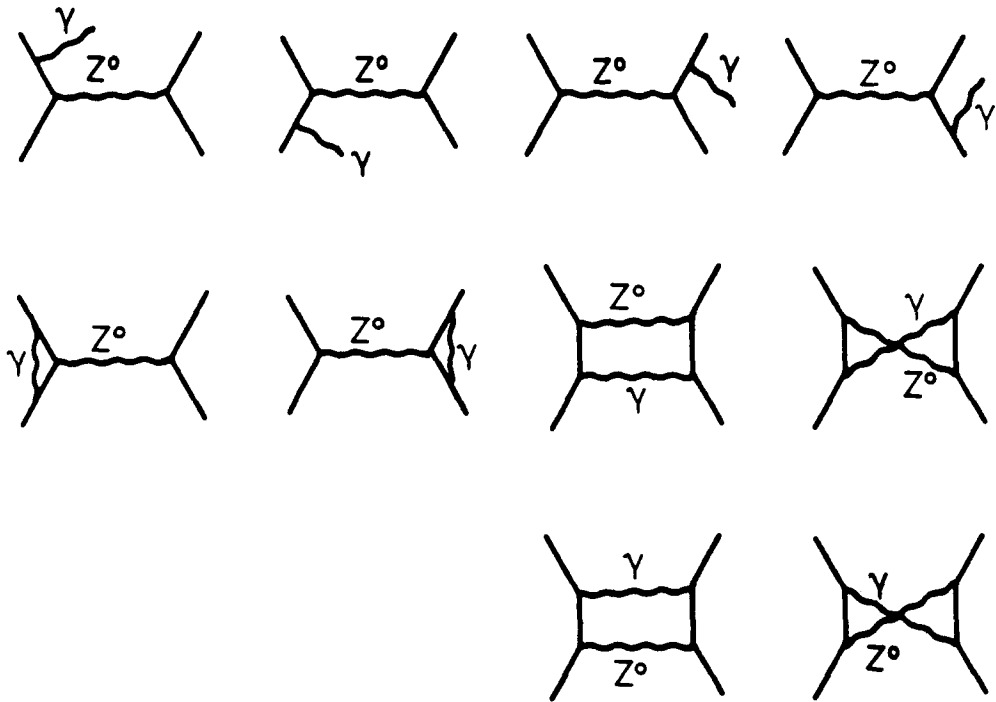
FIGURE 2.5

Feynman diagrams for the radiative corrections to $e^+e^- \rightarrow \ell^+\ell^-$ via Z^o.
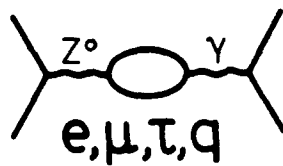

FIGURE 2.6

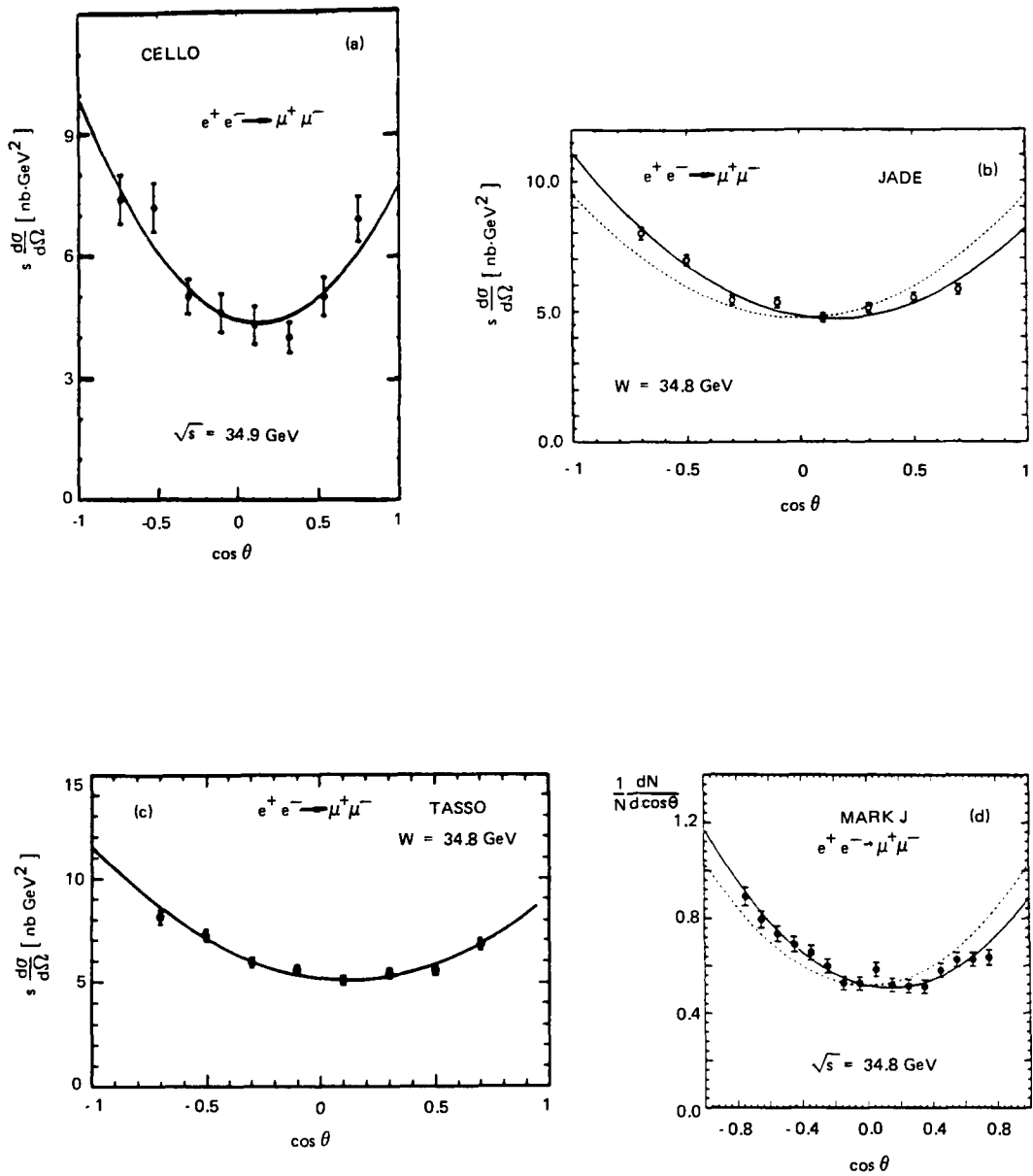Feynman diagram for the self-energy correction to $e^+e^- \rightarrow \ell^+\ell^-$ via Z^o.

FIGURE 2.7

PETRA data on the angular distribution of $e^+e^- \to \mu^+\mu^-$. The solid lines represent the best fits including electroweak interference.

Table 2.2

Results on the Asymmetry in e⁺e⁻ → μ⁺μ⁻

Compiled by Naroska [2.4]

Experiment		$\sqrt{s}(GeV)$	N_μ	$A_\mu(\%)$			$A_\mu(SM)(\%)$
CELLO	(1980-82)	34.2	387	−6.4	±6.4		−8.4
CELLO	(1986)	35.0	2760	−9.2	±3.0	±1.0	−8.9
JADE	(1980-82)	34.4	3400	−11.1	±1.8	±1.0	−8.5
JADE	(1986)	35.0	3901	−10.9	±1.7	±1.0	−8.9
MARK J	(1980-82)	34.6	3658	−11.7	±1.7	±0.5	−8.6
MARK J	(1986)	35.0	3196	−8.1	±1.9	±0.5	−8.9
PLUTO		34.7	1550	−13.2	±2.8	±1.0	−8.7
TASSO	(1980-82)	34.5	2673	−9.1	±2.3	±0.5	−8.6
TASSO	(1986)	35.0	2697	−10.1	±2.2	±0.5	−8.9
combined		34.8	24222	−10.1	±0.9		−8.7
CELLO		39.2	288	−4.8	±6.5	±1.0	−11.6
JADE		38.0	422	−9.7	±5.0	±1.0	−10.8
MARK J		39.2	671	−10.6	±4.0	±0.5	−11.6
TASSO		38.3	173	+2.4	±8.6	±0.5	−11.0
combined		38.8	1554	−8.1	±2.7		−11.3
CELLO		44.0	611	−18.8	±4.5	±1.0	−15.5
JADE		43.7	1258	−19.1	±2.8	±1.0	−15.3
MARK J		44.1	1278	−15.8	±2.8	±0.5	−15.6
TASSO		43.6	614	−17.3	±4.4	±0.5	−15.2
combined		43.9	3761	−17.6	±1.7		−15.4
HRS		29	5057	−4.9	±1.5	±0.5	−5.9
MAC		29	16058	−5.9	±0.7	±0.2	−5.9
MARK II		29	5312	−7.1	±1.7		−5.9
combined		29	26427	−5.9	± 0.6		−5.9

Results from PETRA on the Asymmetry in e⁺e⁻ → μ⁺μ⁻
averaged values for 1980-82 and 1986

Compiled by Naroska [2.4]

Experiment	$\sqrt{s}(GeV)$	N_μ	$A_\mu(\%)$			$A_\mu(SM)(\%)$
CELLO	34.9	387	−8.7	±2.7	±1.0	−8.8
JADE	34.7	7301	−11.0	±1.2	±1.0	−8.7
MARK J	34.8	6854	−10.4	±1.3	±0.5	−8.7
TASSO	34.8	5370	−9.6	±1.6	±0.5	−8.7

Standard model expectations $A_\mu(SM)$ were calculated with
$sin\theta_W = 0.229$ and $m_Z = 92.5$ GeV.

Table 2.3

Combined values of A_μ at different $\sqrt{s}$
Compiled by Naroska [2.4]

Experiment	$\sqrt{s}(GeV)$	$A_\mu(\%)$		$A_\mu(SM)(\%)$
PEP	29	−5.9	±0.62	−5.9
PETRA	34.8	−10.1	±0.9	−8.7
PETRA	38.8	−8.1	±2.7	−11.3
PETRA	43.9	−17.6	±1.7	−15.4
TRISTAN	50-52	−22	±9	−21

PEP   : HRS, MAC, MARK II
PETRA   : CELLO, JADE, MARK J, PLUTO, TASSO
TRISTAN : AMY, TOPAZ, VENUS

Table 2.4

Combined values of a_μ at PEP and PETRA [2.4]

	a_μ
PEP	−1.02±0.12
PETRA	−1.14±0.07
combined	−1.11± 0.06
standard model	−1

Assume $a_e = -1$, $m_Z = 92.5$ GeV and $sin^2\theta_W = 0.229$

for different experiments and in Table 2.3 for combined results at PEP and PETRA at different $\sqrt{s}$. Table 2.4 gives the combined results for the muon axial vector coupling a_μ to be

$$a_\mu = -1.11 \pm 0.06$$

for $a_e = -1$, $m_Z = 92.5$ GeV and $sin^2\theta_W = 0.229$. The expectation from the standard model is $a_\mu = -1$.

2.3.2. Electroweak Interference in $e^+e^- \to \tau^+\tau^-$

For the 1986 data at $\sqrt{s} = 35$ GeV, only the JADE collaboration [2.6] has analyzed the τ-pair asymmetry: $A_\tau = (-8.5 \pm 2.0 \pm 1.0)\%$. The results compiled by Naroska [2.4] are given in Table 2.5 for the τ-pair asymmetry for different experiments and in Table 2.6 for combined results at PEP and PETRA at different $\sqrt{s}$. Table 2.7 gives the combined results for the τ lepton axial vector coupling a_τ to be

$$a_\tau = -0.88 \pm 0.09$$

for $a_e = -1$, $m_Z = 92.5$ GeV and $sin^2\theta_W = 0.229$. The expectation from the standard model is $a_\tau = -1$.

2.3.3. Combined results for μ-pair and τ-pair asymmetry.

Figure 2.8 gives the asymmetry as a function of s for $e^+e^- \to \mu^+\mu^-$ and $e^+e^- \to \tau^+\tau^-$ from combined results of the PEP and PETRA experimental groups. The solid curve is the expectation from the standard model for $m_Z = 92.3$ GeV and $sin^2\theta_W = 0.228$. The combined axial vector coupling for μ and τ is

$$a_{\mu,\tau} = -1.04 \pm 0.05$$

Figure 2.9 show the 95% C.L. contour in $sin^2\theta_W$ versus m_Z plane from fits of data in μ-pair and μ-pair plus τ-pair asymmetry. Fixing $m_Z = 92.5$ GeV one obtains [2.4]

$$sin^2\theta_W = 0.214 \pm 0.014 {\pm}^{0.019}_{0.014}$$

the last error comes from m_Z mass being changed by ± 1.8 GeV. As seen from Figure 2.9, this result agrees well with results from ν-scattering [2.9] and the $p\bar{p}$ collider [2.10].

Table 2.5

Results on the Asymmetry in e$^+$e$^-$ → $\tau^+\tau^-$

Compiled by Naroska [2.4]

Experiment		$\sqrt{s}(GeV)$	N_τ	$A_\tau(\%)$			$A_\tau(SM)(\%)$
CELLO	(1980-82)	34.2	434	−10.3	±5.2		−8.5
JADE	(1980-82)	34.6	1998	−6.0	±2.5	±1.0	−8.7
JADE	(1986)	35.0	2900	−8.5	±2.0	±1.0	−8.9
MARK J	(1980-82)	35.0	811	−8.6	±3.7	±1.5	−8.9
PLUTO	(1980-82)	34.6	419	−5.9	±6.8	±2.5	−8.7
TASSO	(1980-82)	34.6	577	−4.9	±5.3	±1.2	−8.6
combined		34.8	7139	−7.6	±1.4		−8.7
CELLO		38.1	260	−11.8	±6.2	±2.7	−11.5
JADE		38.0	336	+7.5	±6.3	±1.0	−10.8
combined		38.0	596	−1.6	±4.6		−10.8
CELLO		43.8	824	−16.3	±3.5	±1.3	−15.5
JADE		43.7	913	−17.0	±3.6	±1.0	−15.3
MARK J		43.9	222	−12.8	±7.0	±1.5	− 15.4
combined		43.8	1959	−16.3	±2.5		−15.3
HRS		29	7372	−4.4	±1.4	±0.5	−5.9
MAC		29	10153	−5.5	±1.2	±0.5	−5.9
MARK II		29	3714	−4.2	±2.0		−5.9
combined		29	21239	−4.9	±0.9		−5.9

Table 2.6

Combined values of A_τ at different $\sqrt{s}$
Compiled by Naroska [2.4]

Experiment	$\sqrt{s}(GeV)$	$A_\tau(\%)$	$A_\tau(SM)(\%)$
PEP	29	−4.9 ±0.9	−5.9
PETRA	34.8	−7.6 ±1.4	−8.7
PETRA	38.0	−1.6 ±4.6	−10.8
PETRA	43.8	−16.3 ±2.5	−15.3

PEP   : HRS, MAC, MARK II
PETRA : CELLO, JADE, MARK J, PLUTO, TASSO

Table 2.7

Combined Values of a_τ at PEP and PETRA [2.4]

	a_τ
PEP PETRA	−0.84± 0.16 −0.91± 0.11
combined	−0.88±0.09
standard model	− 1

Assume: $a_e = -1$, $m_Z = 92.5$ GeV and $sin^2\theta_W = 0.229$
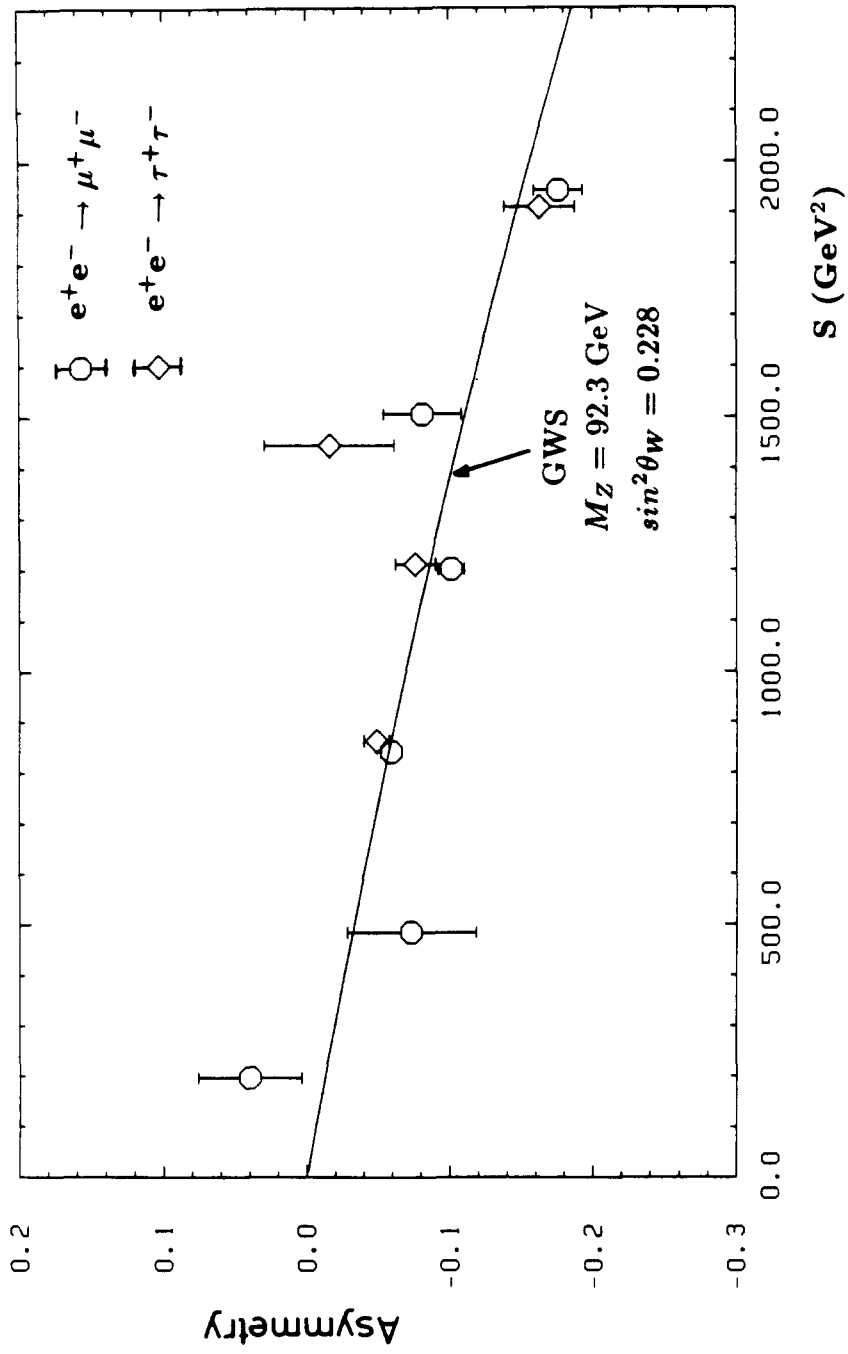
FIGURE 2.8
Asymmetry as a function of s for $e^+e^- \rightarrow \mu^+\mu^-$ and $e^+e^- \rightarrow \tau^+\tau^-$.
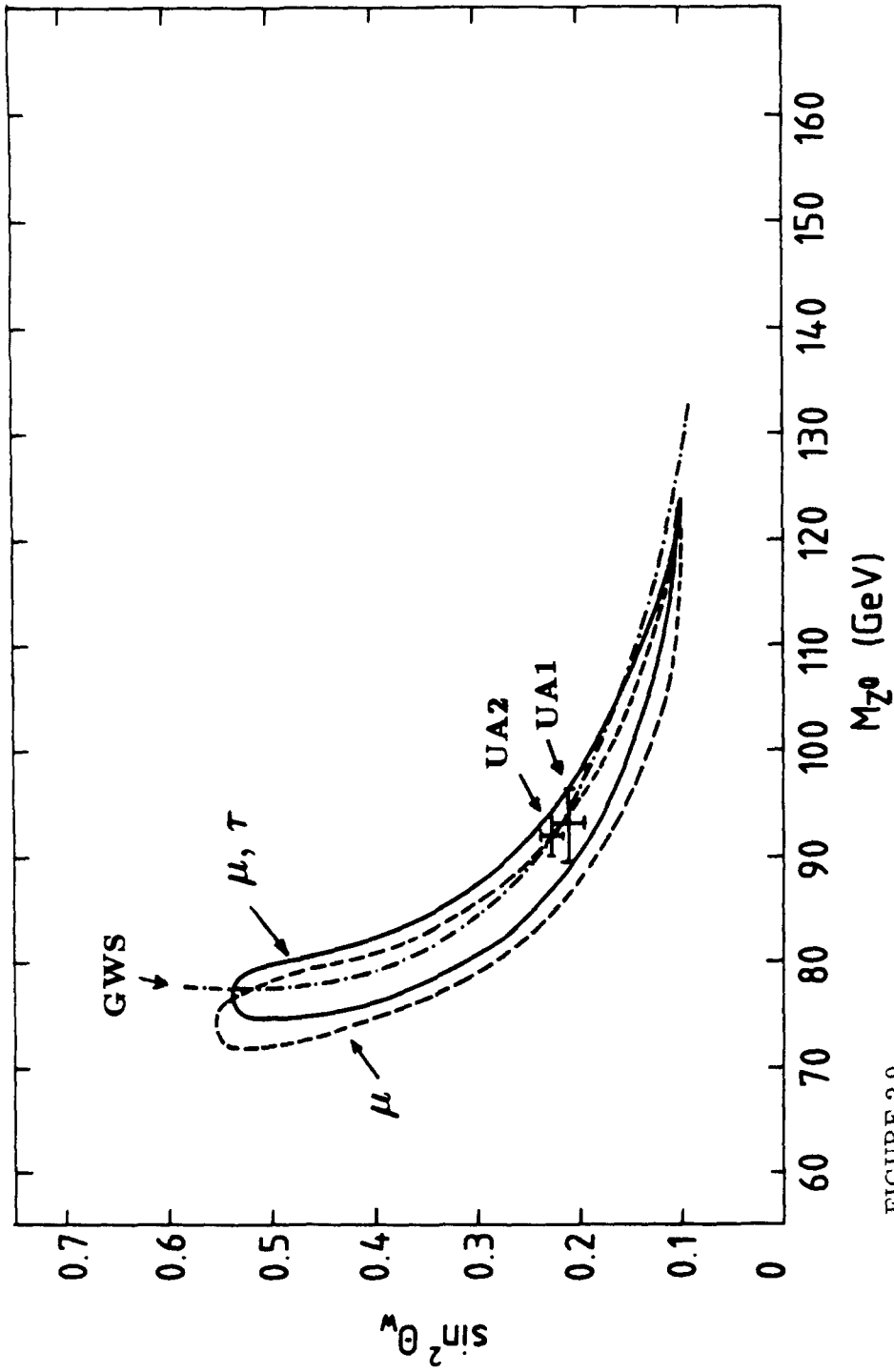
FIGURE 2.9

Contours in the $sin^2\theta_W - m_Z$ plane. The solid line is the 95% C.L. limit on the basis of the PEP and PETRA asymmetry measurements for $e^+e^- \rightarrow \mu^+\mu^-$ and $e^+e^- \rightarrow \tau^+\tau^-$. The dashed line is for $e^+e^- \rightarrow \mu^+\mu^-$ only.

2.4 Electroweak Interference in the Quark Sector

2.4.1. Flavor separation.

To measure the forward-backward asymmetry of $e^-e^+ \to c\bar{c}$ and $e^-e^+ \to b\bar{b}$, one needs to identify the flavors of the heavy quarks. The following two methods are used:

(i) Charm quark identification by $D^{*\pm}$ or $D^{\pm}$.

The identification of $D^{*\pm}$ is based on the fact that the Q value of the decay $D^{*+} \to \pi^+ D^o$ is only 5.8 MeV. As a result, the direction of the π^+ relative to that of the D^o and the momentum of the π^+ are severely restricted. The mass difference $m_{D^*} - m_{D^o}$ can be measured more accurately than the mass of the D^* itself. The D^o has been detected in the decay modes $D^o \to K^-\pi^+$, $K^-\pi^+\pi^o$ or $K^-\pi^+\pi^-\pi^+$. In this method, a cut in the $m(K\pi,\ K\pi\pi$ or $K\pi\pi\pi)$ spectrum around the D peak is made and then the Δm spectrum is plotted. As seen in Figure 2.10 clear $D^{*\pm}$ signals are seen in the Δm spectra measured by JADE [2.11]. HRS [2.12] has good enough resolution to see the charmed mesons directly. They observed the D^o decay into $K^-\pi^+$ and the D^+ decay into $K^-\pi^+\pi^+$ as shown in Figure 2.10. Both of these decays can be used to identify the primary $c(\bar{c})$ quark charge and direction.

This method leads to clean identification of the event $e^-e^+ \to c\bar{c}$ but the statistics are poor. Typically, the number of $D^{*\pm}$ is about 100 from TASSO [2.13] and about 100 from JADE [2.11]. HRS [2.12] obtains about 400 D's.

(ii) Flavor identification from inclusive leptons.

Semileptonic decays of heavy quarks ($c \to s\bar{\ell}\nu_\ell,\ b \to c\ell\bar{\nu}_\ell$) lead to a lepton with large transverse momentum ($P_\perp$) with respect to the jet axis. In the case of a c quark, the average $P_\perp$ of lepton is not as high as that from a b quark, hence background due to misidentification is larger. A large $P_\perp$ lepton gives a cleaner sample of b quark events.

2.4.2 Forward-backward asymmetry in $e^-e^+ \to c\bar{c}$

Figure 2.11 (a) to (c) shows the angular distribution of $D^{*\pm}$ from TASSO [2.13], and from JADE [2.11], and $D^{\pm}$ from HRS [2.12]. The c-quark asymmetries measured by different experiments at PEP and PETRA compiled by Marshall [2.14] and Greenshaw [2.15] and their corresponding axial vector couplings of charm-quark are given in Table 2.8.
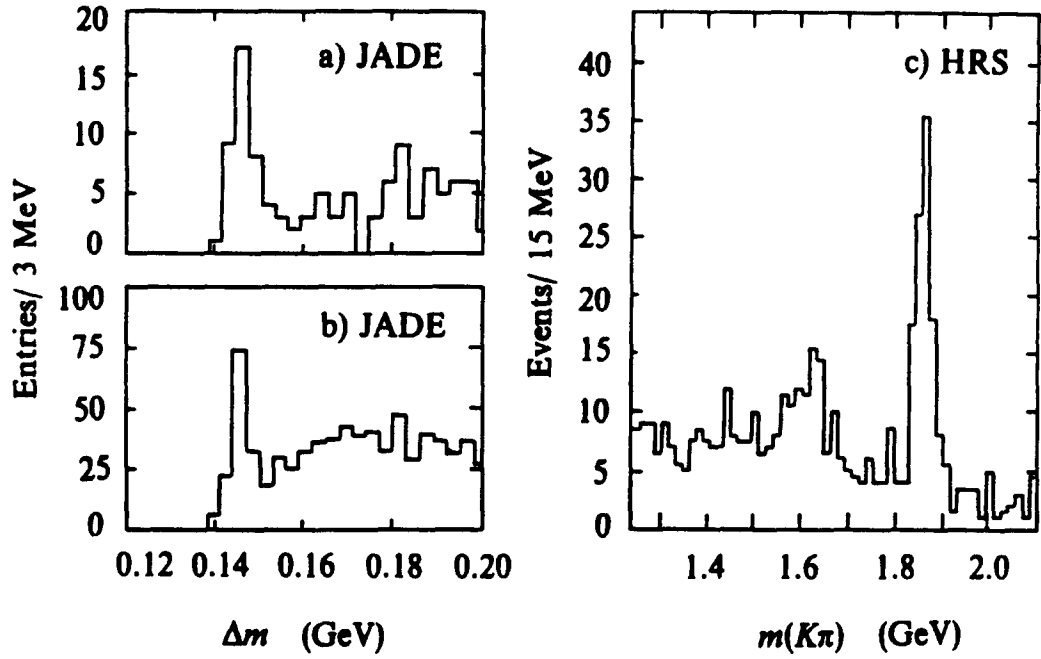
FIGURE 2.10

Observation of charm mesons by JADE and HRS. JADE uses the decays $D^{*+} \rightarrow D^o\pi^+$ with (a) $D^o \rightarrow K^-\pi^+$ and (b) $D^o \rightarrow K^-\pi^+\pi^-\pi^+$. HRS observes (c) $D^o \rightarrow K^-\pi^+$ directly.

Table 2.8

c-quark assymetry

Compiled by Greenshaw and Marshall [2.14, 2.15]

Experiment	$\sqrt{s}$ (GeV)	Method	A_c(meas)	A_c(SM)	$a_e a_c$
HRS	29	D^*	−0.14±0.05	−0.09	−1.47±0.52
TPC	29	e	−0.21±0.12±0.10	−0.09	−2.3±1.4±1.0
TPC	29	μ	−0.14±0.13±0.05	−0.09	−1.5±1.5±0.5
TPC	29	D^*	−0.16±0.16	−0.09	−1.78±1.78
JADE	34.4	D^*	−0.14±0.09	−0.131	−1.0±0.64
MARK J	35.3	μ	−0.16±0.09	−0.139	−1.2±0.6
PLUTO	34.8	μ	−0.16±0.16	−0.134	−1.1±1.1
TASSO	35.6	D^*	−0.17±0.09	−0.140	−1.2±0.6
Average					−1.3±0.3
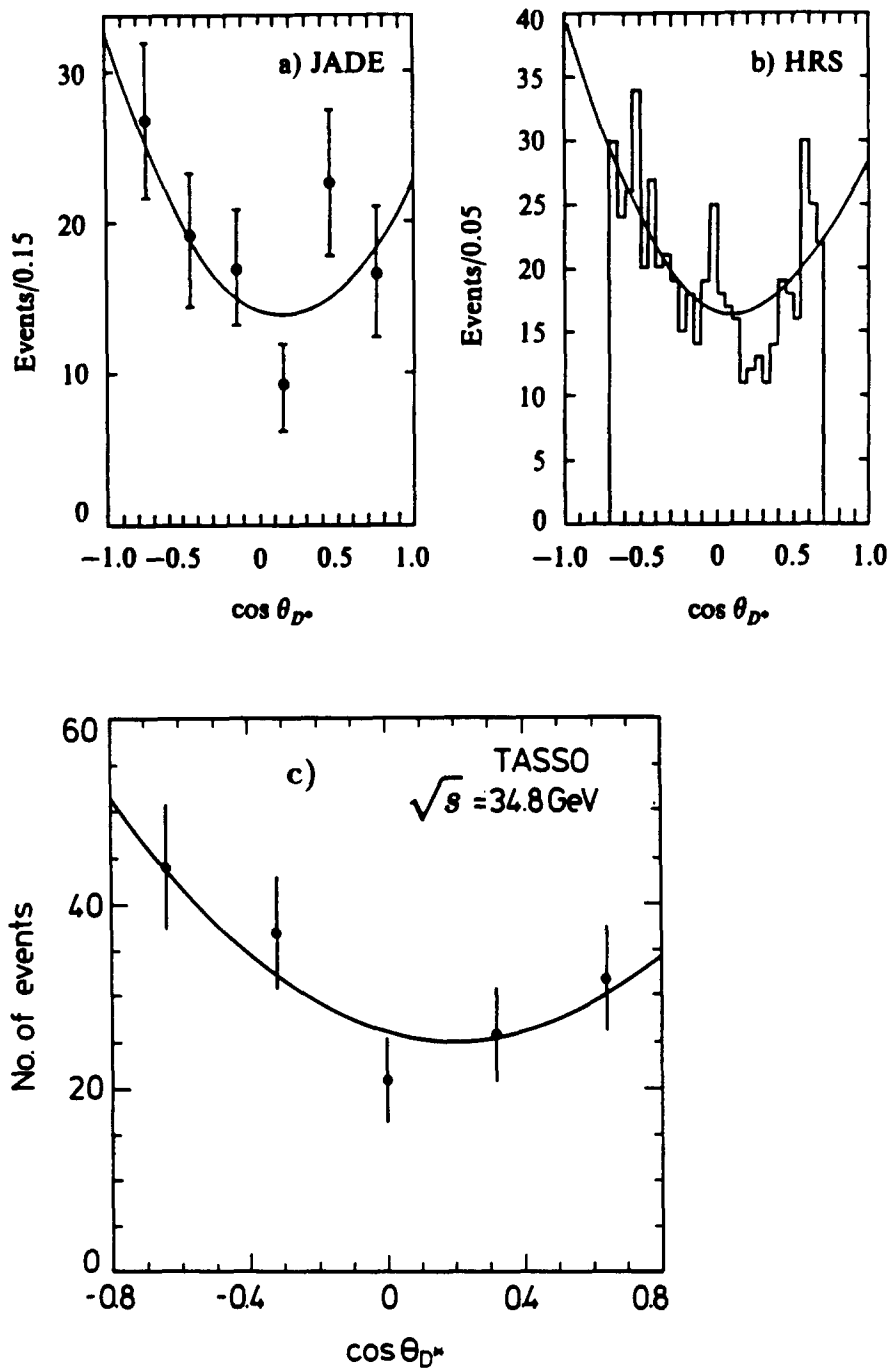
FIGURE 2.11

The measured angular distributions for the process $e^+e^- \rightarrow c\bar{c}$ measured via D^* by a) JADE, b) HRS and c) TASSO.

The combined result is, with $a_e = -1$,

$$a_c = 1.3 \pm 0.3$$

Statistical errors and systematic errors are combined in quadrature. The standard model expectation is $a_c = 1$.

2.4.3 Forward-backward asymmetry in $e^- e^+ \rightarrow b\bar{b}$

The most accurate measurement of the $b\bar{b}$ asymmetry is given by JADE [2.16]. Figure 2.12 shows the JADE angular distribution for the process $e^- e^+ \rightarrow b\bar{b}$ measured from the inclusive muons. The bottom quark asymmetries measured by different experiments at PEP and PETRA and their corresponding axial vector couplings of bottom quark are given in Table 2.9. The combined result is, with $a_e = -1$,

$$a_b = -0.84 \pm 0.21$$

without taking into account possible B^o-$\bar{B}^o$ mixing correction. Statistical errors and systematic errors are combined in quadrature.

Recently UA1 [2.17] and ARGUS [2.18] have observed B^o-$\bar{B}^o$ mixing. Taking this into account, the axial vector coupling of b quark after the B^o-$\bar{B}^o$ mixing correction is, with $a_e = -1$,

$$a_b = -1.08 \pm 0.29$$

The standard model expectation is $a_b = -1$. The correction factor is discussed in the next section.

2.4.4 Correction to b-quark asymmetry due to B^o-$\bar{B}^o$ mixing.

At PEP and PETRA, the ratio of production, in $e^+ e^-$ annihilation, of $B_u^+ : B_d^o : B_s^o$ is expected to be about 1:1:0.3. This is deduced from the fact that quark pairs $u\bar{u} : d\bar{d} : s\bar{s}$ produced from the color field is about 1:1:0.3. If we define the B^o-$\bar{B}^o$ mixing parameter χ by

$$\chi_d = \frac{\Gamma(B_d^o \rightarrow \bar{B}_d^o \rightarrow \bar{X})}{\Gamma(B_d^o \rightarrow X \text{ or } \bar{X})}$$
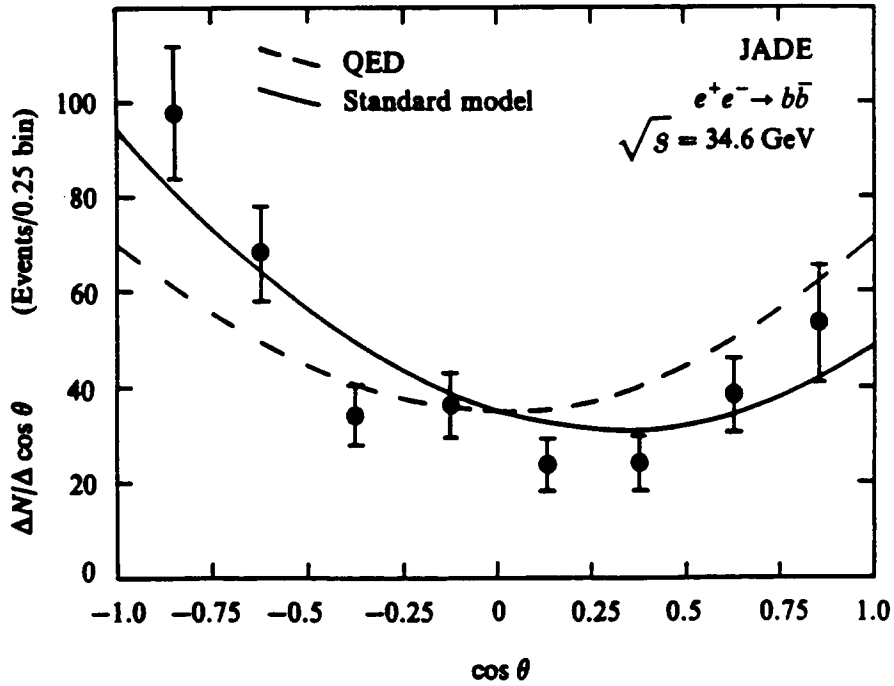
FIGURE 2.12

The measured angular distribution for the process $e^+e^- \rightarrow b\bar{b}$ measured via inclusive μ by JADE.

Table 2.9

b-quark assymetry

Compiled by Greenshaw and Marshall [2.14, 2.15]

Experiment	$\sqrt{s}$ (GeV)	Method	A_b(meas)	A_b(SM)	$a_e a_b$
TPC	29	e	$-0.36\pm0.32\pm0.08$	-0.170	$2.0\pm1.9\pm0.5$
TPC	29	μ	$-0.15\pm0.19\pm0.05$	-0.170	$0.9\pm1.1\pm0.3$
JADE	34.6	μ	$-0.228\pm0.06\pm0.025$	-0.252	$0.90\pm0.24\pm0.10$
MARK J	37	μ	$0\pm0.14\pm0.08$	-0.262	0.00 ± 0.54
PLUTO	34.8	μ	-0.36 ± 0.25	-0.254	1.3 ± 0.9
TASSO	34.4	e	-0.25 ± 0.22	-0.248	1.0 ± 0.9
TASSO	34.5	μ	-0.375 ± 0.275	-0.249	1.5 ± 1.1
CELLO	44.0	e,μ	$-0.51\pm0.38\pm0.20$	-0.41	$1.2\pm0.9\pm 0.5$
Average					0.84 ± 0.21

then the three χ's are χ_d, χ_u, and χ_s. By charge conservation, χ_u must be zero. The ARGUS result is [2.18]

$$\chi_d = 0.17 \pm 0.05$$

Using the 1:1:0.3 ratio above, the average χ is

$$\chi = R_u\chi_\mu + R_d\chi_d + R_s\chi_s$$
$$= (\frac{1}{2.3})\chi_\mu + (\frac{1}{2.3})\chi_d + (\frac{0.3}{2.3})\chi_s$$
$$= \frac{\chi_d + 0.3\chi_s}{2.3}$$

The range of all possible values of χ_s is from 0 to 0.5. If we use $\chi_s = 0.25 \pm 0.25$ together with the above ARGUS value for χ_d, then we have

$$\chi = 0.11 \pm 0.04$$

To relate the measured b-quark asymmetry to be true asymmetry, we have

$$\left.\frac{b - \bar{b}}{b + \bar{b}}\right|_{meas.} = \frac{[(1 - \chi)b + \chi\bar{b}] - [\chi b + (1 - \chi)\bar{b}]}{b + \bar{b}}$$
$$= (1 - 2\chi)\left.\frac{b - \bar{b}}{b + \bar{b}}\right|_{true}$$

For

$$\chi = 0.11 \pm 0.04,$$

we have

$$\frac{1}{1 - 2\chi} = 1.28 \pm 0.14$$

$$(A_b)_{true} = (1.28 \pm 0.14)\,(A_b)_{meas.}$$

and

$$(a_b)_{true} = (1.28 \pm 0.14)(a_b)_{meas.}$$

2.4.5 Jet charge asymmetry.

MAC [2.19] and JADE [2.20] have measured the combined asymmetry for all quarks. The analysis involves the determination of the quark charge from the charges of the particles in the jets. Then one measures the forward-backward asymmetry of the positively charged jet-axis.

If the quark flavors are produced in the proportions f_d, f_u, f_s, f_c and f_b with asymmetries A_d, A_u, A_s, A_c, and A_b and defining θ to be the angle between the positively charged quark or anti-quark direction and that of the incoming positron direction, the hadronic asymmetry is then

$$A_q = f_d A_d - f_u A_u + f_s A_s - f_c A_c + f_b A_b,$$

the negative signs arising because of the signs of the quark charges. At a centre-of-mass energy of 35 GeV, $A_q \approx 0.035$ while at 44 GeV, $A_q \approx 0.071$ from the standard model.

In the standard model, the axial vector couplings of the quarks are related by $a_u = -a_d = -a_s = a_c = -a_b$. Assuming this we define

$$a_q = a_u = -a_d = -a_s = a_c = -a_b$$

MAC [2.19] determines the charge of each jet by

$$Q_{jet} = \sum_i Q_i \eta_i^\kappa$$

where Q_i is the charge of the i'th charged particle of one hemisphere of the event, η_i is the rapidity of the ith particle and κ is a constant. The weight η_i^κ is introduced since particles with larger rapidity are expected to have a higher probability of carrying the parent quark flavor. The value $\kappa = 0.2$ is chosen to maximize the number of events with oppositely charged jets. From Monte Carlo simulation the quark charge misidentification probability is about 20% for the u-type quarks and about 27% for the d-type quarks. MAC measures the angular distribution of the thrust axis, taken in the direction of the positively charged jet, with respect to the direction of the incident positron. This distribution, after efficiency and radiative corrections, is shown in Figure 2.13(a), with the dotted curve representing the pure QED distribution. The difference between the measured cross section and that expected from pure QED is shown in Figure 2.13(b). The average charge asymmetry determined by a maximum likelihood fit is $A_q = 0.028 \pm 0.005$ at $\sqrt{s} = 29$ GeV where the error is statistical. The fit is shown by the solid lines in Figure 2.13(a) and 2.13(b). The Monte Carlo simulated events give a jet charge asymmetry $A = 0.022$. This simulation was based on standard electroweak theory with $sin^2\theta_W = 0.22$. The result for the axial vector coupling of quark is

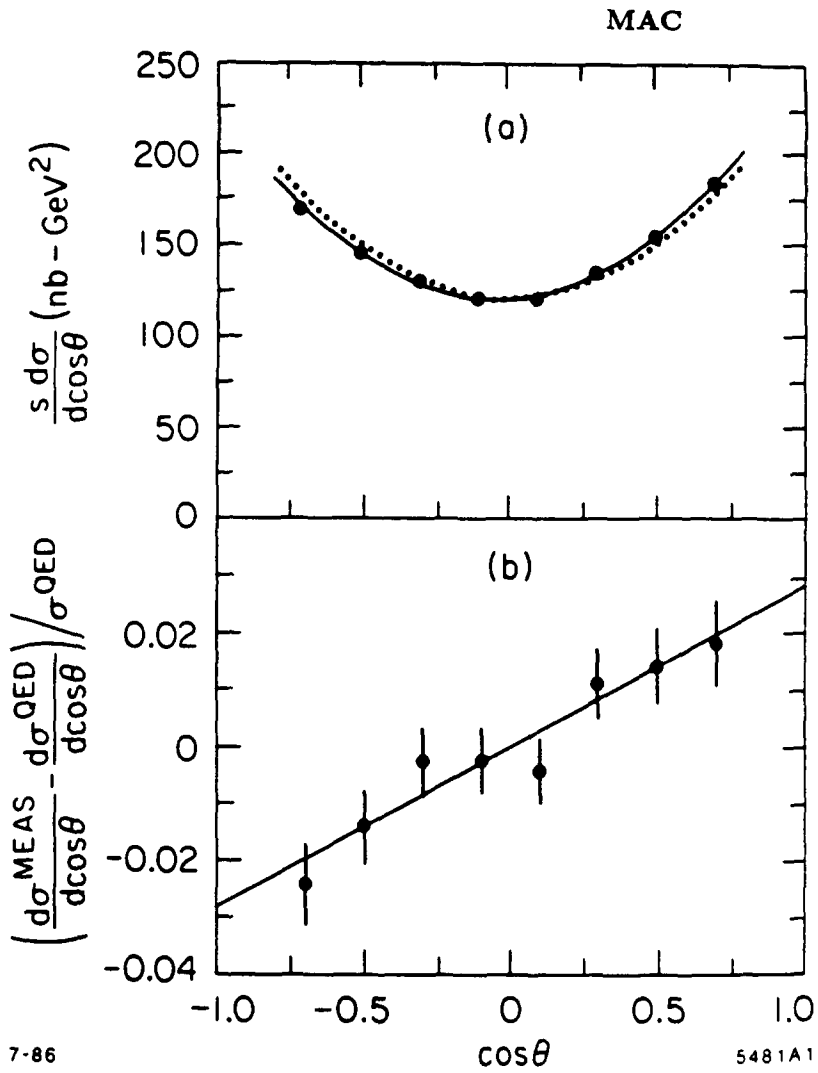$$a_e a_q = -1.36 \pm 0.24 \text{ (stat.)} \pm 0.20 \text{ (syst.)}$$

MAC

FIGURE 2.13

Result from MAC on jet charge asymmetry:

    (a) the measured angular distribution, and

    (b) the difference between the measured cross-section and pure QED.

with no $B^o\bar{B}^o$ mixing correction.

JADE [2.20] determine the charge of each jet by using

$$Z_i = \frac{Q_i P_{Li}}{E_b} \qquad\qquad i = 1, 2, 3$$

of the fastest three particles ($P_1 > P_2 > P_3$) in each jet (two jet events are selected by sphericity < 0.1). Here P_{Li} is the longitudinal momentum of the ith particle along the sphericity axis of the event, Q_i is its charge and E_b is the beam energy. The marginal Z_1, Z_2 and Z_3 distributions ($|Z_1| > |Z_2| > |Z_3|$) from Monte Carlo simulation for jets originating from positive quarks or anti-quarks and negative quarks or antiquarks, at a centre of mass energy of 35 GeV are illustrated in Figure 2.14. It is clear from the figures that for a jet of positive quarks there are more entries for positive Z_1 than negative Z_1. The same is true for Z_2 and Z_3. To identify the charge of the jet, JADE uses a weighting scheme [2.21] with Z_1, Z_2, and Z_3 as the discriminative variables. The results obtained are:

$$A_q = 0.060 \pm 0.013$$

at a mean center-of-mass energy of 34.8 GeV and

$$A_q = 0.082 \pm 0.029$$

at 43.6 GeV. The angular distributions at $\sqrt{s} = 35$ GeV and 44 GeV of the positively charged jet are shown in Figure 2.15. Combining the results of $\sqrt{s} = 34.8$ GeV and 43.6 GeV and including in the systematic error a reasonable estimate of the effects of the uncertainties in the B^o-$\bar{B}^o$ system gives final results of

$$a_e a_q = 1.20 \pm 0.21 \text{ (stat.)} \pm 0.23 \text{ (syst.)}$$

where no correction for B^o-$\bar{B}^o$ mixing effects has been made and

$$a_e a_q = 1.13 \pm 0.20 \text{(stat.)} \pm 0.22 \text{(syst.)}$$

where a correction for B^o-$\bar{B}^o$ mixing effects has been applied, using the result of ARGUS [2.18] as mentioned in the previous section.
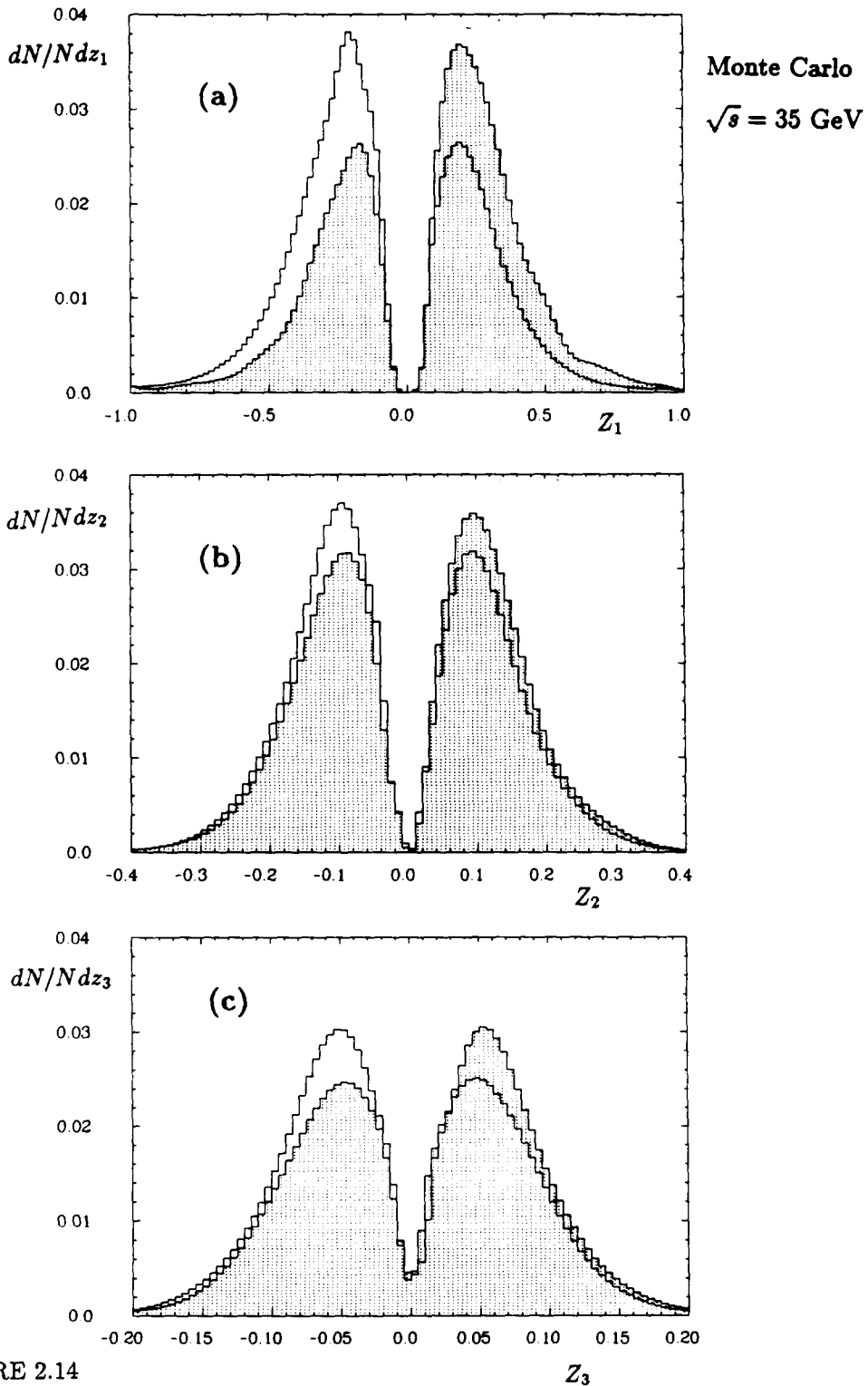
FIGURE 2.14

Monte Carlo simulated z_1, z_2 and z_3 distributions from positive (shaded) and negative jets at a center-of-mass energy of 35 GeV.
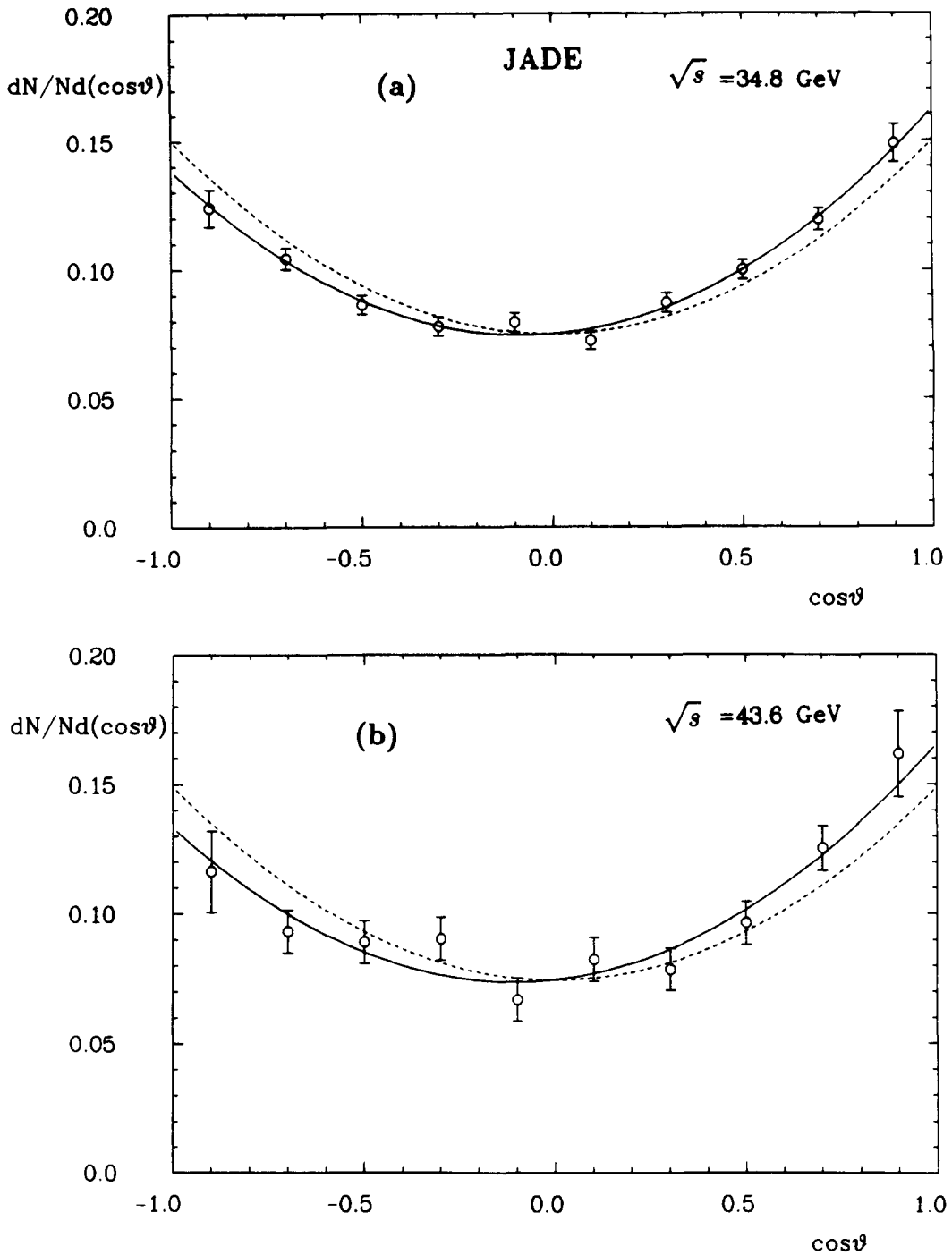
FIGURE 2.15

Result from JADE on jet charged asymmetry. The acceptance corrected *cos* θ distribution of the sphericity axes with the sense of the positively charged quark or anti-quark, at 35 GeV (upper figure) and at 44 GeV (lower figure). The solid lines are fits to the data with asymmetries of 0.060 and 0.082 respectively and the dotted lines are fits with the asymmetry set to zero.

2.4.6 Global fit to R and quark asymmetries.

Marshall [2.14] of the JADE collaboration has performed a global fit to obtain the vector couplings and axial vector couplings of quarks using the R measurements from PEP and PETRA, forward-backward asymmetry measurements of c-quarks and b-quarks, and the jet charge asymmetry reported in this section. The results are:

without B^o-$\bar{B}^o$ mixing correction

$$a_e a_{u,c} = -1.08 \pm 0.15$$

$$a_e a_{d,s,b} = 0.84 \pm 0.18$$

and with B^o-$\bar{B}^o$ mixing correction

$$a_e a_{u,c} = -1.17 \pm 0.15$$

$$a_e a_{d,s,b} = 1.03 \pm 0.20$$

2.5 Quark Bremsstrahlung

In events from the process $e^+e^- \rightarrow q\bar{q}$, if a photon is radiated from the initial state, the hadrons are in a $C = -1$ state, whereas photons emitted from quarks lead to a $C = +1$ state of the hadrons. The interference of these two contributions to the direct photon signal leads to a negative asymmetry in the distribution of the positive quark relative to the positive incoming lepton. Such measurements of charge asymmetry have been carried out previously by JADE [2.22], MAC [2.23] and MARK II [2.24]. The new contribution to this conference from the preliminary results of TASSO [2.25] gives

$$\text{Asymmetry} = -1.11 \pm 0.25 \text{ (stat.)} \pm 0.35 \text{ (syst.)}$$

This value differs by two standard deviations from the standard model value of -0.36.

Section 3   New Particle Search

Since the International High Energy Conference in Berkeley [3.1], July 1986, no new particles have been found in e^+e^- annihilation. However, there has been important progress made in setting limits on masses and couplings in new particle search. We shall cover here the searches for

(1) Neutral and Charged Higgs Bosons

(2) Fourth Generation Charged and Neutral Leptons

(3) Neutrino Counting

(4) Supersymmetric Particles

(5) Magnetic Monopoles

3.1 Search for Neutral Higgs Boson

After the observation of the intermediate vector bosons W and Z at the CERN $p\bar{p}$ collider [3.2], with only two exceptions all the other particles of the three-generation standard model [3.3] have been seen experimentally. The two exceptions are the top quark t and the neutral Higgs boson H^o [3.4]. The recent observation by ARGUS on B^o-$\bar{B}^o$ mixing has led to the conclusion that [3.5]

$$m_t > \frac{1}{2}\,m_Z$$

Similar top quark mass limit has been given by UA1 [3.6]. In other words, within the standard model, the t quark mass is most likely to be heavier than anticipated. This result was discussed elsewhere in this conference. However, as emphasized by Glashow [3.7], with some extensions of the standard model, a lower mass for the t quark is still consistent with the existing experimental data.

While the t quark of the third generation is perhaps not fundamentally different from the c quark of the second generation, the neutral Higgs boson H^o is unique within the standard model. In particular, it is responsible for giving masses to all the particles. Therefore, the experimental search for this particle H^o is of extraordinary importance. In this section we summarize two such searches, one by the CUSB collaboration [3.8] and

the other by the CLEO collaboration [3.9], both at CESR of Cornell. Such searches will undoubtedly continue, and are indeed expected to be a major activity [3.10] at LEP.

3.1.1 Search for neutral Higgs Boson from Υ radiative decay

The CUSB collaboration [3.8] at CESR had searched for the neutral Higgs boson from the radiative decays of 4×10^5 $\Upsilon(1S)$ and 3.5×10^5 $\Upsilon(3S)$ through the Wilczek mechanism [3.11] $\Upsilon(nS) \rightarrow \gamma H^o$ as shown in Figure 3.1. Their decay rate, normalized to the two muon rate, is given by [3.11, 3.12]

$$\Gamma(\Upsilon \rightarrow \gamma H^o)/\Gamma(\Upsilon \rightarrow \mu\mu) = G_F m_\Upsilon^2/(4\alpha\pi\sqrt{2}) \times (1 - m_{H^o}^2/m_\Upsilon^2)x^2, \qquad (3.1)$$

where x is unity in the minimum model where there is only one physical, neutral Higgs. For models with more Higgses, $x = \langle\phi_1\rangle/\langle\phi_2\rangle$ where $\langle\phi_{1,2}\rangle$ are vacuum expectation values of the Higgs fields. QCD radiative corrections [3.13], reduce the branching ratio by about a factor of two. The branching ratio for $\Upsilon(nS) \rightarrow \gamma + H^o$ is small, of the order of 2.5(or 1.3) $\times 10^{-4}(1 - m_{H^o}^2/m_\Upsilon^2$(or $m_{\Upsilon''}^2))x^2$, especially if $m_H \sim m_\Upsilon$(or $m_{\Upsilon''}$).

Combining the data from $\Upsilon(1S)$ and $\Upsilon(3S)$ decays, CUSB obtains the result shown in Figure 3.2. The excluded mass limit for the neutral Higgs Boson is

$$0.6 \text{ GeV } < m_{H^o} < 3.9 \text{ GeV at } 90\% \text{ confidence level}$$

The same data are used to extract an upper limit on the branching ratio for the process $\Upsilon'' \rightarrow \gamma + \eta_{\tilde{g}}$. The $\eta_{\tilde{g}}$ is a bound state of two gluinos, the supersymmetric partners of the gluon. These $\tilde{g}\tilde{g}$ bound states are expected to have similar properties as the Υ and J/ψ. In particular the $\eta_{\tilde{g}}$ is a pseudoscalar state ($J^{PC} = 0^{-+}$), similar to the η_c for $c\bar{c}$. Using the same analysis as described in Ref. [3.14], CUSB obtains the excluded mass limit for gluino

$$0.6 \ GeV < m_{\tilde{g}} < 2.6 \ GeV \qquad \text{at } 90\% \text{ confidence level}$$

3.1.2 Search for neutral Higgs from B-meson decay

The CLEO collaboration [3.9] at CESR looked for decays of the type $B \rightarrow H^o K($ or $K^*)$ where the H^o decays into a two body final state containing a K, or a K^*, dimuons or

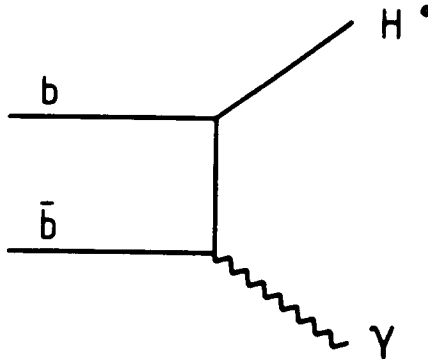FIGURE 3.1

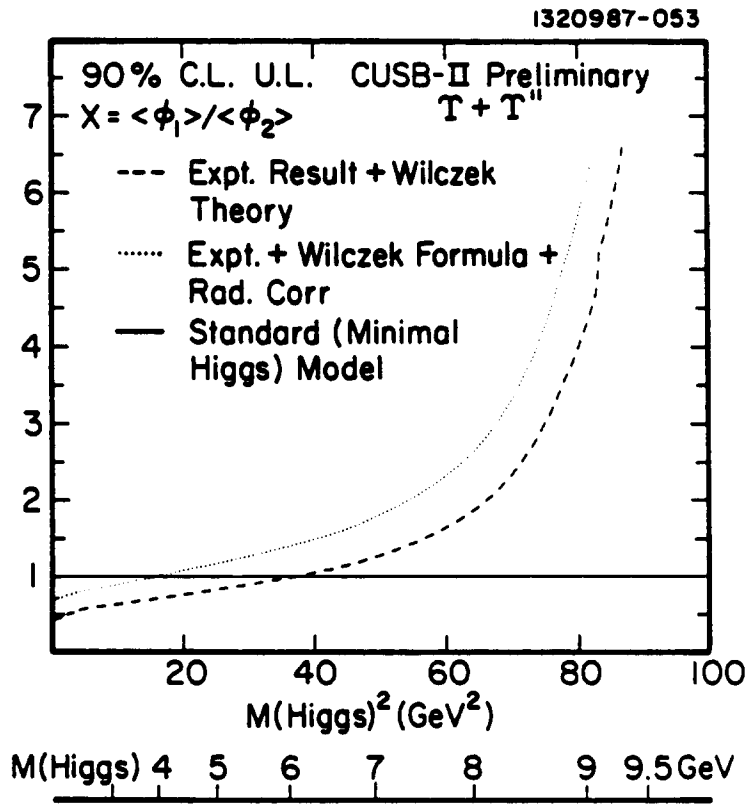Feynman diagram for Wilczek mechanism $\Upsilon(nS) \to \gamma H^\circ$.

FIGURE 3.2

CUSB 90% C.L. upper limit (dotted curve) for $x = <\phi_1> / <\phi_2>$ from $\Upsilon(1S)$ and $\Upsilon(3S)$. The dotted curve intersects $x = 1$ at $m_{H^\circ} = 3.9$ GeV.

dipions. The production of Higgs in the B meson decay involves the coupling of Higgs to the t quark as shown in Figure 3.3. The partial width for this decay relative to the B semileptonic partial width is given by Willey and Yu [3.15] as

$$\frac{\Gamma(B \to H^\circ X)}{\Gamma(B \to e\nu X)} = \frac{|V_{tb}V_{ts}^*|^2}{|V_{cb}|^2} \frac{27\sqrt{2}}{64\pi^2} G_F m_b^2 \left(\frac{m_t}{m_b}\right)^4 \left(1 - \frac{m_{H^\circ}^2}{m_b^2}\right) \frac{1}{r(m_c/m_b)} \qquad (3.2)$$

where m_{H° is the Higgs mass, m_b, m_c and m_t are the b, c and t quark masses and the V_{ij}'s are Kobayashi-Kaskawa matrix [3.16] elements. $r(m_c/m_b)$ is the phase space factor for semileptonic B decay. Using the B semileptonic branching ratio measured in $\Upsilon(4S)$ decays of 0.110 ± 0.007, [3.17], CLEO estimates that

$$BR(B \to H^\circ X) = 0.042 \, (m_t/50 \text{ GeV})^4 \, (1 - m_{H^\circ}^2/m_b^2) \qquad (3.3)$$

At the $\Upsilon(4S)$ resonance, CLEO collected 180,000 B meson decays, of which 76,000 are neutral B's and 104,000 are charged B's. Using the prediction of Haber et al., [3.18], for $BR(B \to H^\circ K)$ and $BR(B \to H^\circ K^*)$ (which is small) and Voloshin's predictions [3.19] for $BR(H^\circ \to \mu^+\mu^-)$ and $BR(H^\circ \to \pi^+\pi^-)$ the upper limits on the branching ratio $B \to H^\circ X$ by CLEO is shown in Figure 3.4. From this figure, one concludes that there is no evidence for the neutral Higgs in B decay. Using equation (3.3), CLEO states that either the t quark mass is less than 47 GeV [3.20] or the H° is excluded from the mass range between 0.3 and 3.0 GeV, and between 3.2 and 3.6 GeV.

We would like to point out here that the above result is subject to large theoretical uncertainties. In particular, one notes:

(1) $\Gamma(B \to H^\circ K)/\Gamma(B \to H^\circ X)$ can be much smaller [3.21] than that given by Haber et al.

(2)   The interpolation of the $BR(H^\circ \to \mu^+\mu^-)$ given by Voloshin between 1.5 GeV to 3.0 GeV Higgs mass is unreliable.

(3)   The result of Willey and Yu as given by (3.2) has been confirmed by Grzadkowski and Krawczyk [3.22] and by Botella and Lim [3.23] but not by Pham and Sutherland [3.24] for the Higgs mass range in question.
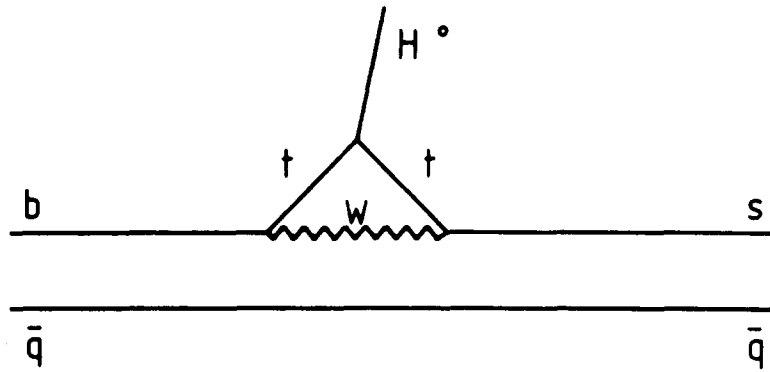
FIGURE 3.3

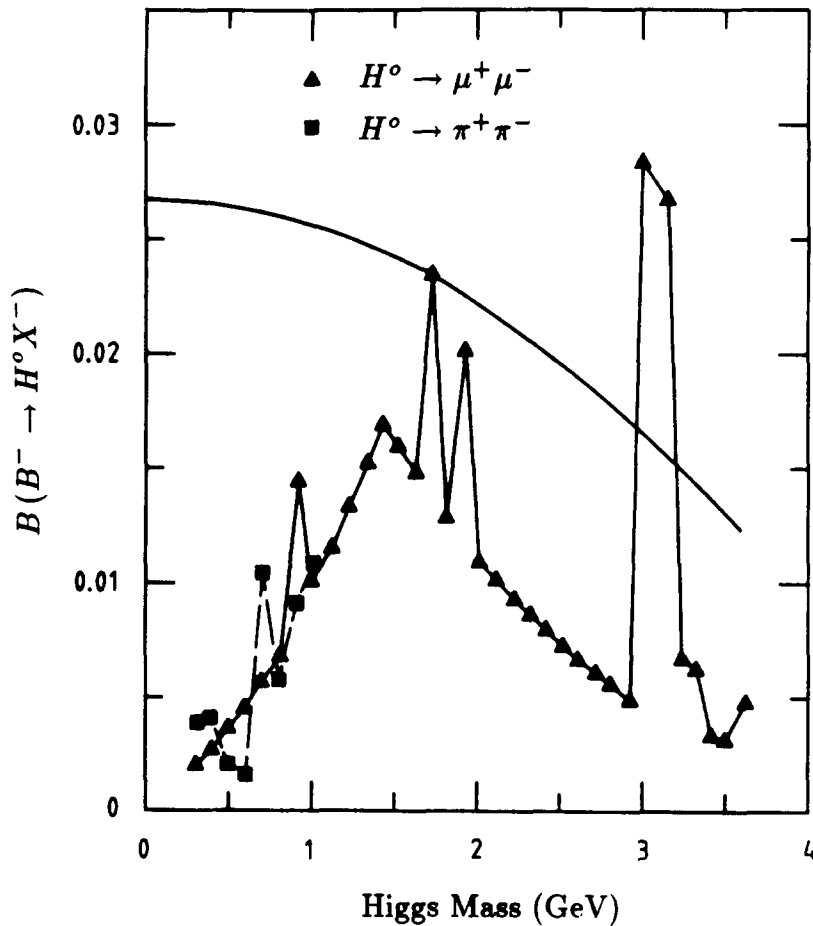Feynman diagram for B decay into Higgs through a virtual t.

FIGURE 3.4

CLEO upper limits on the branching ratio for $B \to H^\circ X$ using $H^\circ \to \mu^+\mu^-$ and $H^\circ \to \pi^+\pi^-$. The smooth curve corresponds to $m_t = 47$ GeV.

3.2 Search for Charged Higgs Boson

In the standard model [3.3] (which is sometimes referred to as the minimal standard model), there is only one scalar Higgs doublet. This one scalar Higgs doublet leads to just one physical particle, which is the neutral Higgs boson discussed in the preceeding subsection.

It is conceivable that there is more than one Higgs doublet. In particular, the supersymmetric version of the standard model requires the presence of at least two Higgs doublets. Since the numbers of the intermediate vector bosons Z^o and W are not doubled, there are in this supersymmetric version five physical Higgs bosons, three neutral and two charged ones (H^+ and H^-).

Charged Higgs bosons ($H^\pm$) can be produced via

$$e^+e^- \to H^+H^-$$

with the differential cross section

$$\frac{d\sigma}{d\Omega}(e^+e^- \to H^+H^-) = \frac{3}{32\pi}\sigma_{\mu\mu}\beta^3 sin^2\theta$$

where $\sigma_{\mu\mu} = \frac{4}{3s}\pi\alpha^2$ is the total μ-pair cross section, β is the Higgs velocity and θ is the relative angle between the incoming and outgoing particles. The total cross section is $\frac{1}{4}\sigma_{\mu\mu}\beta^3$.

With the dominant decay modes assumed to be $H^\pm \to \tau\nu, cs$ and cb [3.25], various PEP and PETRA groups [3.26] have studied the following reactions:

$$e^+e^- \to H^+H^- \to \bar{\tau}\nu\tau\bar{\nu} \qquad \text{Two-tau final state}$$
$$e^+e^- \to H^+H^- \to c\bar{q}\bar{c}q' \; (q, q' = s, b) \qquad \text{Hadronic final state}$$
$$e^+e^- \to H^+H^- \to \bar{\tau}\nu\bar{c}q \; (q = s, b) \qquad \text{Mixed tau and hadronic final state}$$

Higgs production could also be detected through the change of the total cross section of tau pairs and multihadrons.

The new results are given by JADE [3.27] and CELLO [3.28] collaborations and are shown in Figure 3.5 and Figure 3.6 respectively. Charged Higgs are excluded from 3.5 GeV to 19 GeV independent of the hadronic and leptonic decay branching ratios.
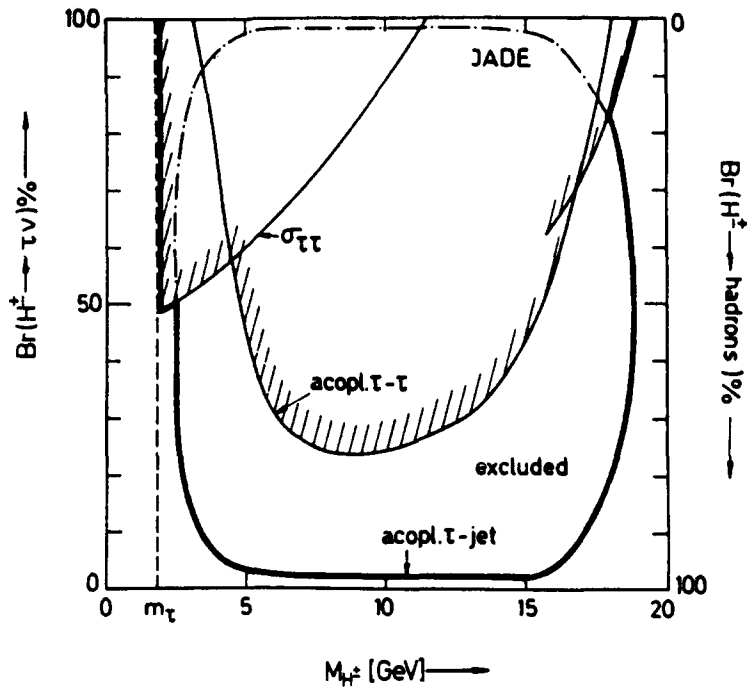
FIGURE 3.5

JADE result on lower limits at 95% C.L. for the production of a charged scalar Higgs $H^{\pm}$ decaying into τ's or hadrons.
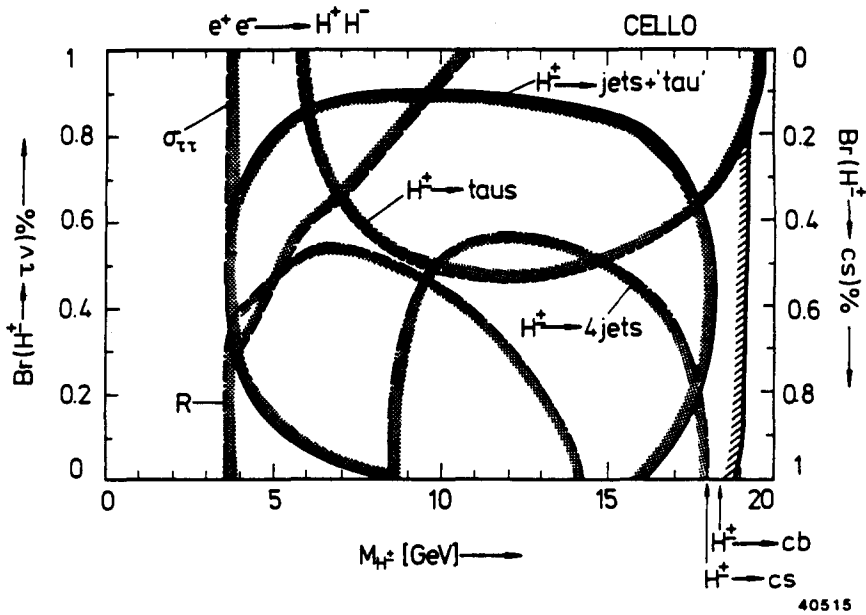

FIGURE 3.6

CELLO result on limits at 95% C.L. on the mass of the charged Higgs $H^{\pm}$. The area on the shaded side of the contour is excluded in each case. The combined limit for all of them (thick line) shows that charged Higgs bosons below 19 GeV/c² are excluded.

3.3 Search for Fourth Generation Leptons

So far as we know, the three leptons – the electron, the muon, and the tau – together with their respective neutrinos form three generations in the sense that their interactions are identical (except for the differences in masses). Yet there is at present no understanding why there are three generations. In particular, there is no reliable argument why there is, or there is not, a fourth generation. In view of this situation, there have been repeated efforts to look for leptons of a fourth generation. Such searches are further encouraged by the empirical observation that the leptons are the lightest fermions in the three known generations, and we may hope that this is also true for the fourth generation.

3.3.1 Charged heavy leptons

Charged sequential heavy leptons are produced via the reaction

$$e^+e^- \to \gamma_{virtual} \to L^+L^-$$

and decay through the processes

$$L^- \to \quad L^o + \ell^- + \bar{\nu}_\ell, \qquad \ell = e, \mu, \tau$$
$$\to \quad L^o + \text{hadrons}$$

as shown in Figure 3.7 where L^o is the neutral lepton associated with L^-.

If m_{L^o} is negligible compared with $m_{L^\pm}$ the best limits so far are:

JADE :	$m_{L^\pm} > 22.7$ GeV	[3.27]
CELLO :	$m_{L^\pm} > 22$ GeV	[3.29]
VENUS :	$m_{L^\pm} > 24.5$ GeV	[3.30]

These limits are to be compared with the 41 GeV obtained by UA1 [3.31]

3.3.2 Close-mass lepton pairs

The above results are obtained under the assumption that m_{L^o} is much less than $m_{L^\pm}$ There is no reason why this has to be true. Perl [3.32] was first to search for the case where m_{L^o} is close to $m_{L^\pm}$. The results in mass difference ($\delta = m_{L^\pm} - m_{L^o}$) versus charged heavy lepton mass ($m_{L^\pm}$) is shown in Figure 3.8. The following regions are excluded (Regions A to D are given by Perl [3.32]).
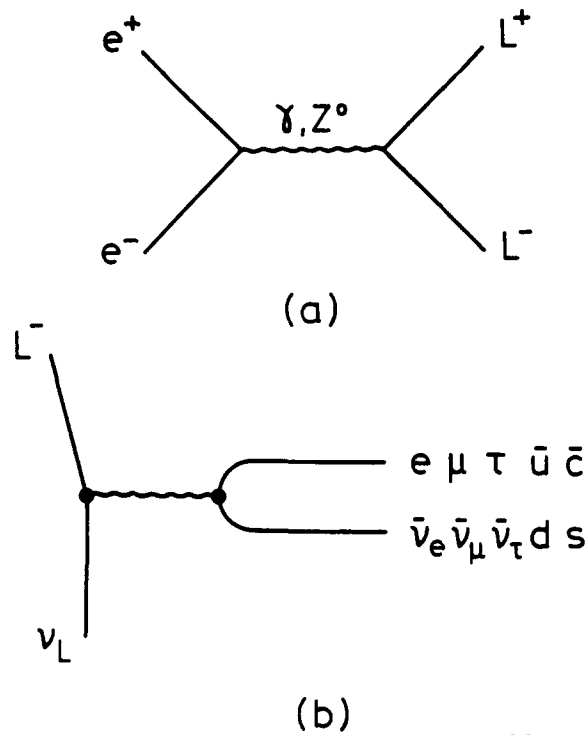
FIGURE 3.7

Production and major decay modes of a heavy charged sequential lepton.

Region A :   By definition $\delta \leq m_{L\pm}$; therefore this region A where $\delta > m_{L\pm}$ is excluded.

Region B :   This region B, where the decay length of $L^{\pm}$ is quite long, is excluded by the JADE [3.33] and CELLO [3.34] collaborations.

Region C :   Excluded by extending the null result of searching for $L^{\pm}$ with $m_{L^{\circ}} \ll m_{L\pm}$ to $m_{L^{\circ}}^2 \leq 0.2 m_{L\pm}^2$.

Region D :   Excluded by the charginos search of the JADE collaboration [3.33].

Region E :   Excluded by Perl and Stoker [3.35] of the MARK II collaboration. They look for e-μ events and events with three or more charged hadrons versus isolated e or μ.

Region F :   Excluded by the TPC/Two-Gamma collaboration [3.36]. They look for candidate events where one of the charged leptons is detected through the decay $L^- \to L^{\circ}e^-\bar{\nu}_e$ and the other through the decays $L^- \to L^{\circ}\pi^- +$ neutral particles and $L^- \to L^{\circ}\mu^-\bar{\nu}_\mu$.
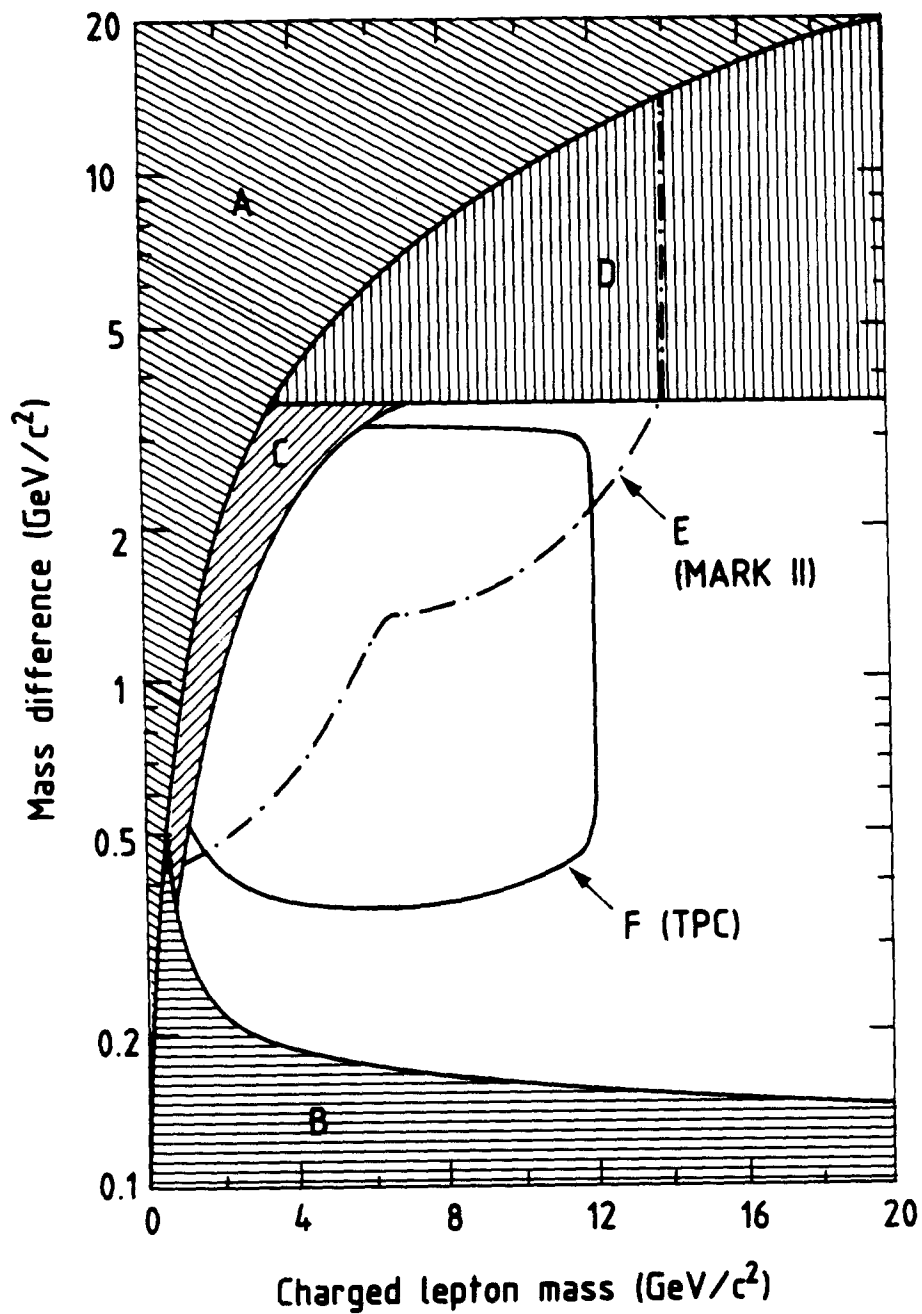
FIGURE 3.8

Perl plot of the excluded regions of the charged lepton mass, m_{L^-}, and the mass difference $m_{L^-} - m_{L^0}$. The excluded regions A-F are defined in the text.
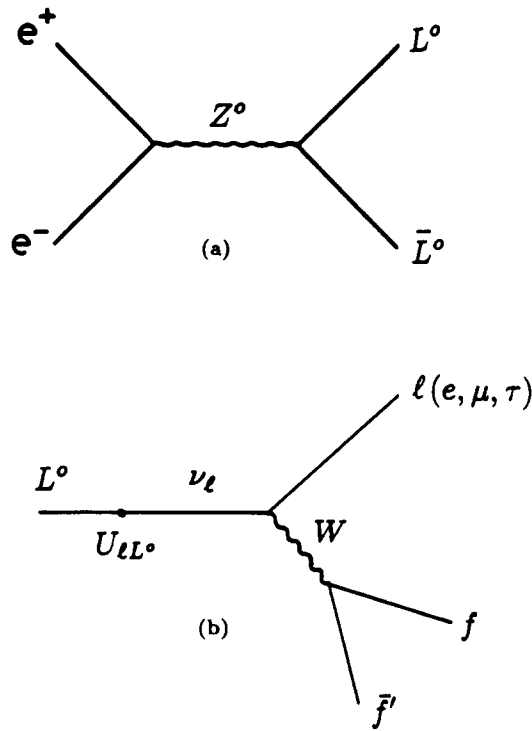
FIGURE 3.9

(a) Production and (b) decay through mixing of heavy neutral lepton L^o.

3.3.3 Heavy neutral leptons

For the first three generations, the neutrino has the lowest mass, perhaps zero. If there is a fourth generation, then it is quite possible the neutral lepton L^o still has the lowest mass. If so, the detection of the L^o may be the most hopeful way of finding this fourth generation.

If the mass of this L^o is very low, then the best way of finding it is through neutrino counting, to be discussed below in the next section. So far, the results from neutrino counting are not accurate enough to tell whether there is a fourth generation or not.

If $m_{L^\pm}$ is less than 22.7 GeV, then it would have been pair produced at PETRA; if it is less than 41 GeV, then it would have been seen at the CERN $p\bar{p}$ collider. The interesting case is thus the one where the mass of $L^\pm$ is above these limits. In this case, if the fourth generation neutral lepton L^o does not mix with those of the first three generations, then it is stable and its detection is extremely difficult. We therefore consider the case where there is mixing between the four neutral leptons.

In the presence of this mixing, there are many ways to try to detect this fourth generation heavy neutral lepton. For example, if the mass is less than that of the pion, then we can look for the decay $\pi^+ \to e^+ L^o$. In entirely the same way, the pion may be replaced by $K^\pm$, or charmed meson, or even bottom meson. A compilation of such low energy results has been given by Gilman [3.37], and reported in recent conferences.

If the mass of this fourth generation neutral lepton is higher, then it is useful to look for it at PEP and PETRA. We summarize these recent results.

MARK II [3.38], HRS [3.39] and CELLO [3.29] collaborations have carried out the search through the process

$$e^+e^- \to L^o \bar{L}^o$$

as shown in Figure 3.9(a) together with the decay process of Figure 3.9(b) via mixing with neutrino of other flavors. Here we denote the coupling of L^o with ν_e, ν_μ, and ν_τ as U_{eL^o}, $U_{\mu L^o}$, and $U_{\tau L^o}$ respectively where $|L^o\rangle = \sum_\ell U_{\ell L^o} |\nu_\ell\rangle$. With these notations, if ℓ is the lepton to which L^o primarily couples, then its lifetime can be expressed as

$$\tau(L^o \to \ell^- X^+) = (\frac{m_\mu}{m_{L^o}})^5 \frac{\tau_\mu B(L^o \to \ell^- e^+ \nu_e)}{f(m_{L^o}, \ell)|U_{\ell L^o}|^2}$$

where $f(m_{L^o}, \ell)$ is phase-space correction which differs appreciably from 1 only when $\ell = \tau$.

Since smaller coupling $|U_{\ell L^o}|$ leads to longer lifetime, the MARK II [3.38] collaboration looks for events with two back-to-back vertices (each > 2mm from the interaction point) and with no tracks coming from the interaction point. The HRS collaboration [3.39] looks for L^o through the process

$$e^+e^- \to L^o \bar{L}^o$$
$$\begin{array}{l} \vert \quad \vert\!\!\longrightarrow \text{ anything} \\ \vert\!\!\longrightarrow e^\pm X^\mp \end{array}$$

where X is a non-showering particle (i.e. not an electron). This $e^\pm X^\mp$ pair may be accompanied by possible light, unobserved neutrinos. The CELLO collaboration [3.29] looks for events with one isolated lepton and at least one other lepton of opposite sign but of the same type.

Assuming that the mixing is predominately with only one of the neutrinos ν_e, ν_μ, or ν_τ, the excluded regions for $|U_{eL^o}|^2$, $|U_{\mu L^o}|^2$, and $|U_{\tau L^o}|^2$ from the MARK II (90% C.L.

for $U_{e,\mu L^\circ}$), HRS (90% C.L. for $U_{e,\mu L^\circ}$ and 80% C.L. for $U_{\tau L^\circ}$) and CELLO (95% C.L. for $U_{e,\mu L^\circ}$) collaborations are shown in Figure 3.10.

As recently summarized by Caldwell [3.40], mass limits have also been provided by non-accelerator experiments, especially for Majarana heavy neutral leptons.

3.4 Neutrino counting

In section 3.3.3, we have described the search for an additional neutral lepton which decays through mixing with the three known neutrinos. Here we consider the opposite case where the additional neutral lepton is stable, or at least has a sufficiently long lifetime such that it does not decay within the detector. It is also assumed that the mass of this additional neutral lepton, or neutrino, is small compared with the center-of-mass energy at PEP and PETRA. (The term "neutrino" is used here to mean a stable or nearly stable neutral lepton of low mass).

Under these circumstances, the number of neutrino families N_ν (including the three known ones) is most directly counted by detecting single photons from the process

$$e^+e^- \to \gamma\nu\bar{\nu}.$$

This process proceeds through annihilation into Z°; for an electron neutrino there is an additional contribution from W exchange. Both types of diagrams are shown in Figure 3.11. The total cross-section for $e^+e^- \to \gamma\nu\bar{\nu}$ is [3.41]

$$\frac{d\sigma(e^+e^- \to \gamma\nu\bar{\nu})}{dxdy} = \frac{2\alpha}{\pi} \frac{s(1-x)}{x(1-y^2)}((1-\frac{x}{2})^2 + x^2\frac{y^2}{4})\sigma(e^+e^- \to \nu\bar{\nu})$$

$$\sigma(e^+e^- \to \nu\bar{\nu}) = \frac{G_F^2}{6\pi}[2 + \frac{N_\nu(v_e^2 + a_e^2) + 2(v_e + a_e)(1 - \frac{s(1-x)}{m_Z^2})}{(1 - \frac{s(1-x)}{m_Z^2})^2 + \frac{\Gamma_Z^2}{m_Z^2}}]$$

where x is the energy of the photon divided by the beam energy, $\sqrt{s}$ is the center-of-mass energy, $y = cos\ \theta$ is the photon polar angle with respect to the beam axis, v_e and a_e are the vector and axial vector couplings of the electron and Γ_Z is the total width of the Z°.

Since the background from the reaction $e^+e^- \to \gamma e^+e^-$ is severe due to the fact that the e^+e^- can be easily escape detection by going along the beam pipe, a hard kinematic cut for the photon is necessary. The event rate for the process $e^+e^- \to \gamma\nu\bar{\nu}$ hence is small.
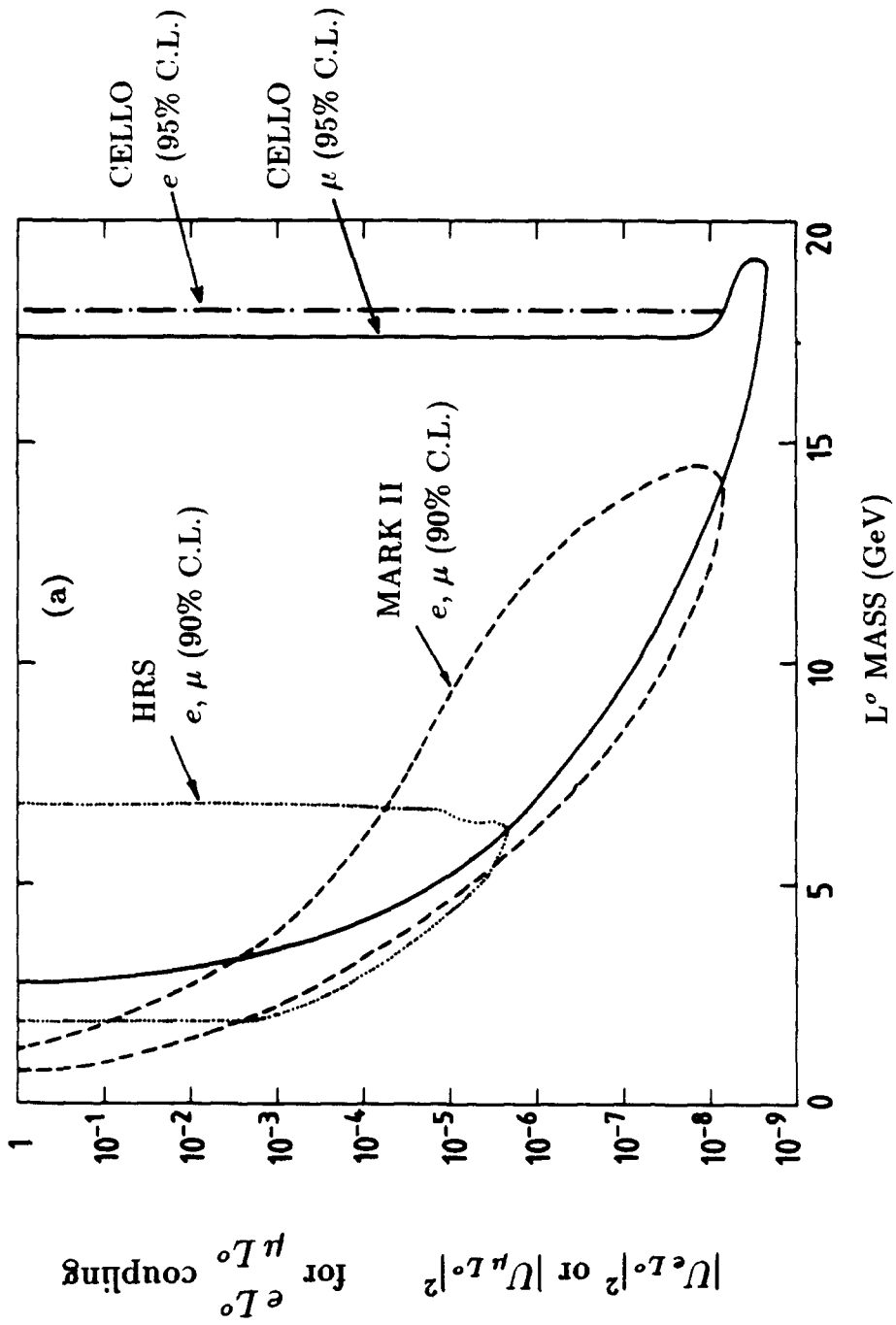
FIGURE 3.10(a)

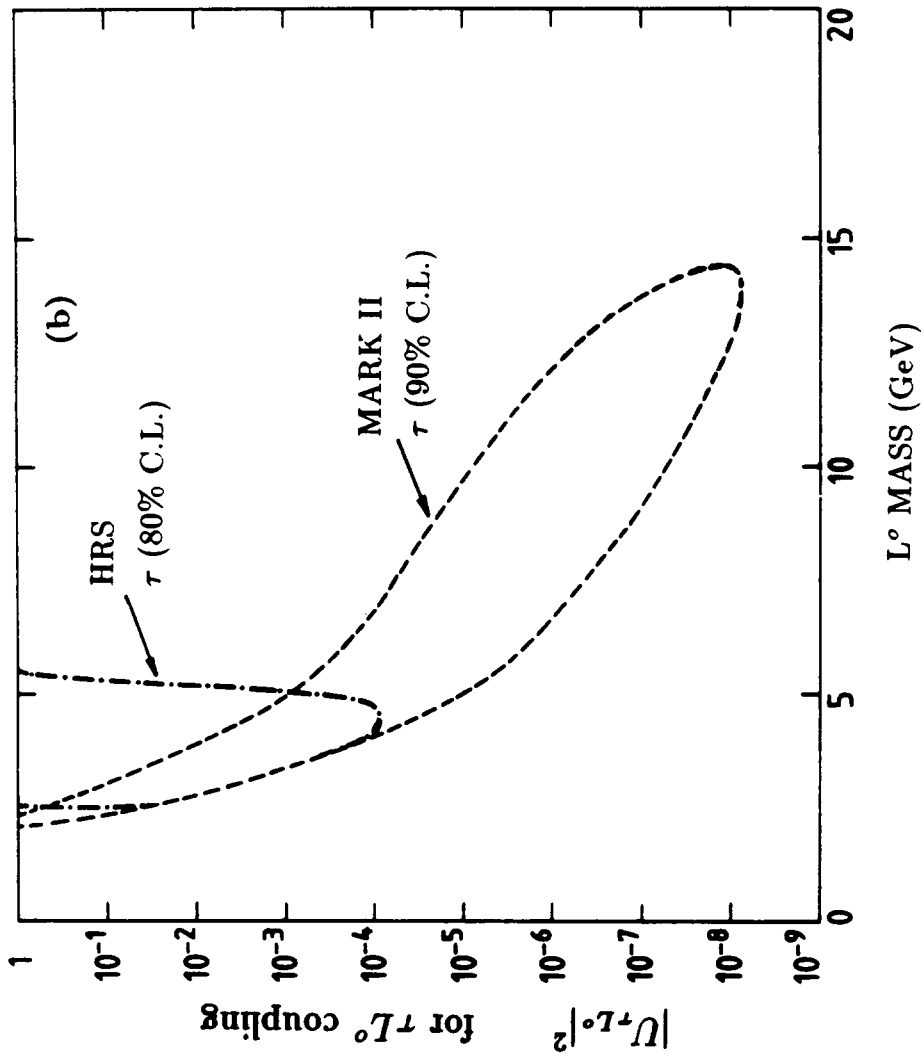Excluded regions of the mass of heavy neutral lepton L^o from PEP and PETRA. This L^o is assumed to mix predominately with ν_e or ν_μ.

FIGURE 3.10(b)

Excluded regions of the mass of heavy neutral lepton L^o from PEP and PETRA. This L^o is assumed to mix predominately with ν_τ.
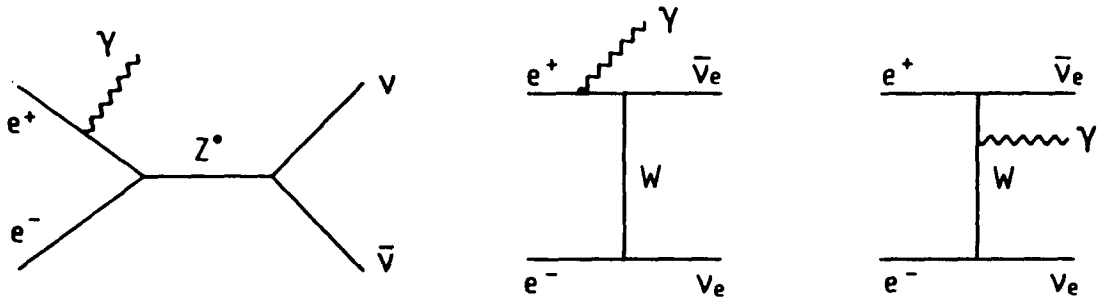
FIGURE 3.11

Feynman diagram for neutrino counting through $e^+e^- \to \gamma\nu\bar{\nu}$. The first diagram through annihilation into Z^o applies to all neutrinos, and the other two diagrams from W exchange apply only for electron neutrino.

The CELLO collaboration [3.41] uses the method described in Ref. [3.42] and with the statistical approach of Ref. [3.43], they combine the results with those obtained by ASP [3.44] and MAC [3.45] at PEP, and CELLO [3.41] and MARK J [3.46] at PETRA, as summarized in Table 3.1.

The expected single photon yield, calculated for each experiment is

$$N = \sum L_i \bar{\epsilon}_i \sigma_i$$

where L is the integrated luminosity, $\bar{\epsilon}$ is the averaged efficiency and σ is the cross section integrated over the search region. The product $L\bar{\epsilon}$ is also indicated in Table 3.1. With 4 events observed in the combined search, the following results are obtained [3.47]:

$$N_\nu < 4.5 \qquad \text{at } 90\% \ C.L.$$

$$N_\nu < 5.5 \qquad \text{at } 95\% \ C.L.$$

These results are comparable with those from the $p\bar{p}$ collider [3.6].

3.5 Search for Supersymmetric Particles

3.5.1 Introduction

Supersymmetry refers to the symmetry between bosons and fermions [3.48]. The study of supersymmetry has theoretical, but not experimental, motivation, and it is not possible to judge at present whether it will eventually be a useful concept in particle physics [3.49]. Nevertheless, it is interesting because it introduces a very large number of new particles.

Table 3.1

Single photon searches and their neutrino generation limits.

The expected yields are calculated for the three known neutrino species.

All limits are at 90% C.L.

Search	$\sqrt{s}$	Acceptance cuts	$L\bar{\epsilon}$	Expected yield $(N_\nu = 3)$	Observed yield	N_ν
MAC 1	29.0	$E_{\perp\gamma} > 4.5$ GeV $\theta_\gamma > 40°$	27	0.11	0	
MAC 2	29.0	$E_{\perp\gamma} > 2$ GeV $\theta_\gamma > 40°$	51.2	0.64	1	< 17
MAC 3	29.0	$E_{\perp\gamma} > 2.6$ GeV $\theta_\gamma > 40°$	42.7	0.40	0	
ASP	29.0	$E_{\perp\gamma} > 0.8$ GeV $\theta_\gamma > 20°$	70.15	$2.7 + 0.4$	2	< 7.5
CELLO 1	42.6	$E_{\perp\gamma} > 2.13$ GeV $\theta_\gamma > 34°$	14.8	0.63	0	< 10
CELLO 2	35.0	$E_{\perp\gamma} > 1.75$ GeV $\theta_\gamma > 34°$	37.0	1.01	1	
MARK J	39			0.39	0	< 26
Combined				6.28	4	< 4.5

<div align="center">

Table 3.2

List of Particles in $N = 1$ Supersymmetric Standard Model

</div>

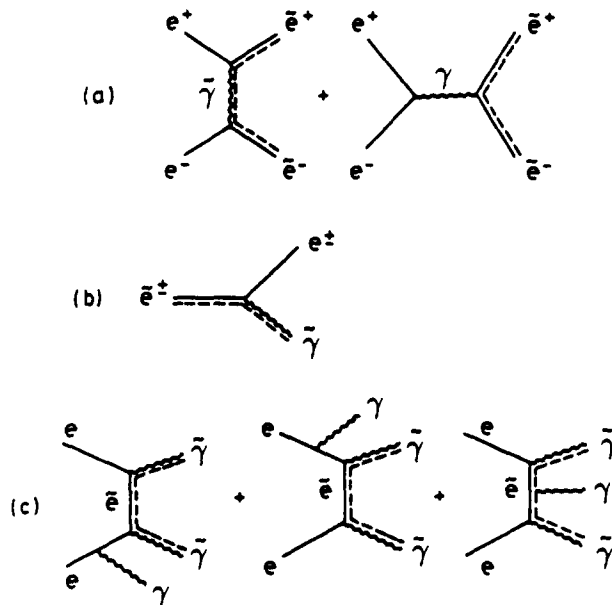| Spin 0	Spin $\frac{1}{2}$	Spin 1
scalar neutrino $\tilde{\nu}$	Goldstino $\tilde{G}$ photino $\tilde{\gamma}$ neutrino ν gluino $\tilde{g}$	photon γ gluon g
scalar leptons $\tilde{\ell}_R, \tilde{\ell}_L$ scalar quarks $\tilde{q}_R, \tilde{q}_L$	lepton ℓ quark q wino $\tilde{W}^\pm$ zino $\tilde{Z}^\circ$	charged intermediate boson $W^\pm$ neutral intermediate boson Z°
neutral Higgs H° charged Higgs $H^\pm$	neutral higgsino $\tilde{H}^\circ$ charged higgsino $\tilde{H}^\pm$	

FIGURE 3.12

Feynman diagrams for the production of the scalar electron (a) and stable photino (c) together with that for the decay of the scalar electron (b).

Hence we give an up-to-date summary of the recent results from a heroic effort at PEP and PETRA to search for supersymmetric particles.

In view of the success of the standard model [3.3], we shall, as a framework of discussion, use the supersymmetric version of the standard model [3.50, 3.51]. As already mentioned, in order for the supersymmetric version to be consistent, the standard model has to be modified to contain at least two Higgs doublets, leading to five physical Higgses, three neutral and two charged ones (H^+ and H^-). Their supersymmetric partners are called neutral and charged higgsinos. The resulting list of particles is shown in Table 3.2.

While the supersymmetric version of the standard model is not unique, especially concerning supersymmetry breaking, the particles listed in Table 3.2 are all present. The only possible exception is the Goldstino $\tilde{G}$. In most supersymmetry theories, there is an operator R such that all the usual particles are even under R while the supersymmetric partners are odd, with the consequence that the supersymmetric partner must be produced in pairs. We shall use an additional dotted line to indicate $R = -1$ particles. If this R-parity is exact, then the lightest particle with $R = -1$ is stable. It is not known which one of these supersymmetric particles is the lightest; some of the likely candidates are the Goldstino, the photino, and the scalar neutrino.

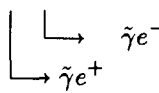### 3.5.2 Mass limits for scalar electrons $\tilde{e}^\pm$ and stable photinos $\tilde{\gamma}$

The best mass limits given by PEP and PETRA are those of the scalar electrons. The search [3.1] for scalar electrons $\tilde{e}$ and stable photinos $\tilde{\gamma}$ has been carried out by ASP [3.44], MAC [3.45] and MARK II [3.52] collaborations of PEP and CELLO [3.41], JADE [3.27], MARK J [3.46] and TASSO [3.53] collaborations of PETRA. The following processes have been used.

A. Pair production of stable $\tilde{e}^\pm$

$$e^+e^- \to \tilde{e}^+\tilde{e}^-$$

The signature is a collinear heavy muon-pair-like event.

B. Pair production of unstable $\tilde{e}^{\pm}$

$$e^+e^- \rightarrow \tilde{e}^{\pm} + \tilde{e}^-$$
$$\qquad\qquad \lfloor\; \xrightarrow{\;\;\;} \;\; \tilde{\gamma}e^-$$
$$\qquad\quad \lfloor\!\!\longrightarrow \tilde{\gamma}e^+$$

The diagrams for the production and decay are shown in Figure 3.12(a) and (b). The signature of such events is acoplanar e^+e^- pair with missing energies and momenta.

C. Radiative photino pair production

$$e^+e^- \rightarrow \gamma\tilde{\gamma}\tilde{\gamma}$$

The diagrams for this process are given in Figure 3.12(c). For stable photinos, the signature for this event is a single photon with nothing else.

The experimentally excluded region in the $m_{\tilde{e}} - m_{\tilde{\gamma}}$ plane is shown in Figure 3.13. If the photino mass is assumed to be small, the mass limits can be read off from Figure 3.13 by the intercept with the $m_{\tilde{e}}$-axis. The best result, 58 GeV at 90% confidence level, is obtained by ASP collaboration [3.44] using process C. In this figure it is assumed that the masses of the two scalar electrons are the same, i.e., $m_{\tilde{e}_R} = m_{\tilde{e}_L}$.

H. Jung of the CELLO collaboration [3.47] has carried out an analysis to combine the updated results of ASP, CELLO, MAC, and MARK J. The 95% C.L. combined limits for $\tilde{e}^{\pm}$ are

For $\quad m_{\tilde{e}_L} = m_{\tilde{e}_R}$ (mass degenerate case)

$\quad m_{\tilde{e}} > 64.5$ GeV $\qquad$ for $m_{\tilde{\gamma}} = 0$

$\quad m_{\tilde{e}} > 44.5$ GeV $\qquad$ for $m_{\tilde{\gamma}} = 10$ GeV

For $\quad m_{\tilde{e}_L} >> m_{\tilde{e}_R}$ (mass non $-$ degenerate case)

$\quad m_{\tilde{e}_R} > 52.7$ GeV $\qquad$ for $m_{\tilde{\gamma}} = 0$

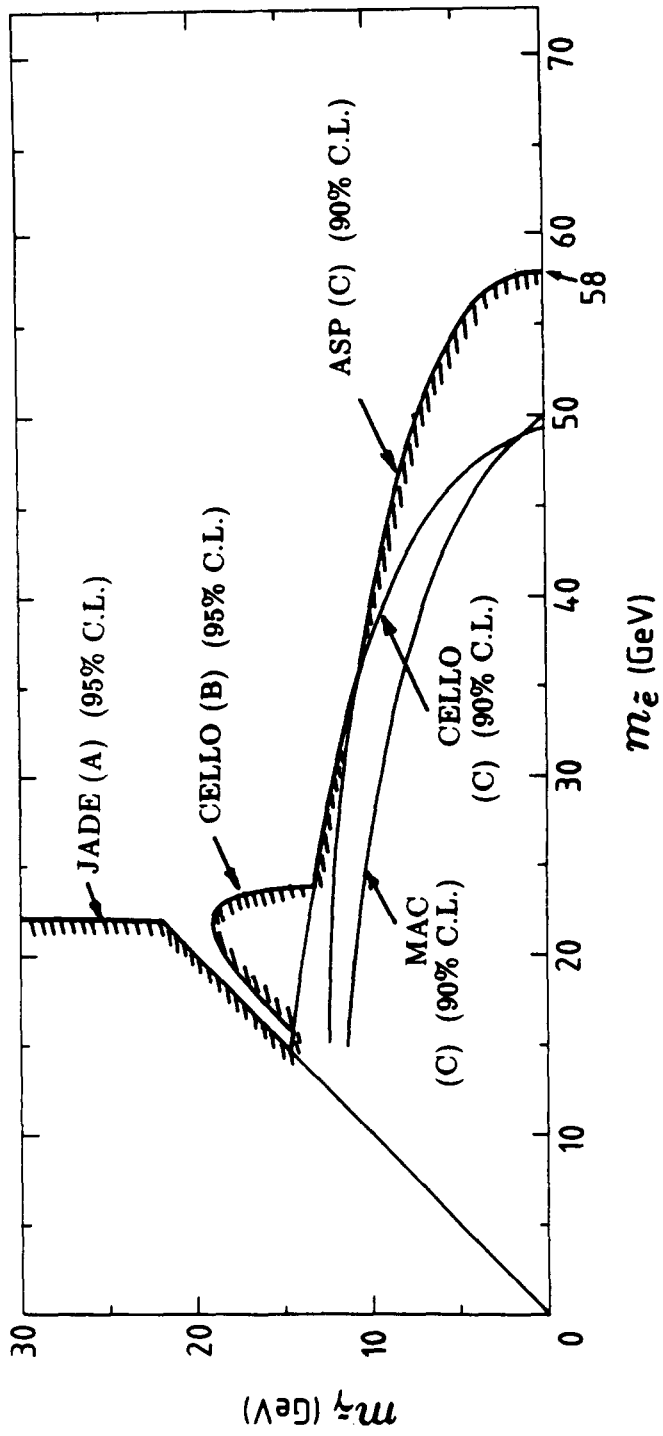$\quad m_{\tilde{e}_R} > 35.7$ GeV $\qquad$ for $m_{\tilde{\gamma}} = 10$ GeV

FIGURE 3.13
Excluded region in the $m_{\tilde{\gamma}} - m_{\tilde{e}}$ plane for stable photino.
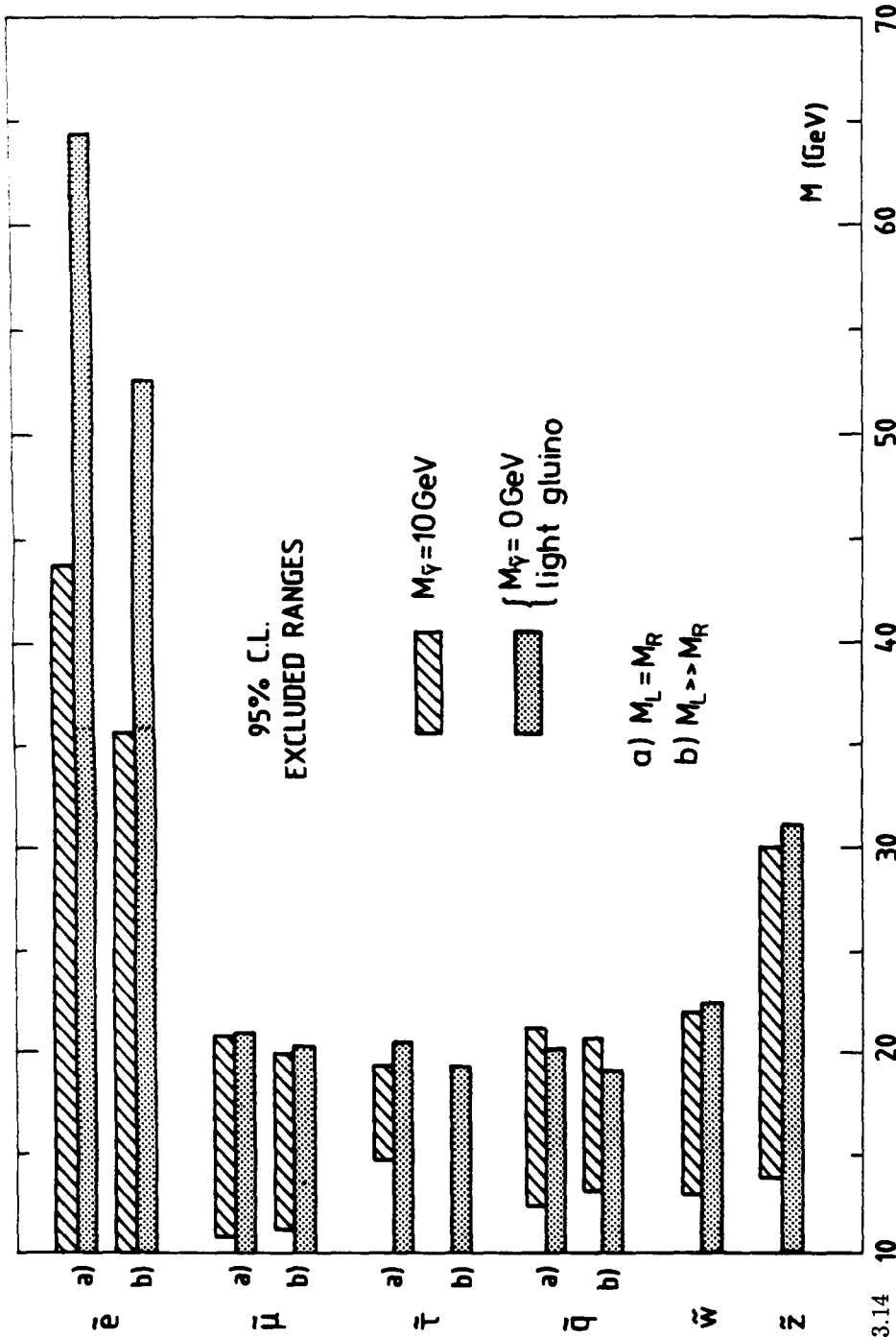
FIGURE 3.14

Updated version of supersymmetric particle mass domains excluded at 95% C.L., taking the photino to be the LSP and with two assumptions on the mass: $m_{\tilde{\gamma}} = 10$ GeV (and a heavy $\tilde{g}$), and for massless photinos (with a light $\tilde{g}$). The wino mass limits have been computed, in the case of massless photinos, for a leptonic branching ratio of 1/3. The zino mass limits have been computed for $m_{\tilde{e}_L} = m_{\tilde{e}_R} = 70$ GeV.

3.5.3 Mass limits for supersymmetric particles

CELLO collaboration [3.34] recently published their latest mass limits for the search of $\tilde{e}^\pm, \tilde{\mu}^\pm, \tilde{\tau}^\pm, \tilde{q}^\pm, \tilde{W}^\pm$ and $\tilde{Z}^o$. Figure 3.14 shows the best mass limits for these SUSY particles adapted from Figure 9.1 of the Ref. [3.34] modified with the latest results submitted to this conference. Not shown in this figure is the additional information that, for small scalar neutrino mass ($m_{\tilde{\nu}} \sim 0$), the combined results of ASP, CELLO, JADE and MARK J give $m_{\tilde{W}^\pm} > 62.5$ GeV at 90% C.L. [3.47].

3.6 Search for Monopole

The TASSO collaboration [3.54] presents limits on the production of magnetic monopoles [3.55] via the process

$$e^+e^- \to \gamma^* \to M\bar{M}$$

of masses up to 17 GeV and of magnetic charges between 5e and 70e. The method used is to consider the effect of the solenoidal field in an e^+e^- detector on the trajectory of monopoles. This method was previously used by the CLEO collaboration [3.56]. The solenoidal field will exert a Lorentz force on the particle causing it to accelerate in the direction parallel to the solenoid's axis and thereby appear curved in the detector's $(s-z)$ view. s is defined as the distance a track travels if projected onto the $r - \phi$ plane, the plane perpendicular to the beampipe and z is the direction of the positron beam.

The results from TASSO can be summarized, for magnetic charge $g < 50e$ and mass up to 14 GeV, as:

$$R = \frac{\sigma(e^+e^- \to M\bar{M})}{\sigma(e^+e^- \to \mu^+\mu^-)} < 10^{-3}$$

One word of caution is that the existence of magnetic monopole with charge smaller than the Dirac charge (Dirac charge: $g = \frac{137}{2}e$) would violate quantum mechanics [3.55].

Section 4   Measurements of the Average Bottom Hadron Lifetime

4.1   Introduction

The measurement of the B-hadron lifetime, τ_B, the lifetime of hadrons which contain a b-quark, provides constraints to the elements of the Kobayashi-Maskawa matrix [4.1]. The JADE collaboration [4.2] was the first one to give an upper limit for τ_B and MAC [4.3] and MARK II [4.4] were the first to obtain finite values of τ_B. Significant improvements on the measurements of the average Bottom hadron lifetime have been made since the report at the 1986 Berkeley Conference [4.5]. Table 4.1 summarizes all the updated B lifetime measurements from experiments at PEP and PETRA. The left column (marked "*New*") indicates the new results since the Berkeley Conference.

Three methods are used for selection of hadronic events to be used for the measurement of B lifetime: (i) No $b\bar{b}$ event enrichment, i.e., all hadronic events are used; (ii) select events with leptons with large transverse momentum with respect to the jet axis in order to enrich events containing $B, \bar{B}$ hadrons; (iii) select events with large boosted sphericity product [4.6], $S_1 \times S_2$, to enrich $b\bar{b}$ events.

Four quantities have been used to measure the average lifetime of B-hadron:

 (i) The impact parameter of the lepton

 (ii) The impact parameters of all charged particles

(iii) The dipole moment

(iv) The decay distance by vertex reconstruction.

The results from different experiments with different methods are listed in the last column of Table 4.1 with the statistical error as the first error and the systematic error as the second. In all cases, the sphericity or thrust axis is taken to be a good approximation to the direction of flight of the B-hadrons produced in the event. For all detectors with a solenoidal magnet, the resolution is much better in the plane perpendicular to the beam direction. Therefore, all measurements of impact parameters and decay distances are carried out in this plane.

Since the different methods of identifying B-decays cannot distinguish between the

various B-hadrons (B^o, B^+, Λ_b^o, etc.), the measurements are some average value of τ_B. However, different methods of B-hadron tagging may measure different averages.

4.2 Methods of $b\bar{b}$ Event Enrichment

There are basically two methods of $b\bar{b}$ event enrichment currently in use.

(a) Method of high transverse momentum lepton

The popular method of enriching $b\bar{b}$ events is to select events with at least one lepton (e or μ) with large transverse momentum ($P_\perp$) with respect to the sphericity or thrust axis of the overall event. Due to the large mass of the b-quark, leptons from semi-leptonic decay of B-hadrons carry large transverse momentum with respect to the B-hadron flight direction. Typical selection criteria is to require the leptons to have momentum $P > 2$ GeV/c and $P_\perp > 1$ GeV/c. For example, at a PEP center-of-mass energy of 29 GeV, MARK II attains a lepton purity of 65% from B-hadron decay [4.9]. Note that, without the high $P_\perp$ lepton selection, only about 1/11 of hadronic events are from $b\bar{b}$ events.

(b) Boosted sphericity product method [4.6]

Since the semi-leptonic decay branching ratio of the B-hadrons is only about $\frac{1}{4}$, it is desirable to have an alternative method that makes use of the non-leptonic decays. This second $b\bar{b}$ event enrichment scheme is based on the fact that since a b quark has a much higher mass than lighter quarks, the average transverse momenta with respect to the jet axis from these events should be correspondingly higher and therefore the $b\bar{b}$ events should be more spherical. Since this method depends on tagging events with high sphericities, it is desirable to remove the $q\bar{q}g$ three jet background. For example, the TASSO collaboration uses the Wu-Zobernig three jet finding algorithm [4.16] to eliminate them from the event sample. The events are then split into two hemispheres defined by the plane perpendicular to the sphericity or thrust axis and each jet is boosted in the direction of the rest frame of a b quark by using, for example, a β value of 0.74 by TASSO for $\sqrt{s} = 35$ GeV (the β value varies with $\sqrt{s}$ and is such that the separations of b-quark from c-quark events are optimized). Due to the fact that the produced b quark gives most of its momentum to the B-hadron, the purpose of the boost is to reduce the
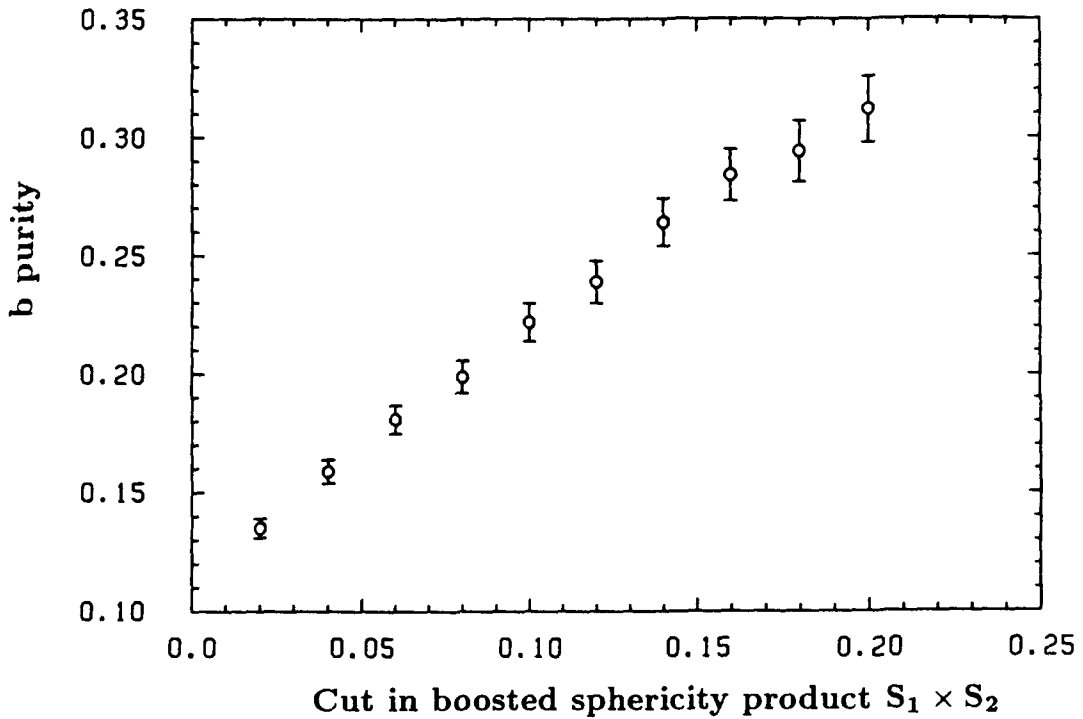
FIGURE 4.1

The method of boosted sphericity product. This plot shows the purity of b events as a function of the cut on the sphericity product $S_1 \times S_2$. The error bars show the statistical error from the Monte Carlo simulation.

momentum of the B-hadron so that the higher sphericity of the $b, \bar{b}$ jets is more clearly seen. The sphericity of each jet is then calculated in its boosted frame. The product of the two sphericities S_1 and S_2 of the jet 1 and jet 2 in their respective boosted frame is defined as the boosted sphericity product $S_1 \times S_2$. Figure 4.1 shows the purity of b events (purity = $b\bar{b}$ events/all events) obtained for different minimum cuts on $S_1 \times S_2$ as it has been calculated by the TASSO collaboration from Monte Carlo events [4.12]. A minimum of 0.18 for this variable has been chosen for the b enriched sample for a TASSO measurement of the B-hadron lifetime. $12.2 \pm 0.3\%$ of the data and $12.0 \pm 0.3\%$ of the Monte Carlo simulated events pass this cut, giving a b purity of $29.4 \pm 0.12\%$. In this case 35% of the $b\bar{b}$ events are kept.

It is clear from the above description that the first method gives higher purity while the second method retains a larger fraction of $b\bar{b}$ events. Therefore, from the same event sample, the method of high transverse momentum lepton gives a smaller systematic error while the boosted sphericity product method gives a smaller statistical error.
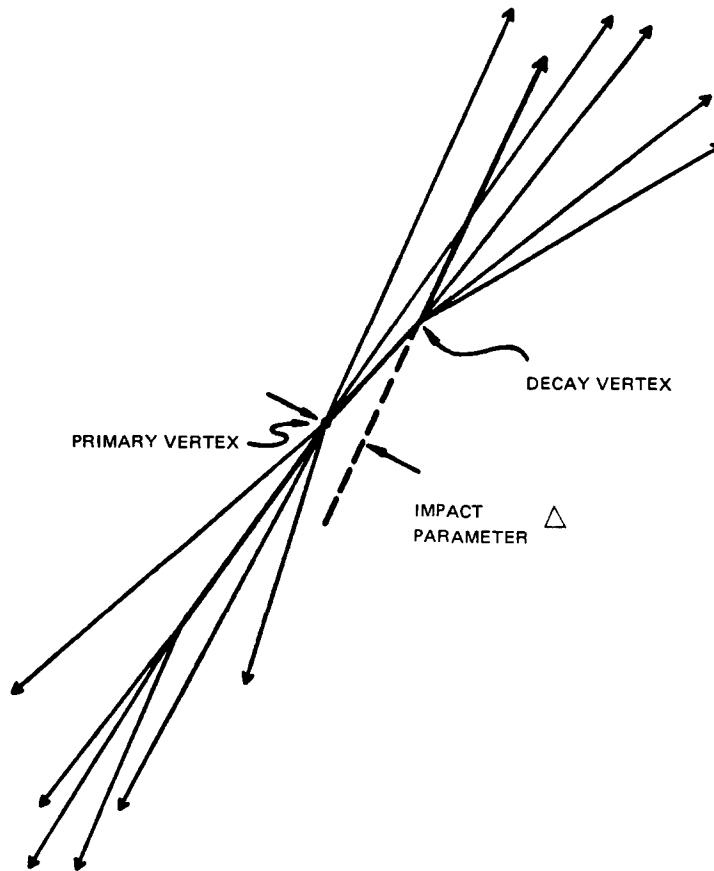
FIGURE 4.2

Definition of impact parameter: the impact parameter is signed positive when the intersection of the lepton direction and the thrust vector corresponds to a positive decay length.

4.3   Impact Parameter of the Lepton

In this and the following three sections, the four quantities listed in section 4.1 for measuring the average lifetime of B-hadrons are discussed.

JADE [4.7], DELCO [4.8], MARK II [4.9] and HRS [4.10] measure the impact parameters of the high $P_\perp$ leptons to determine the average B-hadron lifetime. Since the MARK II result is the most accurate, and is also not yet published, we concentrate here on their specific procedure.

The impact parameter of a lepton is defined as in Figure 4.2. The distance of the closest approach of a lepton from the primary interaction vertex is defined as the impact parameter of a lepton.

MARK II uses $\sim 200pb^{-1}$ of data, all after their vertex chamber was installed. This corresponds to 70000 hadronic events with a total of 4000 leptons with momentum greater than 2 GeV/c. They select events with high $P_\perp$ leptons to enrich $b\bar{b}$ events as described in section 4.2. Applying cuts of thrust > 0.75, $P_{e,\mu} > 2$ GeV/c and $P_{\perp\,e,\mu} > 1$ GeV/c, they find that 65% of the leptons selected come from B-hadron decays.

The following improvements have been made over the analysis made in 1984 which yielded a result [4.17] of $\tau_B = (0.85 \pm 0.17 \pm 0.21) \times 10^{-12}$ sec..

(i) Resolution studies: better understanding of the resolution function of the impact parameter enables MARK II to reduce both the statistical and systematic errors.

(ii) Inclusive leptons: an improved analysis of the leptons from B-decay with six times more statistics allows MARK II to determine the B-hadron semi-leptonic branching ratio and the b quark fragmentation function with better precision. This reduces the systematic errors of the B-hadron lifetime measurement.

(iii) Determination of production point: in order to improve the impact parameter resolution for tracks above an azimuthal angle of 45 degrees (ones that get a large error contribution from the beam size), MARK II uses a jet vertex technique to determine the primary production point on an event by event basis. They reconstruct a secondary vertex using all good tracks in a jet. This vertex is used to extrapolate back along the thrust axis into the beam spot as shown in Figure 4.3 to find the most likely production point using the decay length technique. The error in the thrust direction is accounted for. By determining the production point, the lepton impact parameter error is improved by about a factor of two.

Figure 4.4 shows the lepton impact parameter distribution of 634 leptons from MARK II. A maximum likelihood fit gives

$$\tau_B = (0.98 \pm 0.12 \pm 0.13) \times 10^{-12} \text{ sec.}$$

Figure 4.5 and 4.6 give the lepton impact parameter distributions from DELCO [4.8] and HRS [4.10] and their results of B-hadron lifetime measurements are given in Table 1.
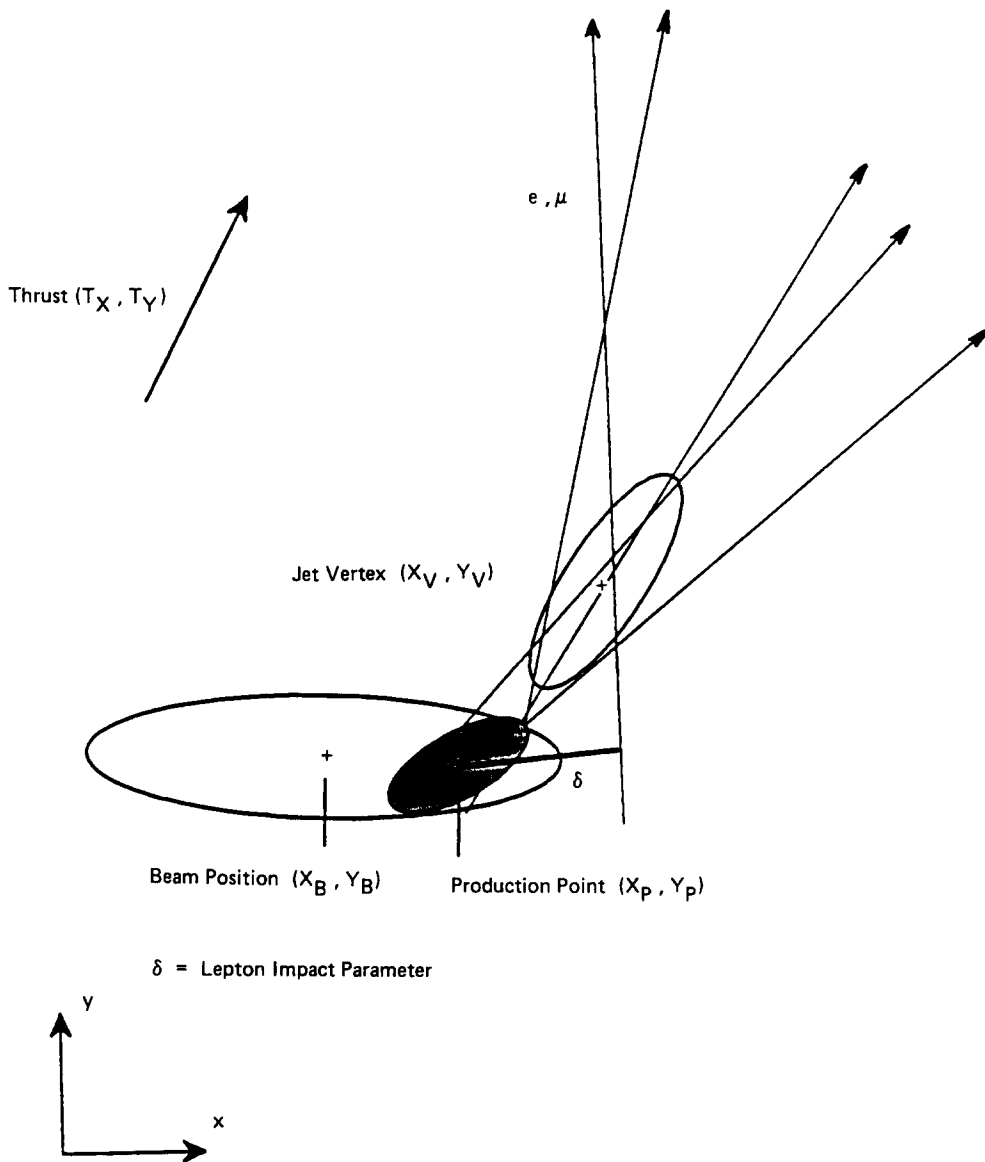
FIGURE 4.3

Extrapolation of the secondary jet vertex back along the thrust axis into the beam spot to find the production point using the decay length technique. This method is used by MARK II.
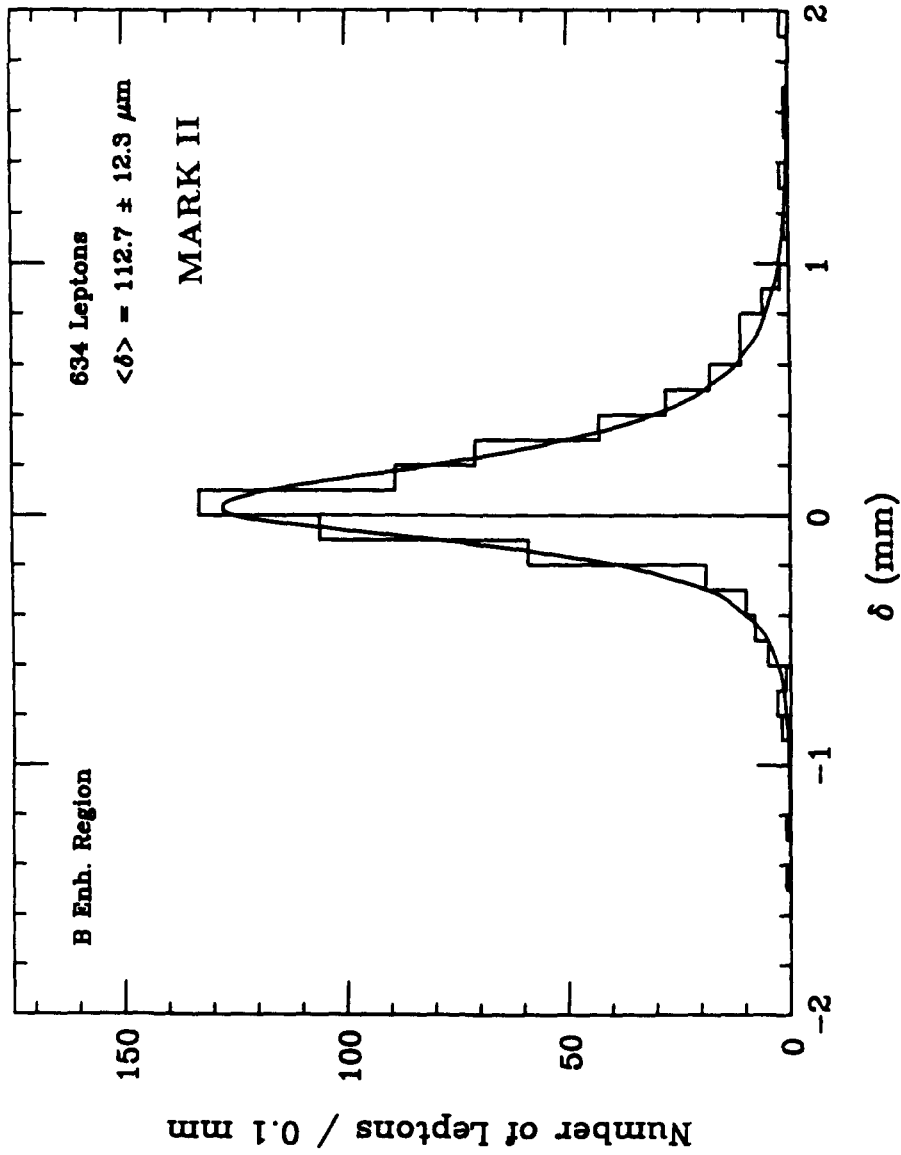
FIGURE 4.4

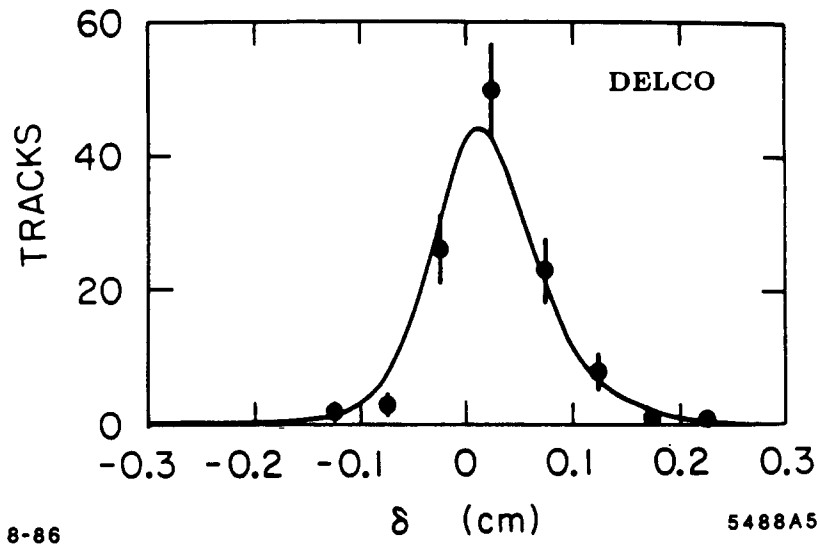Lepton impact parameter distribution from MARK II. The curve is the result of maximum likelihood fit.

FIGURE 4.5

Lepton impact parameter distribution from DELCO. The points are the data and the smooth curve is the expected distribution based on $\tau_B = 1.17 \times 10^{-12}$ sec.
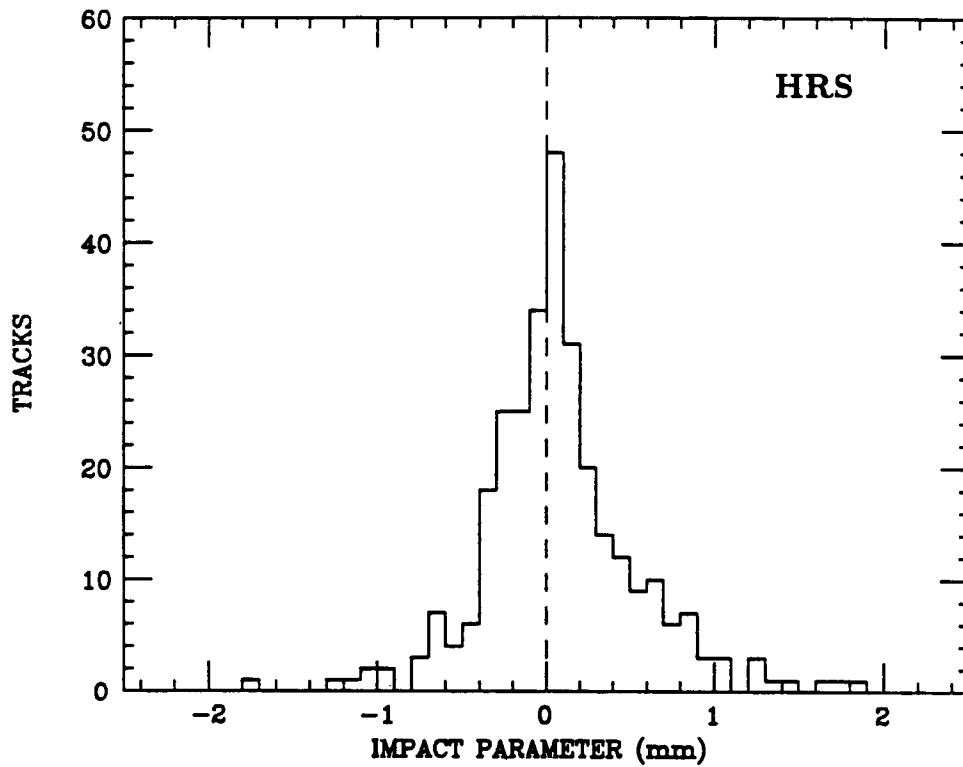

FIGURE 4.6

Lepton impact parameter distribution from HRS.

4.4　The Impact Parameters of All Charged Particles

MAC [4.11] and TASSO [4.12] determine the B-hadron lifetime from the impact parameter distributions of all charged particles in an event instead of only the lepton impact parameters. Since the B-hadron lifetime is obtained by comparison of distributions of data to Monte Carlo simulation, this method is more fragmentation model dependent.

MAC employs a $b\bar{b}$ event enrichment scheme by selecting events with high $P_\perp$ leptons. The impact parameter distributions of all charged particles are shown in Figure 4.7(a) and (b) for before and after the installation of their vertex detector. Since this measurement is published, no details will be given here. The result is [4.11]

$$\tau_B = (1.29 \pm 0.20 \pm 0.21) \times 10^{-12} \text{ sec.}$$

TASSO makes use of the boosted sphericity product, $S_1 \times S_2$, method as described in section 4.2 as a $b\bar{b}$ event enrichment scheme. TASSO starts with 32,000 events at a center-of-mass energy of 35 GeV taken with their precision vertex detector. After removing the three-jet event candidates, the B-hadron enriched data sample is obtained by selecting events with $S_1 \times S_2 > 0.18$. The signed impact parameters for all high quality tracks with momentum greater than 1 GeV/c are found. These tracks are weighted by their tracking errors determined by the track refitter described by Saxon [4.18]. Figure 4.8 shows the distribution of weighted impact parameters from data with the Monte Carlo distribution whose mean coincides with that from the data overlaid. The mean of this distribution from the data is $(86.8 \pm 6.2) \mu m$. A comparison of the mean of the distribution of the weighted impact parameters of the data to those from Monte Carlo simulations with different lifetimes resulted in a lifetime of

$$\tau_B = (1.52 \pm 0.18 \pm 0.24) \times 10^{-12} \text{ sec.}$$

The systematic error for this measurement mainly comes from the enrichment scheme and from the uncertainty in heavy quark fragmentation.
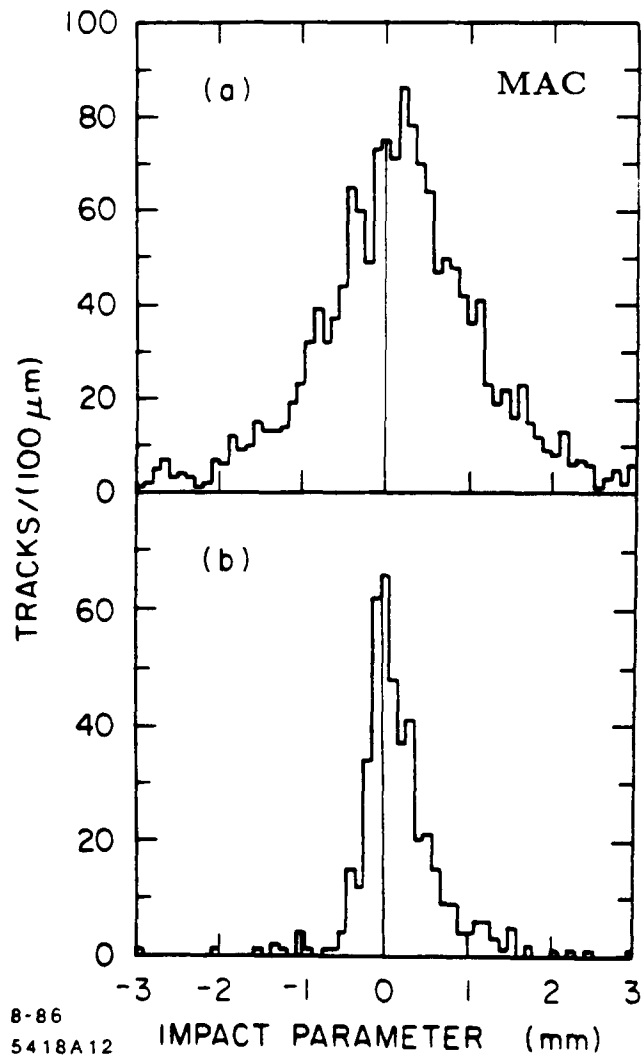
FIGURE 4.7

Charged particle impact parameter distribution from MAC (a) without and (b) with vertex chamber.
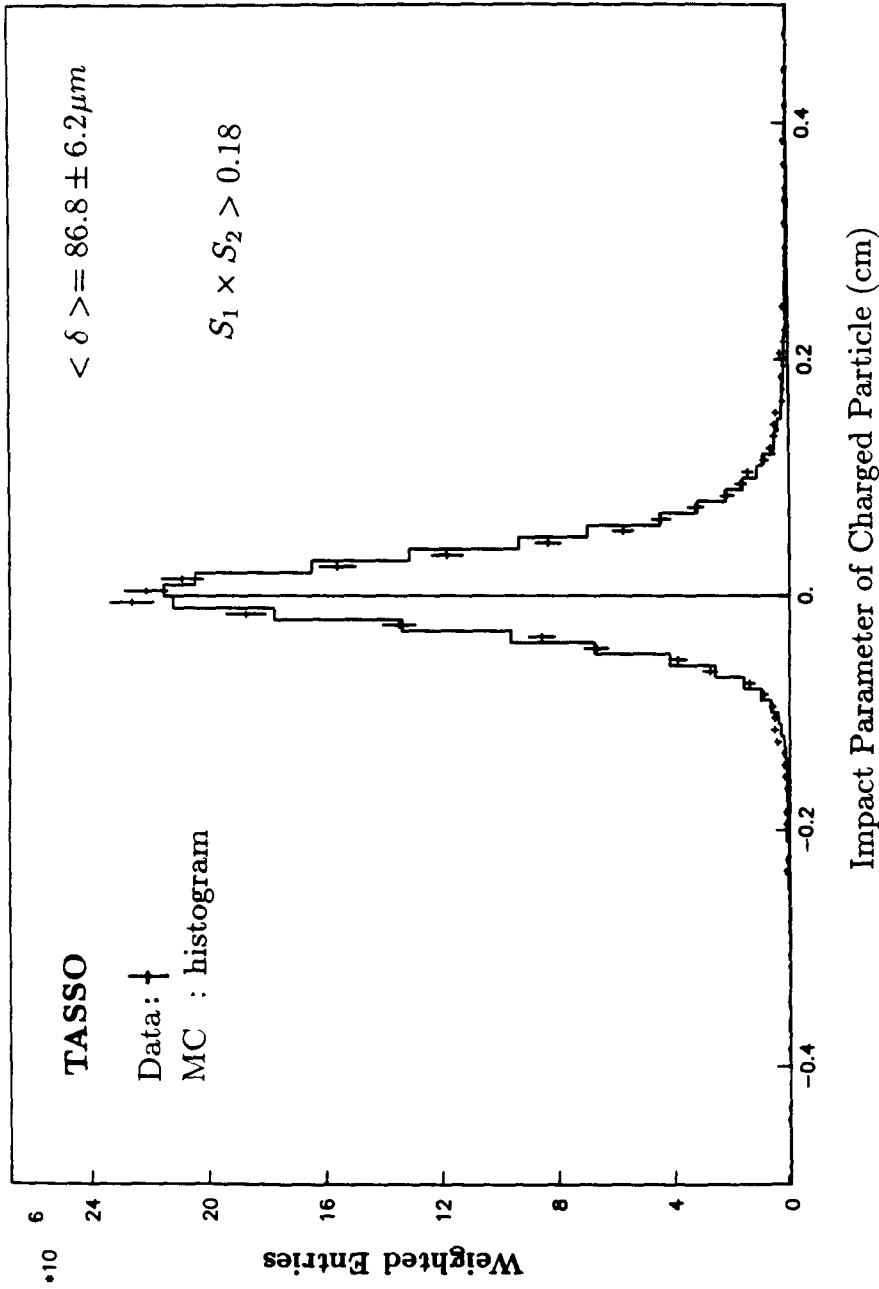
FIGURE 4.8

Weighted charged particle impact parameter distribution from TASSO. The data (†) are shown with error bars, and the Monte Carlo simulated distribution with the same mean is shown overlaid as the solid histogram.

4.5   Dipole Moment

The TASSO collaboration also uses a variable called the dipole moment, ρ, to estimate the decay distance of a B-hadron [4.13]. The definition of the dipole moment ρ is illustrated in Figure 4.9(a). In the plane perpendicular to the beam axis, a common vertex of all tracks for each of the two jets is calculated. For $b\bar{b}$ events these vertices will contain a majority of tracks from the B-hadron decays. To obtain ρ the distance between these 2 vertices is projected onto the sphericity axis, taken as an approximation for the B-hadron flight direction. Note that by this definition no reference to the beam spot is needed. The sign of ρ is defined in such a way that it is positive when the primary e^+e^- vertex lies between the two jet vertices with two B-hadrons flying from the primary vertex to their decay vertices. For each measured dipole moment ρ a weight is calculated from the error on the measured distance. In this error propagation not all tracks enter with the same weight; they are weighted by their rapidity. This additional weight enhances the contribution from tracks coming from first rank fragmentation particles as the B-hadrons are of that kind.

Figure 4.9(b) shows the distribution of the weighted dipole moments. The mean value of this distribution is $305\pm13\mu m$. In this analysis no b enrichment has been used. Comparison with Monte Carlo simulation with different B-hadron lifetime, this mean value of the dipole moment distribution yields

$$\tau_B = (1.37 \pm 0.14 \pm 0.32) \times 10^{-12} \text{ sec.}$$

The JADE collaboration uses a method similar to the method of the dipole moment. They obtain a pseudo decay length ℓ as follows [4.14]:

(i) Divide the event into two hemispheres by the normal to the sphericity axis of the event.

(ii) Determine a vertex (x_i, y_i) and its covariance $cov(x_i, y_i)$ for each hemisphere i, where $i = 1, 2$. The vertex 1 is assumed to be precisely known and the error of the other scaled accordingly $cov(x, y) = cov(x_1, y_1) + cov(x_2, x_2)$.

(iii) The sphericity axis is shifted so that it passes through vertex 1. A pseudo decay length ℓ with error σ_ℓ is calculated by minimizing the following χ^2-function

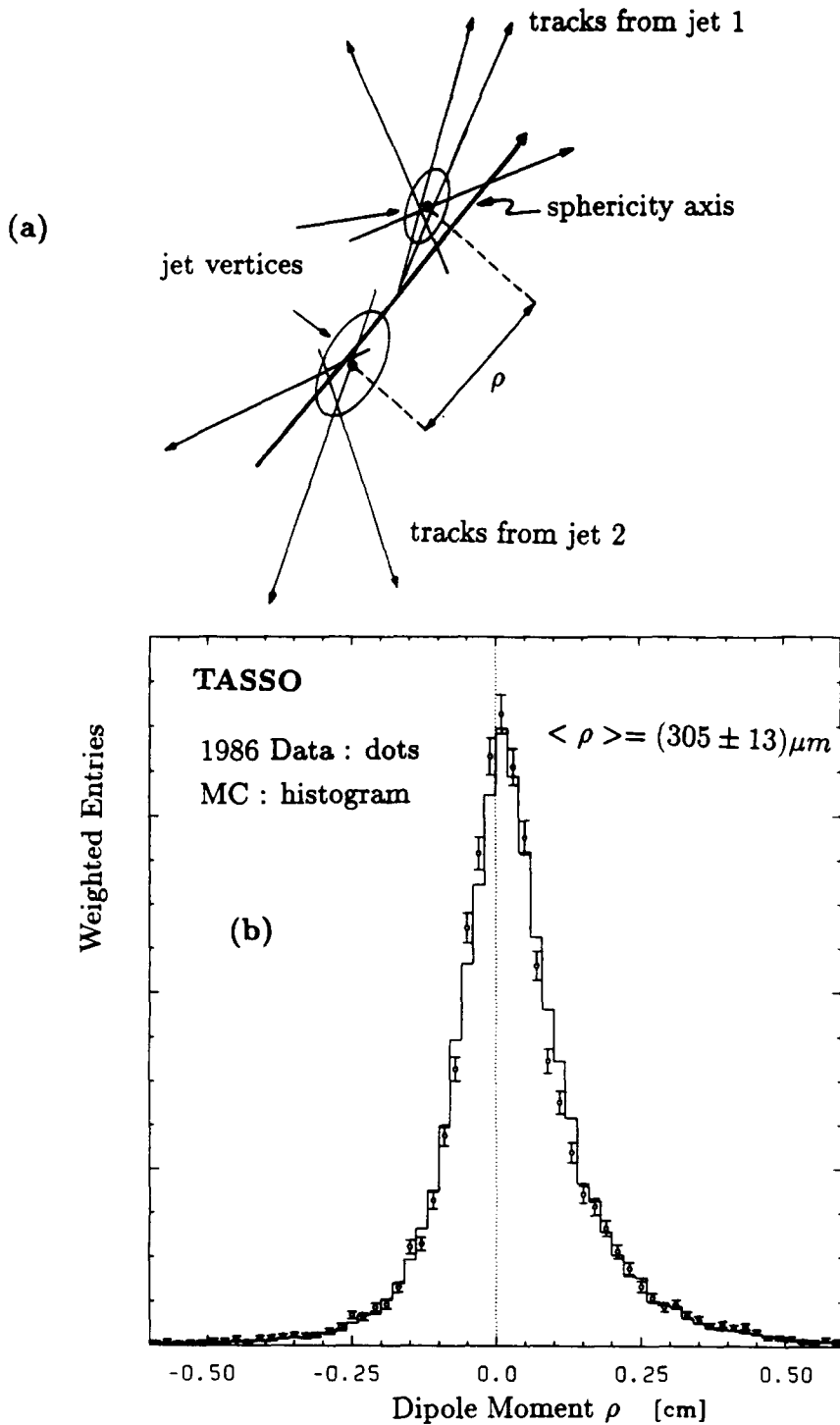$$\chi^2 = \vec{\Delta}\, cov^{-1}(x, y)\vec{\Delta}^T$$

FIGURE 4.9

(a) The definition of the dipole moment ρ. (b) TASSO distribution (ϕ) of the weighted dipole moments. The solid histogram is a Monte Carlo simulated distribution with the same mean.

where $\vec{\Delta}$ is defined in Figure 4.10(a).

The analysis of JADE is based on a data sample of 3170 multihadronic events at an average center-of-mass energy of 41.7 GeV and 11941 events at 35 GeV. These data have been accumulated after the installation of an additional small jet chamber as the vertex detector.

The distribution of the pseudo decay distance ℓ is separated into a signal and a background distribution by means of the weighting technique described in Ref. [4.19]. The discriminating quantity is the product of the boosted sphericities $S_1 \times S_2$ as described in section 4.2.

The trimmed mean $<\ell>$ of the distribution of the weighted pseudo decay distances is used to estimate τ_B. Monte Carlo simulations with different τ_B are used to "calibrate" $<\ell>$ versus τ_B. Figure 4.10(b) shows the distribution of ℓ for the $b\bar{b}$ enriched data sample together with the Monte Carlo simulation of $\tau_B = 1.5$ps. The distribution of the data yields $<\ell> = 1.008 \pm 0.080$mm. This gives

$$\tau_B = (1.46 \pm 0.19 \pm 0.30) \times 10^{-12} \text{ sec.}$$

4.6 Decay Distance by Vertex Reconstruction

Although B-hadrons have not been reconstructed at PEP and PETRA, TASSO attempts to reconstruct the decay vertices from B-hadrons [4.15]. Again, TASSO starts with 32,000 hadronic events at a center-of-mass energy of 35 GeV with their precision vertex detector installed. The selected tracks in an event are divided into two jets using the plane perpendicular to the sphericity axis. In each jet vertices are fitted in the plane perpendicular to the beam axis for all combinations of 3 tracks with momentum greater than 0.6 GeV and not all with the same charge. The tracks are then refitted with the addition of a constraint that they come from a common vertex [4.18] and the combination with the best vertex fit is selected. This procedure selects vertices near the B-hadron decay point in $b\bar{b}$ events, but near the primary interaction point in lighter quark events. Approximately 12% of the vertices found are in b quark jets.

Similar to the event-by-event vertex reconstruction of MARK II as described in section 4.3, the most likely decay distance to the event vertex (beam position) as shown
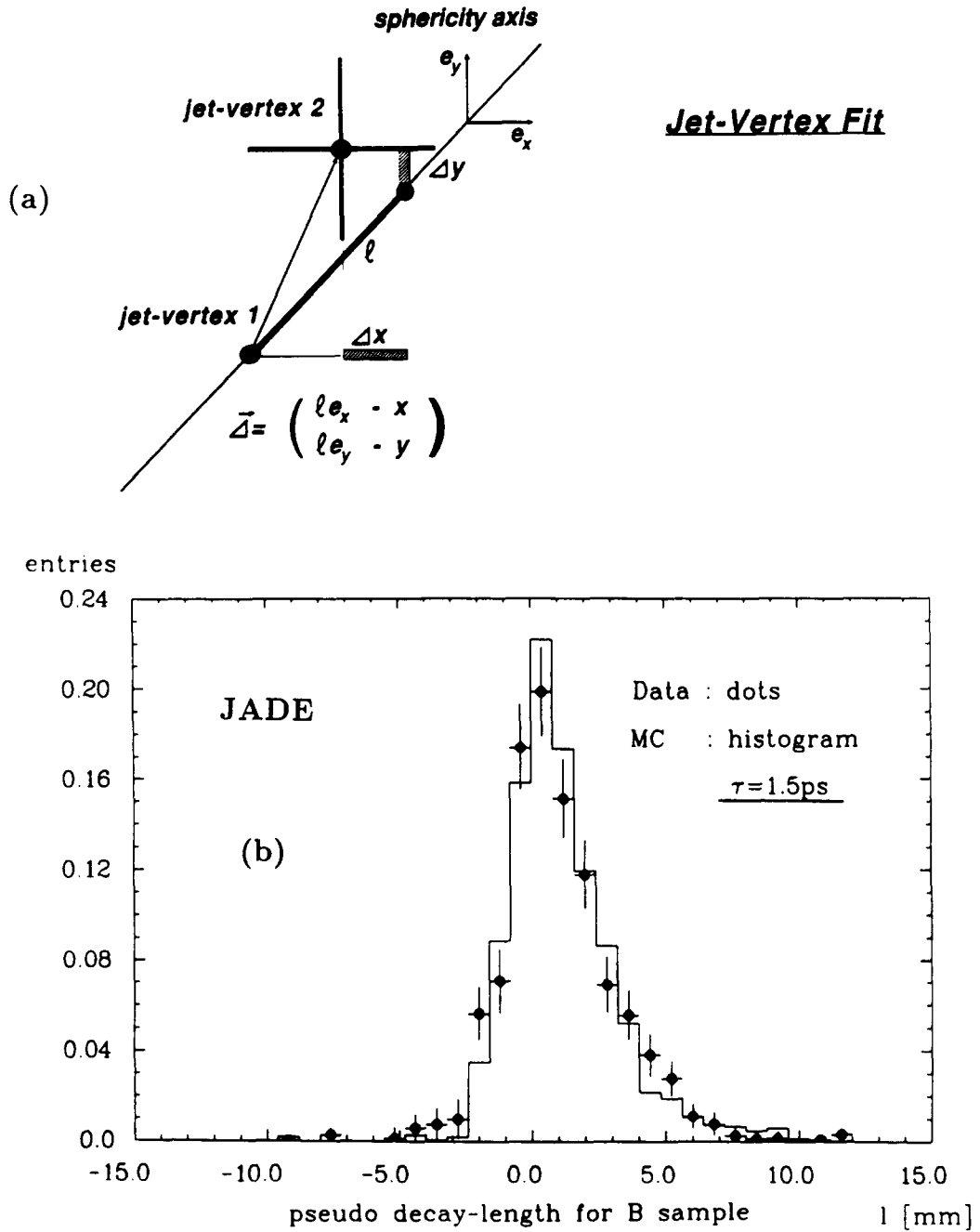
(a)

Jet-Vertex Fit

sphericity axis

e_y

e_x

jet-vertex 2

Δy

ℓ

jet-vertex 1

Δx

$$\vec{\Delta} = \begin{pmatrix} \ell e_x - x \\ \ell e_y - y \end{pmatrix}$$

entries

JADE

(b)

Data : dots

MC : histogram

$\tau = 1.5\text{ps}$

pseudo decay-length for B sample

l [mm]

FIGURE 4.10

(a) The definition of the pseudo decay length. (b) JADE distribution (♦) of the pseudo decay length. The solid histogram is a Monte Carlo simulated distribution with $\tau_B = 1.5 \times 10^{-12}$ sec.

in Figure 4.11(a) is computed in the plane perpendicular to the beam according to the formula

$$\ell_{2D} = \frac{x\sigma_{yy}\cos\,\phi + y\sigma_{xx}(x\,\sin\,\phi - y\,\cos\,\phi)}{\sigma_{yy}\,\cos^2\,\phi + \sigma_{xx}\sin^2\,\phi - 2\sigma_{xy}\sin\,\phi\,\cos\,\phi}$$

where (x, y) is the position of the decay vertex with respect to the beam position, σ is the sum of the decay vertex and beam position error matrices, and ϕ is the azimuth of the sphericity axis. Entries are weighted by the longitudinal component of the vertex error matrix to reduce the dependence on the fragmentation and decay models. The histogram of these decay distances is compared to a Monte Carlo simulated distribution bin by bin. The chi squared of this comparison is minimized with respect to the B lifetime assumed in the Monte Carlo simulation. Figure 4.11(b) shows the distribution of decay distances of the 15,364 vertices with the Monte Carlo simulated distribution giving the best fit overlaid. Agreement between the two curves is very good, particularly in the negative side of the distribution which demonstrates a good understanding of the detector resolution. The result of the bin by bin fit gives, using no B enrichment scheme,

$$\tau_B = (1.39 \pm 0.10 \pm 0.25) \times 10^{-12} \text{ sec.}$$

Using the B enrichment scheme of requiring the boosted sphericity product $S_1 \times S_2 >$ 0.18 as described in section 4.2, TASSO obtains the distribution of decay distances of 2075 vertices as shown in Figure 4.12. The result of the bin by bin fit gives

$$\tau_B = (1.35 \pm 0.16 \pm 0.27) \times 10^{-12} \text{ sec.}$$

It is interesting to compare the measurement in this section with that of the dipole moment in the preceding section. One of the major differences is that, while only one of the two B-decay vertices of the $b\bar{b}$ event is reconstructed here, both must be reconstructed in the measurement of the dipole moment. Consequently, in obtaining the dipole moment, either the number of usable events is quite small or tracks of relatively low quality must be accepted. This is the reason why the errors are larger when the dipole moment is measured (see Table 4.1).
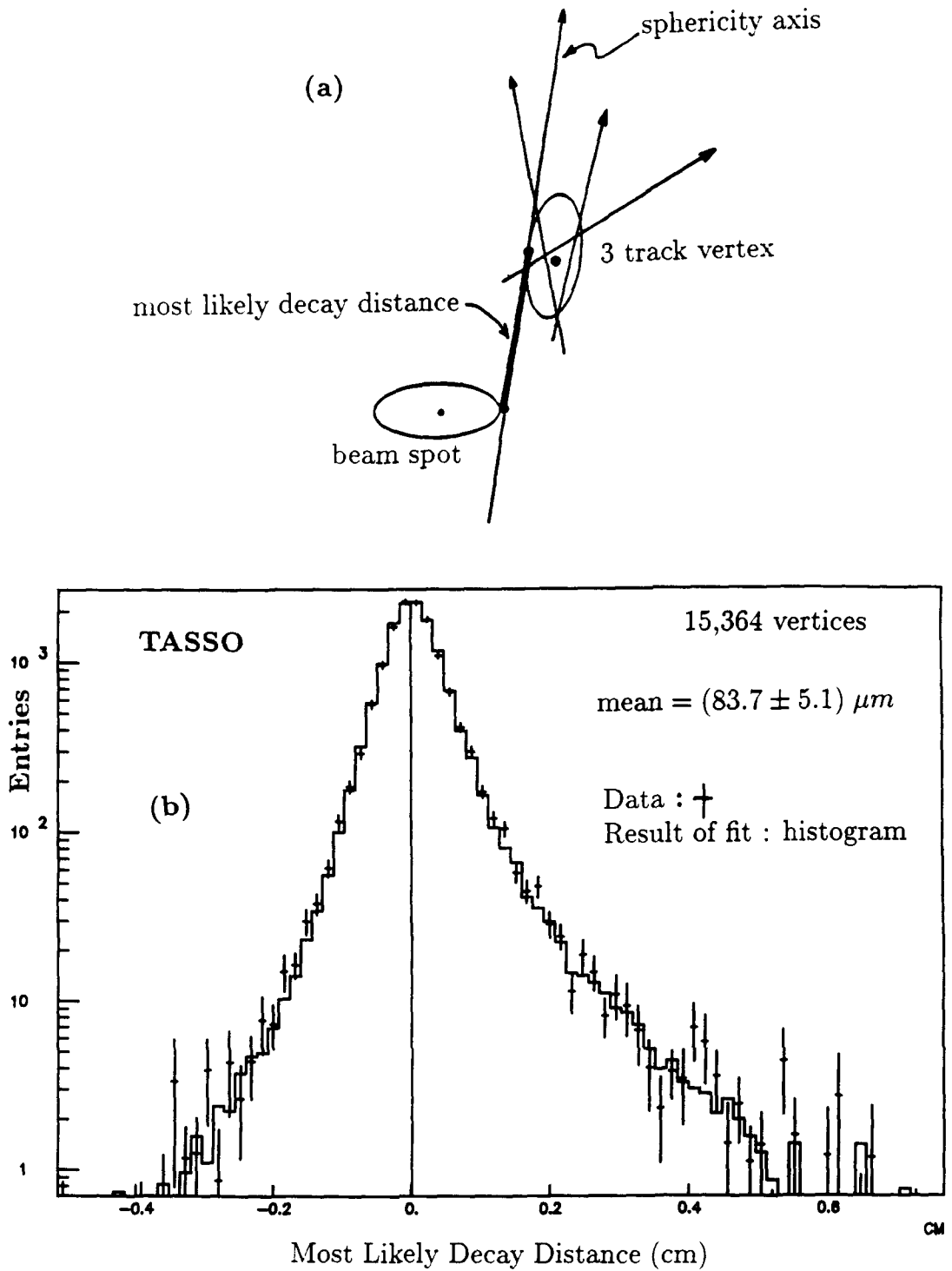
(a)

FIGURE 4.11

(a) The definition of the most likely decay distance. (b) TASSO distribution (✛) of the most likely decay distance. The solid histogram is the Monte Carlo simulated distribution giving the best fit.
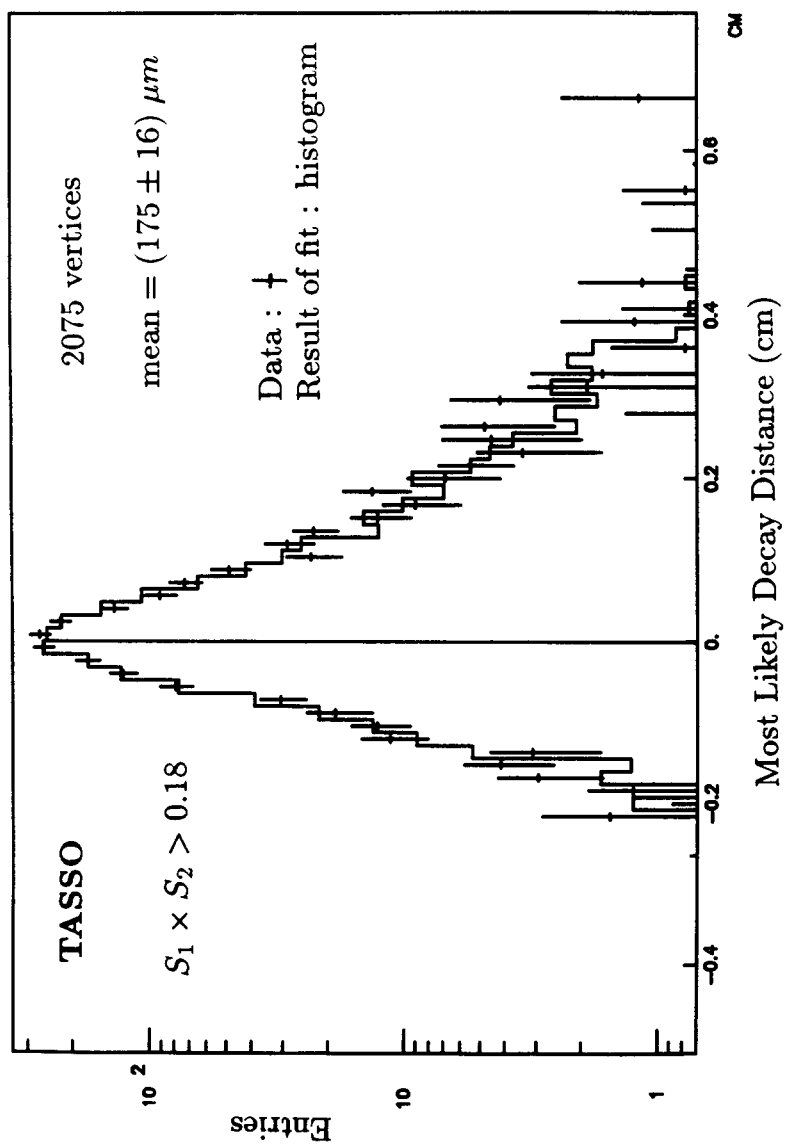
FIGURE 4.12
Same as Fig. 4.11(b) with B enrichment using boosted sphericity product $S_1 \times S_2 > 0.18$.

Table 4.1

	Experiment	$B\bar{B}$ event Enrichment	Quantity Measured	τ_B 10^{-12} sec
	JADE [4.7]	High $p_\perp$ lepton	Lepton Impact Parameter	$1.8^{+0.5}_{-0.4} \pm 0.4$
	DELCO [4.8]	High $p_\perp$ lepton	Lepton Impact Parameter	$1.17^{+0.27}_{-0.22} {\,}^{+0.17}_{-0.16}$
New	MARK II [4.9]	High $p_\perp$ lepton	Lepton Impact Parameter	$0.98 \pm 0.12 \pm 0.13$
New	HRS [4.10]	High $p_\perp$ lepton	Lepton Impact Parameter	$1.02^{+0.41}_{-0.37}$
	MAC [4.11]	High $p_\perp$ lepton	Impact Parameters of all Charged Particles	$1.29 \pm 0.20 \pm 0.21$
New	TASSO [4.12]	$S_1 \times S_2$ Boosted sphericity product	Impact Parameters of all Charged Particles	$1.52 \pm 0.18 \pm 0.24$
New	TASSO [4.13]	None	Dipole Moment	$1.37 \pm 0.14 \pm 0.32$
New	JADE [4.14]	$S_1 \times S_2$ Boosted sphericity product	Dipole Moment (pseudo decay length)	$1.46 \pm 0.19 \pm 0.30$
New	TASSO [4.15]	None	Decay Distance by Vertex Reconstr.	$1.39 \pm 0.10 \pm 0.25$
New	TASSO [4.15]	$S_1 \times S_2$ Boosted sphericity product	Decay Distance by Vertex Reconstr.	$1.35 \pm 0.16 \pm 0.27$

New = New since Berkeley Conference 1986

4.7   World Average of the B-Hadron Lifetime

It remains to find an average value of the B-hadron lifetime measurements given in Table 4.1. First, as already mentioned in section 4.1, it is by no means clear that the same quantity is measured in the various experiments, i.e., the average B-hadron lifetimes in the various experiments may refer to different averages. However, it is not known how one can derive any quantitative result from this observation. Therefore, the errors to be given in this section do not reflect these possible different averages.

Secondly, the four TASSO measurements given in Table 4.1 are based on the same data sample and thus are in no way independent. Therefore we take the value with the smallest error i.e. $\tau_B = (1.39 \pm 0.10 \pm 0.25) \times 10^{-12}$ sec. The other three measurements are taken as supporting evidence but are not included in calculating the average. After this deletion, the average B-hadron lifetime is found to be

$$\tau_B = (1.19 \pm 0.11) \times 10^{-12} \text{ sec.}$$

where the different measurements are assumed to be independent and the statistical errors and systematic errors are combined in quadrature.

This new result $\tau_B = (1.19 \pm 0.11) \times 10^{-12}$ sec. is to be compared with $\tau_B = (1.16^{+0.16}_{-0.15}) \times 10^{-12}$ sec. as reported a year ago at the Berkeley Conference [4.5] with again, all errors were added in quadrature. It is clear that more precise measurements are given at this conference.

The question to be asked: are the systematic errors for all the measurements independent? Close examination indicates that errors from uncertainty in b quark fragmentation and b fraction in data sample can be in common for all experiments due to the fact that the same B-decay model and the same b fragmentation scheme are used in the Lund Monte Carlo generator.

To estimate the error of the world average taking into account errors which could be common to all measurements, I propose to do the following:

(i) Assume $\sigma\% =$ error in % of τ_B common to all experiments.

   Take this error out from the systematic error from each experiment.

(ii) Calculate the world average of the B-hadron lifetime using the remaining errors.

(iii) Put back $\sigma\%$ into the final error in quadrature.

For the choice of the value of $\sigma\%$, we observe that, for the MARK II measurement, 8.5% of τ_B is attributed to the systematic error which is due to uncertainty in b fragmentation and b fraction. For other experiments, it is about 8% to 10%. In Figure 4.13 the world average τ_B is plotted as a function of the value of $\sigma\%$. Note that τ_B changes very slowly as $\sigma\%$ changes. Hence using $\sigma\% = 8.5\%$ we obtain

$$\tau_B = (1.18 \pm 0.14) \times 10^{-12} \text{ sec.}$$

as the best estimate of the world average of the B-hadron lifetime. Figure 4.14 gives graphically all the results listed in Table 4.1. The vertical line indicates the world average of $\tau_B = 1.18 \times 10^{-12}$ sec.

4.8 Update of the K-M Matrix Elements Involving the b Quark

The knowledge of τ_B clearly implies information about the Kobayashi-Maskawa matrix elements V_{ub} and V_{cb}. Following a recent review [4.20], the relation is

$$|V_{ub}|^2 + 0.48\,|V_{cb}|^2 = B_{SL}/(\tau_B\,\Gamma_o) = (0.90 \pm 0.24) \times 10^{-3}$$

where B_{SL} = semi-leptonic branching ratio of the B-hadron

$$= (11.4 \pm 0.5)\%$$
$$\tau_B = (1.18 \pm 0.14) \times 10^{-12} \text{ sec.}$$
$$\Gamma_o = G_F^2\,m_b^5/(192\pi^3) = 1/(0.92 \times 10^{-14} \text{ sec.})$$
$$m_b = (5.0 \pm 0.25) \text{ GeV/c}^2$$

The width of the elliptical band in $|V_{ub}|, |V_{cb}|$ plane given by τ_B as shown in Figure 4.15 is dominated by the uncertainty in m_b. Since m_b enters in Γ_o to the 5th power, the error in τ_B does not dictate the error in V_{cb} as much as the uncertainty in m_b.

Also shown in Figure 4.15 are the bounds

$$0.19 > |V_{ub}/V_{cb}| > 0.07.$$

The upper bound of 0.19 is the updated result from the CLEO collaboration [4.21]; it has been obtained using the model of Grinstein et al., [4.22] (the upper bound is 0.09 if the
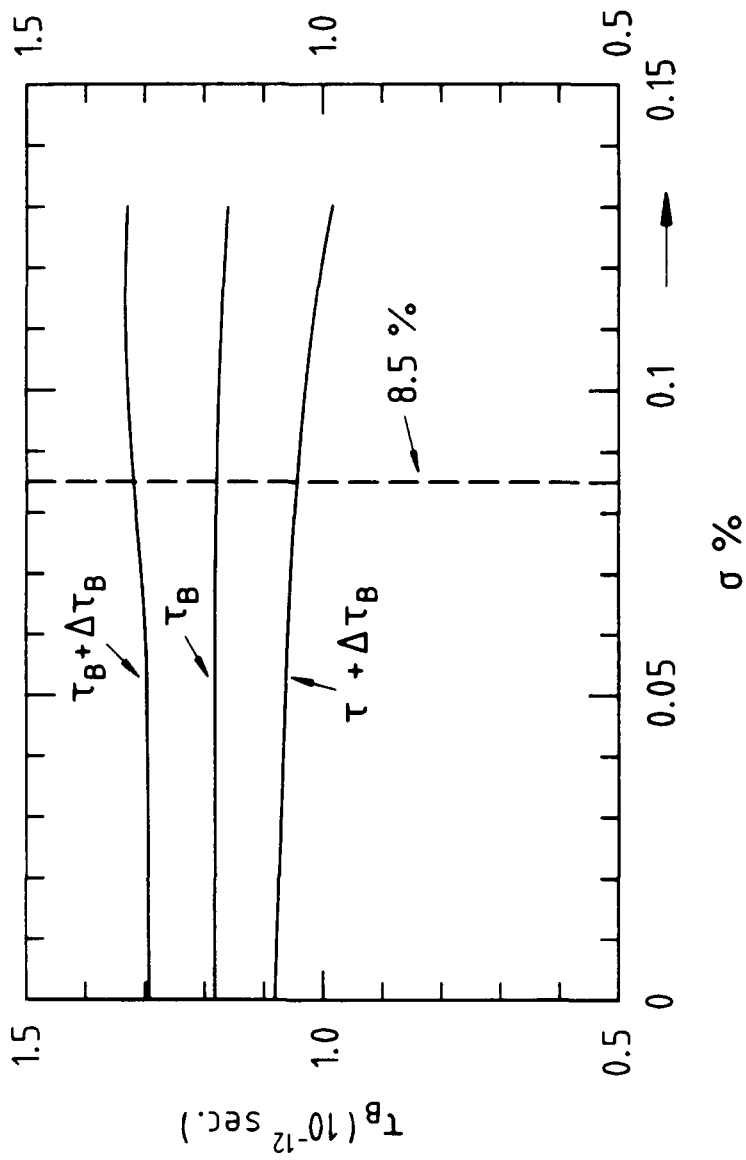
FIGURE 4.13

The world average τ_B as a function of the systematic error $\sigma\%$, which is common to all experiments. This $\sigma\%$ is due to uncertainty in b fragmentation and b fraction.
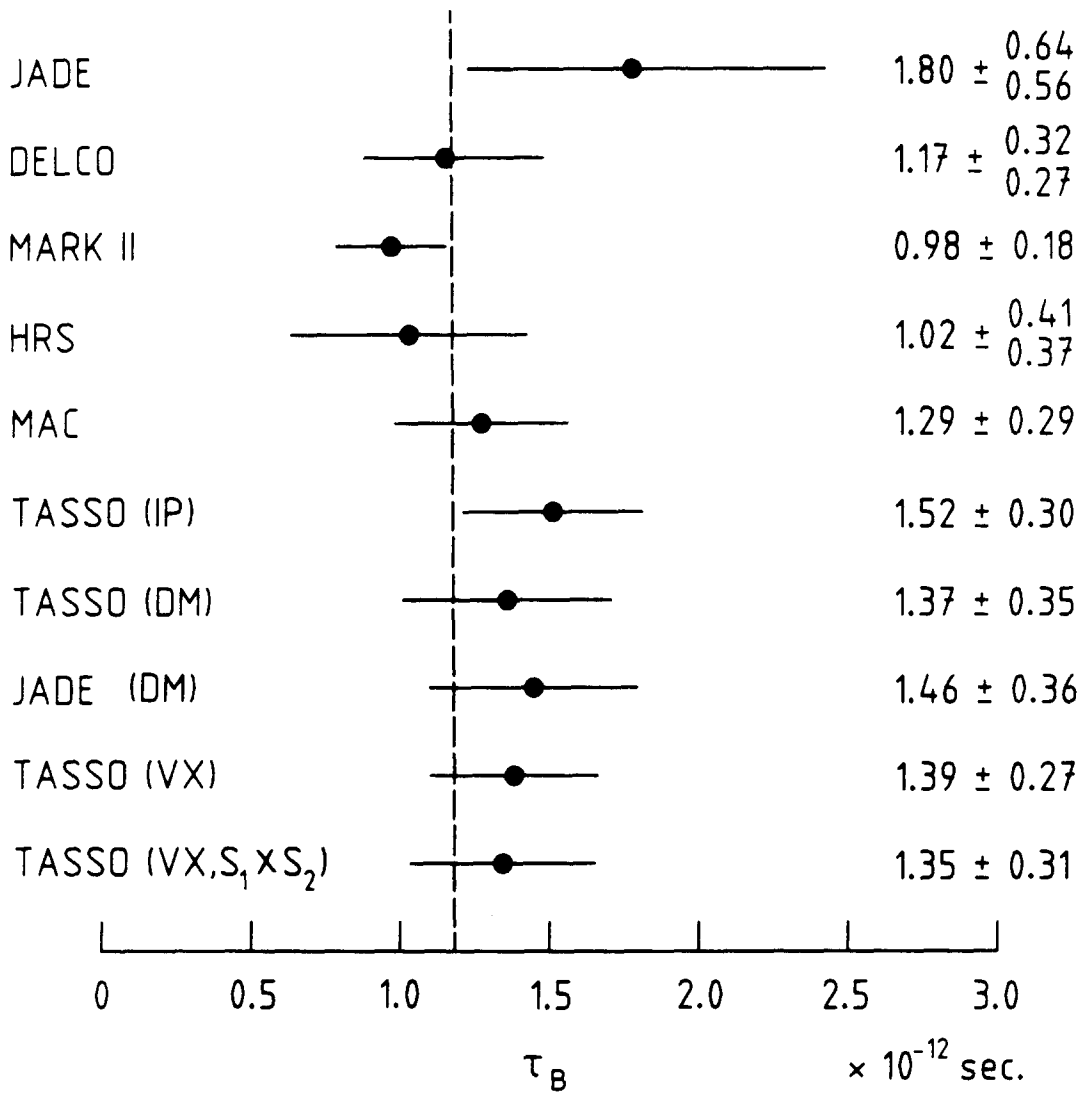
FIGURE 4.14

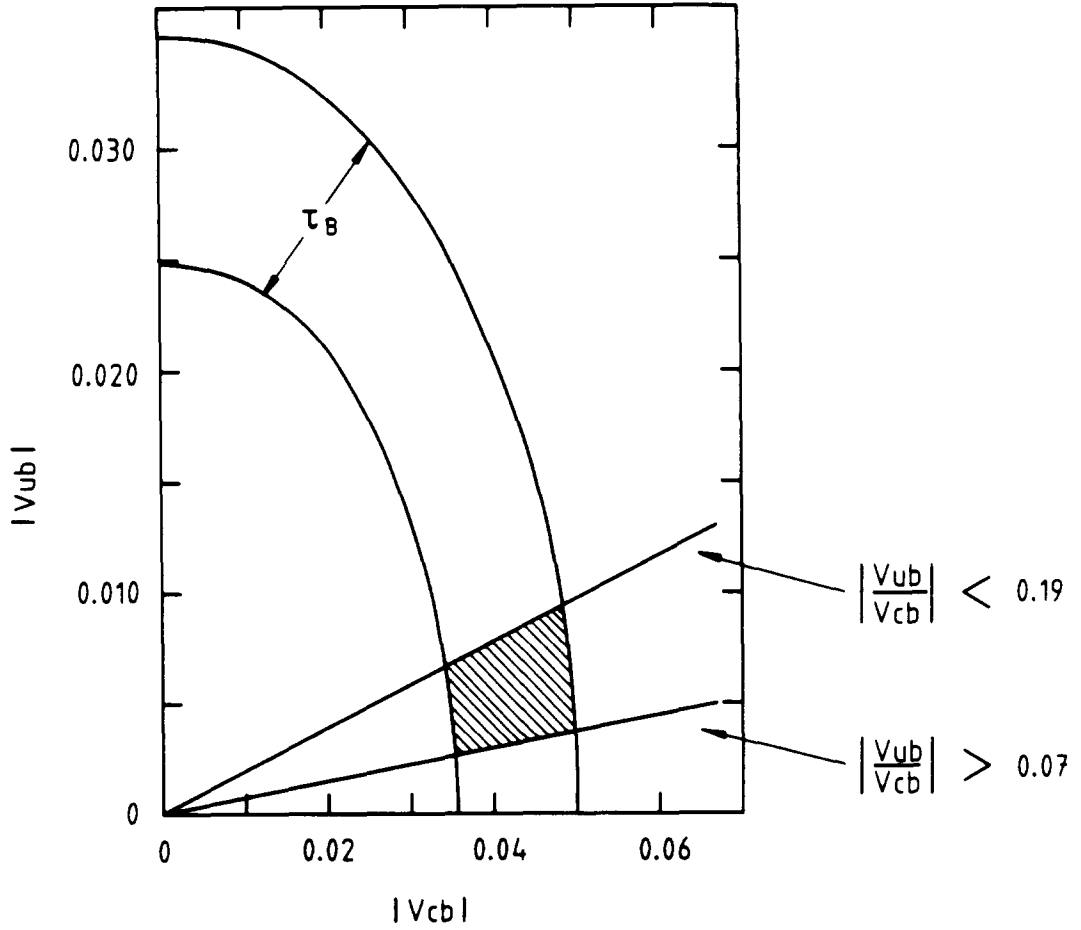A summary of PEP and PETRA measurements of average B-hadron lifetimes.

FIGURE 4.15

V_{ub} vs V_{cb} constraints set by the B-hadron lifetime measurement and the two $|V_{ub}|/|V_{cb}|$ limits by ARGUS and CLEO.

Altarelli model [4.23] is used instead). The lower bound of 0.07 is the recent result from the ARGUS collaboration discussed by Schmidt-Parzifall [4.24] at this conference.

With all these experimental results taken into account, the remaining allowed region in the $|V_{ub}| - |V_{cb}|$ plane is shown hatched in Figure 4.15.

Outlook

The study of e^+e^- interactions at high energies has been very exciting for many years. What is more important is that it promises to become even more exciting. As already mentioned, TRISTAN started operation only in November 1986. SLC is going to become operational in the very near future, and LEP in two years. If we also include BEPC, to be completed by the end of 1988, then four high-energy electron-positron colliding beam accelerators will start operation in a period of less than three years. Nothing of this magnitude has ever happened before in experimental particle physics.

We look forward to learning what kind of surprises are in store for us. With DORIS and PEP and in particular CESR having already achieved phenomenally high luminosity, e^+e^- interactions at high energies, including Z^o physics, will certainly be the main topic for the next conference to be held at SLAC.

Acknowledgements

References

Section 1:

[1.1] G. Altarelli, Proceedings of the XXIII International Conference on High Energy Physics, Berkeley, July 1986.

[1.2] CELLO Collaboration, H.-J. Behrend et al., Phys. Lett. **183B** (1987) 400.
W. de Boer, private communication.

[1.3] S.L. Glashow, Nucl. Phys. **22** (1961) 579;
S. Weinberg, Phys. Rev. Lett. **19** (1967) 1264;
A. Salam, Proc. Eighth Nobel Symp., May 1968, ed. N. Svartholm (Wiley, 1968), p. 367;
S.L. Glashow, J. Iliopoulos and L. Maiani, Phys. Rev. **D2** (1970) 1285.

[1.4] CELLO Collaboration, H.-J. Behrend et al., contribution to this conference;
W. de Boer, private communication.

[1.5] MARK II Collaboration, D.R. Wood et al., to be published in Physical Review **D**.

[1.6] R. Rau, private communication.

[1.7] TASSO Collaboration, W. Braunschweig et al., DESY Report 87-081 (1987)

[1.8] C.L. Basham, L.S. Brown, S.D. Ellis and S.T. Love, Phys. Rev. Lett. **41** (1978) 1585; Phys. Rev. **D17** (1978) 2298; Phys. Rev. **D19** (1979) 2018; Phys. Lett. **85B** (1979) 297;
L.S. Brown and S.D. Ellis, Phys. Rev. **D24** (1981) 2383.

[1.9] W.E. Caswell, Phys. Rev. Lett. **33** (1974) 244;
D.R.T. Jones, Nucl Phys. **B75** (1974) 531;
A.A. Belavin, A.A. Migdal, JETP Lett. **19** (1974) 181;
Particle Data Group, Review of Particle Properties, Phys. Lett. **170B** (1986), see p. 72.

[1.10] B. Naroska, DESY Report 86-113 (1986) and Phys. Reports **148** (1987) 1.

[1.11] M. Dine, J. Sapirstein, Phys. Rev. Lett. **43** (1979) 668;
K.G. Chetyrkin et al., Phys. Lett. **B85** (1979) 277;
W. Gelmaster, R.J. Gonsalves, Phys. Rev. Lett **44** (1980) 560.

[1.12] T.W. Appelquist, J.D. Polizer, Phys. Rev. Lett. **34** (1975) 43, Phys. Rev. **D12** (1975) 1404;
A. De Rujula, H. Georgi, Phys. Rev. **D13** (1976) 1296;
J. Jersak et al., Phys. Rev. **D25** (1982) 1219;
S. Güsken et al., Phys. Lett. **B155** (1985) 185.

[1.13] JADE Collaboration, W. Bartel et al., Phys. Lett. **B129** (1983) 145;
JADE Collaboration, W. Bartel et al., Phys. Lett. **B160** (1985) 337;
B. Naroska, DESY Report 86-113 (1986) and Phys. Reports **148** (1987) 1;
R. Marshall, RAL-84-088, RAL-85-087 and RAL-87-031.

[1.14] MARK J. Collaboration, D.P. Barber, Phys. Rev. Lett. **46** (1981) 1663;
MARK J Collaboration, B. Adeva et al., Phys. Rev. **D34** (1986) 681;
MARK J Collaboration, D. Linnhöfer, Ph.D. Thesis, Aachen (1986).

[1.15] TASSO Collaboration, R. Brandelik et al., Phys. Lett. **B113** (1982) 499;
TASSO Collaboration, M. Althoff et al., Phys. Lett. **B138** (1984) 441.

[1.16] W. de Boer, MPI-PAE/Exp.E1. 167, (1986). Talk given at the XVIIth International Symposium on Multiparticle Dynamics, Austria, (1986).

[1.17] Crystal Ball Collaboration, Z. Jakubowski et al., contribution to this conference.

[1.18] F. Takasaki, Proceedings of this conference. This is a combined result from AMY, TOPAZ and VENUS collaborations. The error given here is the combined error of statistics and systematics in quadrature.

[1.19] H. Wachsmuth, Proceedings of the 1987 International Europhysics Conference on High Energy Physics, Uppsala, Sweden, 1987.

[1.20] P. Jenni, Proceedings of this conference.

[1.21] P. Hoyer, P. Osland, H.G. Sander, T.F. Walsh and P.M. Zerwas, Nucl. Phys. **B161** (1979) 349;
A. Ali, E. Pietarinen, G. Kramer and J. Willrodt, Phys. Lett. **93B** (1980) 155;
A. Ali, Phys. Lett. **110B** (1982) 67.

[1.22] B. Andersson et al., Z. Phys. C-Particles and Fields **1** (1978) 105;
B. Andersson and G. Gustafson, Z. Phys. C-Particles and Fields **3** (1980) 223;
B. Andersson, G. Gustafson and T. Sjöstrand, Z. Phys. C-Particles and Fields **6** (1980) 235;
T. Sjöstrand, Lund Preprint, LU TP 80-3 (1980), LU TP 82-3 (1982);
B. Andersson, G. Gustafson and T. Sjöstrand, Phys. Lett. **94B** (1980) 211;
B. Andersson, G. Gustafson and T. Sjöstrand, Nucl. Phys. **B197** (1982) 45;
T. Sjöstrand, Comput. Phys. Commun. 27 (1982) 243; ibid. 28 (1983) 229;
B. Andersson, G. Gustafson, G. Ingelman, T. Sjöstrand, Phys. Reports **97** (1983) 33;
T. Sjöstrand, Comput. Phys. Commun. 39 (1986) 347.

[1.23] R.K. Ellis, D.A. Ross and A.E. Terrano, Nucl. Phys. **B178** (1981) 421.

[1.24] F. Gutbrod, G. Kramer and G. Schierholz, Z. Phys. C-Particles and Fields (1984) 235.

[1.25] A. Ali and F. Barreiro, Phys. Lett. **118B** (1982) 155.

[1.26] T.D. Gottschalk and M.P. Shatz, Phys. Lett. **150B** (1985) 451.

[1.27] R. Rau, private communication. The MARK J results in Table 1.1 were given to the speaker after the conference. They combine the results of independent jet and Lund fragmentation models and hence are not directly comparable to the other four based on Lund model alone.

Section 2:

[2.1] S.L. Glashow, Nucl. Phys. **22** (1961) 579;

S. Weinberg, Phys. Rev. Lett. **19** (1967) 1264;

A. Salam, Proceedings of the Eighth Nobel Symposium, May 1969, ed. N. Svartholm (Wiley, 1968) p. 367;

S.L. Glashow, J. Iliopoulos and L. Maiani, Phys. Rev. **D2** (1970) 1285.

[2.2] N. Cabibbo and R. Gatto, Phys. Rev. **124** (1961) 1577;

T. Kinoshita, J. Pestieau, P. Roy and H. Terazawa, Phys. Rev. **D2** (1970) 910;

J. Codine and A. Hankey, Phys. Rev. **D6** (1972) 3301;

R. Budny, Phys. Lett. **45** (1973) 340.

[2.3] M. Bohm et al., Z. Phys. C-Particles and Fields **27** (1985) 523; and DESY preprint 84-027, to be published in Progr. Phys.;

W. Hollik, DESY Preprint 86-049 and references therein, to be published in Proceedings of the XXIst Rencontre de Moriond (1986).

[2.4] B. Naroska, private communication.

[2.5] CELLO Collaboration, contribution to this conference.

[2.6] JADE Collaboration, contribution to this conference.

[2.7] MARK J Collaboration, contribution to this conference.

[2.8] TASSO Collaboration, contribution to this conference.

[2.9] H. Wachsmuth, Proceedings of the 1987 International Europhysics Conference on High energy Physics, Uppsala, Sweden, 1987.

[2.10] P. Yenni, Proceedings of this conference.

[2.11] JADE Collaboration, W. Bartel et al., Phys. Lett. **146B** (1984) 121.

[2.12] HRS Collaboration, S. Abachi et al., Purdue University preprint, PU-85-536.

[2.13] TASSO Collaboration, M. Althoff et al., Phys. Lett. **126B** (1983) 493 and erratum Phys. Lett. **130B** (1983) 463;

TASSO Collaboration, W. Braunschweig et al., contribution to this conference.

[2.14] R. Marshall, RAL-87-031 and private communication.

[2.15] T. Greenshaw, private communication.

[2.16] JADE Collaboration, W. Bartel et al., Phys. Lett. **146B** (1984) 437.

[2.17] UA1 Collaboration, C. Albajar et al., Phys. Lett. **186B** (1987) 247.

[2.18] ARGUS Collaboration, H. Albrecht et al., DESY Preprint 87-029.

[2.19] MAC Collaboration, W.W. Ash et al., Phys. Rev. Lett. **58** (1987) 1080.

[2.20] JADE Collaboration, W. Bartel et al., to be published.

[2.21] R. Barlow, Manchester University Preprint M/C HEP 85/21, to be published in the Journal of Computational Physics.

[2.22] JADE Collaboration, W. Bartel et al., Z. Phys. C-Particles and Fields **28** (1985) 343.

[2.23] MAC Collaboration, E. Fernandez et al., Phys. Rev. Lett. **54** (1985) 95.

[2.24] M.S. Gold, Ph.D. Thesis, LBL-22433 (1986).

[2.25] TASSO Collaboration, W. Braunschweig et al., contribution to this conference.

Section 3:

[3.1] M. Davier, Proceedings of the XXIII International Conference on High Energy Physics. Berkeley, July 1986.

[3.2] UA1 Collaboration, G. Arnison et al., Phys. Lett. **122B** (1983) 95;
UA2 Collaboration, M. Banner et al., Phys. Lett. **122B** (1983) 476;
UA1 Collaboration, G. Arnison et al., Phys. Lett. **126B** (1983) 398;
UA2 Collaboration, P. Bagnaia et al., Phys. Lett. **129B** (1983) 130.

[3.3] S.L. Glashow, Nucl. Phys. **22** (1961) 579;
S. Weinberg, Phys. Rev. Lett. **19** (1967) 1264;
A. Salam, Proceedings of the Eighth Nobel Symposium, May 1968, ed. N. Svartholm (Wiley, 1968) 367;
S.L. Glashow, J. Iliopoulos and L. Maiani, Phys. Rev. **D2** (1970) 1285.

[3.4] P.W. Higgs, Phys. Lett. **12** (1964) 132; Phys. Rev. Lett. **13** (1964) 508; Phys. Rev. **145** (1966) 1156;
F. Englert and R. Brout, Phys. Rev. Lett. **13** (1964) 321;
G.S. Guralnik, C.R. Hagen and T.W.B. Kibble, Phys. Rev. Lett. **13** (1964) 585;
T.W.B. Kibble, Phys. Rev. **155** (1967) 1554.

[3.5] ARGUS Collaboration, H. Albrecht et al., Phys. Lett. **192B** (1987) 245.

[3.6] P. Yenni, Proceedings of this conference.

[3.7] S.L. Glashow, talk given in this conference.

[3.8] CUSB Collaboration, M. Narain et al., contribution to this conference.

[3.9] CLEO Collaboration, P. Avery et al., contribution to this conference.

[3.10] Sau Lan Wu, Proceedings of the ECFA Workshop - LEP 200, Aachen, September 1986;
H. Baer et al., CERN 86-02, Vol. 1 (1986), edited by J. Ellis and R. Peccei (see p. 297).

[3.11] F. Wilczek, Phys. Rev. Lett. **40** (1978) 220.

[3.12] S. Weinberg, Phys. Rev. Lett. **40** (1978) 223.

[3.13] M.I. Vysotsky, Phys. Lett. **97B** (1980) 159;
P. Nason, Phys. Lett. **175B** (1986) 223;
J. Ellis, K. Enqvist and D.N. Nanopoulos, Phys. Lett. **158B** (1985) 417.

[3.14] CUSB Collaboration, P.M. Tuts et al., Phys. Lett. **186B** (1987) 233.

[3.15] R.S. Willey and H.L. Yu, Phys. Rev. **D26** (1982) 3086.

[3.16] M. Kobayashi and T. Maskawa, Prog. Theor. Phys. **49** (1973) 652.

[3.17] S. Behrends et al., "$\Gamma(b \rightarrow u\ell\nu)/\Gamma(b \rightarrow c\ell\nu)$ from the End Point of the Lepton Momentum Spectrum in Semileptonic B decay", Cornell preprint CLNS 87/78 (1987).

[3.18] H.E. Haber, A.S. Schwarz and A.E. Snyder, "Hunting the Higgs in B-decays", SCIPP-87/85 (1987).

[3.19] M.B. Voloshin, Sov. J. Nucl. Phys. **44** (1986) 478.

[3.20] In Ref. [3.9], CLEO gave the mass limit for the t quark as 43 GeV. This is a misprint; it should be 47 GeV.

[3.21] J. Ellis, P. Franzini and S. Ritz, private communication.

[3.22] B. Grzadkowski and P. Krawczyk, Z. Phys. C-Particles and Fields **18** (1983) 43.

[3.23] F.J. Botella and C.S. Lim, Finite Renormalization Effects in induced $\bar{s}dH$ Vertex, BNL 37566.

[3.24] T.N. Pham and D.G. Sutherland, Phys. Lett. **151B** (1985) 444.

[3.25] C.F. Abbot, Skivie, and Wise, Phys. Rev. **D21** (1980) 1393;
G.G. Athanasiu and F.J. Gilman, Phys. Lett. **153B** (1985) 274;
G.G. Athanasiu, P.J. Franzini, and F.J. Gilman, Phys. Rev. **D32** (1985) 3010;
M. Drees, M. Glück, and K. Grassie, Phys. Lett. **159B** (1985) 118;
E. Reya, Phys. Rev. **D33** (1986) 773;
L.A.T. Bauerdick, Z. Phys. C-Particles and Fields **32** (1986) 459.

[3.26] CELLO Collaboration, H.-J. Behrend et al., Phys. Lett. **114B** (1982) 287;
JADE Collaboration, W. Bartel et al., Phys. Lett. **114B** (1982) 211 and Z. Phys. C-Particles and Fields **31** (1986) 359;
MARK J Collaboration, B. Adeva et al., Phys. Lett. **115B** (1982) 345 and Phys. Lett. **152B** (1985) 439;
TASSO Collaboration, M. Althoff et al., Phys. Lett. **122B** (1983) 95;
MARK II Collaboration, C.A. Blocker et al., Phys. Rev. Lett. **49** (1982) 517.

[3.27] B. Naroska, DESY Report 86-113 (1986) and Phys. Reports **148** (1987) 1.

[3.28] CELLO Collaboration, H.-J. Behrend et al., Phys. Lett. **193B** (1987) 376.

[3.29] CELLO Collaboration, H.-J. Behrend et al., contribution to this conference.

[3.30] F. Takasaki, Proceedings of this conference.

[3.31] UA1 Collaboration, C. Albajar et al., Phys. Lett. **185B** (1987) 241;
M.M. Mohammadi, Ph.D. Thesis, Wisconsin (1987).

[3.32] M. L. Perl, Proceedings of the XXIII International Conference on High Energy Physics, Berkeley, July 1986.

[3.33] S. Komamiya, Proceedings of the 1985 International Symposium on Lepton and Photon Interactions at High Energies, Kyoto, 1985; ed. by M. Konuma and K. Takahashi, p. 612; JADE Collaboration, W. Bartel et al., Z. Phys. C-Particles and Fields **29** (1985) 505.

[3.34] CELLO Collaboration, H.-J. Behrend et al., Phys. Lett. Z. Phys. C-Particles and Fields **35** (1987) 181.

[3.35] M.L. Perl and D.P. Stocker, Invited talk at the XXIIth Rencontres de Moriond (Electroweak Interactions and Unified Theories), Les Arcs, Savoie, March 1987.

[3.36] TPC/Two-Gamma Collaboration, H. Aihara et al., contribution to this conference.

[3.37] F.J. Gilman, Comments in Nuclear and Particle Physics Vol.XVI, No. 5 (1986) 231.

[3.38] MARK II Collaboration, C. Wendt et al., Phys. Rev. Lett. **58** (1987) 1810.

[3.39] HRS Collaboration, D. Errede et al., contribution to this conference.

[3.40] D.O. Caldwell, University of California Santa Barbara Preprint UCSB-HEP-87-10 (1987) (to be published in the Proceedings of Rochester Conference on Non-Accelerator Physics).

[3.41] CELLO Collaboration, Single photon search with the CELLO detector, contribution to this conference;
E. Ma and J. Okada, Phys. Rev. Lett. **41** (1978) 287;
K.J.F. Gaemers, R. Gastmans and F.M. Renard, Phys. Rev. **D19** (1979) 1605.

[3.42] T. Lavine, Ph.D. Thesis, Wisconsin (1986), Rep. No. WISC-EX-86/275.

[3.43] J.F. Grivaz, Proceedings of the XXIIth Rencontres de Moriond, ed. J. Tran Than Van (Les Arcs, 1987) to be published; and preprint LAL 87-20.

[3.44] ASP Collaboration, C. Hearty et al., Phys. Rev. Lett. **58** (1987) 1711.

[3.45] MAC Collaboration, W.T. Ford et al., Phys. Rev. **D33** (1986) 3472;
M. Davier, Proceedings of the XXIII International Conference on High Energy Physics, Berkeley, July 1986 and preprint LAL 86-31.
J.F. Grivaz, ibid. and preprint LAL 86-28.
W. de Boer, Proceedings of the 17th International Symposium on Multiparticle Dynamics, Seewinkel, Austia, (1986), and preprint MPI-PAE/ Exp.El.167.

[3.46] MARK J Collaboration, contribution to this conference (private communication H. Jung).

[3.47] H. Jung of CELLO Collaboration, private communication.

[3.48] Yu. A. Gol'fand and E.P. Likhtman, JETP Lett. **13**, (1971) 323;
D.V. Volkov and V.P. Akulov, Phys. Lett. **46B**, (1973) 109;
J. Wess, and B. Zumino, Nucl. Phys. **B70**,(1974) 39;
A. Salam, and J. Strathdee, Nucl. Phys. **B76**, (1974) 477.

[3.49] P. Fayet, Phys. Lett. **69B**, (1977) 489;
D.V. Nanopoulos, A. Savoy-Navarro and Ch. Tao (organizers), Proceedings of the Workshop on Supersymmetry versus Experiment, CERN, Geneva, Switzerland, April 1983.

[3.50] P. Fayet, Unification of the Fundamental Particle Interactions, ed. S. Ferrara, J. Ellis, and P. van Nieuwenhuizen, p. 587 (Plenum Press, New York, 1980).

[3.51] H.E. Haber and G.L. Kane, Phys. Reports **117**, (1985) 75.

[3.52] MARK II Collaboration, L. Gladney et al., Phys. Rev. Lett. **51** (1983) 2253; and B. LeClaire, private communication.

[3.53] TASSO Collaboration, R. Brandelik et al., Phys. Lett. **117B** (1982) 365.

[3.54] TASSO Collaboration, W. Braunschweig et al., contribution to this conference.

[3.55] P.A.M. Dirac, Proceedings. Royal Soc. London **A133** (1931) 60; and Phys. Rev. **74** (1948) 817.

[3.56] CLEO Collaboration, T. Gentile et al., Phys. Rev. **D35** (1987) 1081.

Section 4

[4.1] M. Kobayashi and T. Maskawa: Prog. Theor. Phys. **49** (1973) 652.

[4.2] JADE Collaboration, W. Bartel et al., Phys. Lett. **114B** (1982) 71.

[4.3] MAC Collaboration, E. Fernandez et al., Phys. Rev. Lett. **51** (1983) 1022;

[4.4] MARK II Collaboration, N.S. Lockyer et al., Phys. Rev. Lett. **51** (1983) 1316.

[4.5] M.G.D. Gilchriese, Proceedings of the XXIII International Conference on High Energy Physics, Berkeley, July 1986.

[4.6] M. Cherney, M.D. Takashima and Sau Lan Wu (to be published);
M. Cherney, Ph.D. Thesis, Wisconsin (1987);
M. Althoff et al., Phys. Lett. **149B** (1984) 524.

[4.7] JADE Collaboration, W. Bartel et al., Z. Phys. C-Particles and Fields **31** (1986) 349.

[4.8] DELCO Collaboration, D.E. Klem et al., SLAC-PUB-4025, September 1986, Submitted to Physical Review D.

[4.9] MARK II Collaboration, R. Ong et al., contribution to this conference;
R. Ong, Ph.D. Thesis, Stanford (1987), SLAC-Report 320, and private communication.

[4.10] HRS Collaboration, D. Blockus et al., IUHEE-87-1, ANL-HEP-PR-86-144, UM HE-86-19, PU-87-694, contribution to this conference.

[4.11] MAC Collaboration, W.W. Ash et al., Phys. Rev. Lett. **58** (1987) 640.

[4.12] TASSO Collaboration, W. Braunschweig et al., contribution to this conference;
M.D. Takashima, private communication.

[4.13] TASSO Collaboration, W. Braunschweig et al., contribution to this conference;
K.-U. Pösnecker, Ph.D. Thesis, Universität Hamburg (1987).

[4.14] JADE Collaboration, W. Bartel et al., contribution to this conference;
R. Ramcke, private communication.

[4.15] TASSO Collaboration, W. Braunschweig et al., contribution to this conference;
D. Muller, private communication.

[4.16] Sau Lan Wu and G. Zobernig, Z. Phys. C-Particles and Fields **2** (1979) 107.

[4.17] J. Jaros, Proceedings of the International Conference on Physics in Collision, Santa
Cruz, 1984.

[4.18] D.H. Saxon, Nucl. Inst. Methods **A234** (1985) 258.

[4.19] R. Barlow, Manchester University Preprint M/C HEP 85/21, to be published in the
Journal of Computational Physics.

[4.20] B. Gittelman and S. Stone, CLNS 87/81 (1987).

[4.21] CLEO Collaboration, S. Behrends et al., CLNS 87/78 (1987), to be published.

[4.22] B. Grinstein, N. Isgur and M. Wise, Phys. Rev. Letter **56** (1986) 298.

[4.23] G. Altarelli et all., Nucl. Phys. **B208** (1982) 365.

[4.24] W. Schmidt-Parzefall, Proceedings of this conference.

Comment from R. Rau, Brookhaven

I would like to point out firstly that you did not include the latest α_S measurement from MARK J and secondly that our result, $\alpha_S = 0.12 - 0.15$ depending on the fragmentation model used, was first published in 1983 and has remained stable since then. The lastest value is consistent with our first measurement and other PETRA experiments now quote values compatible with ours. Furthermore, our result using the planar triple energy correlation, a method which selects three jet events, is also consistent with $\alpha_S = 0.12 - 0.15$.

Reply

The published MARK J results are shown in my transparency. I apologize for not having included the latest MARK J results. I did ask MARK J to provide me with the results they wanted to have presented at this conference and was told they had none.

Comment from R.M. Godbole, Dortmund

The calculation for $B \rightarrow HK$ was also simultaneously done by a group from Dortmund and contributed to this conference. Both calculations use the B/D decay model of Wirbel, Stech and Bauer.

Question from W. Wallraff, RWTH Aachen, I Phys. Inst.

Could you please comment on the precision of the α_S measurements using energy-energy correlations you have described. I personally find it difficult to understand how a precision of 0.005 can be achieved.

Answer

Systematic errors arising from the modelling of the fragmentation are not included and must be added. They can be large.

Question from G. Barbiellini, CERN

Since the values of α_S you quoted from fits to R (with the further fitted parameter being $sin^2\theta_W$) are obtained over a large energy range, what is the chance of proving that α_S is running, in particular what contribution will TRISTAN make?

Answer

I think TRISTAN will be able to make some statement on this problem.

Question from G. Wolf, DESY

The CUSB data exclude gluinos with masses between 0.3 and 2.2 GeV, is it true that there are still windows of possible gluino mass between 0.0-0.3 GeV and 2.2-3.0 GeV?

Answer from J. Lee-Franzini.

CUSB only excludes masses between 0.6 and 2.6 GeV.

Comment from B.F.L. Ward, Tennessee

In response to the question concerning the running of α_S. the QCD Physics Working Group of the SLC has found that, by counting the ratio of 2:3:4 jet events, the SLC will be able to make a strong statement about the running of α_S, while at TRISTAN the issue will be marginal.

Comment from Y. Eisenberg, Weizmann Inst.

You showed limits on the masses of heavy neutrinos. I am sure that some of the regions allowed in the plots you showed are excluded by the results of neutrino oscillation experiments. I presume these are to be discussed in a different session.

Comment from Min Chen, MIT

MARK J has measured $\alpha_S(q^2)$ from 22 to 46 GeV and has showed that the variation of α_S from 46 GeV to TRISTAN energies is too small to be used for verification of its running properties. Would you please show the MARK J data here for me, to illustrate the above point.
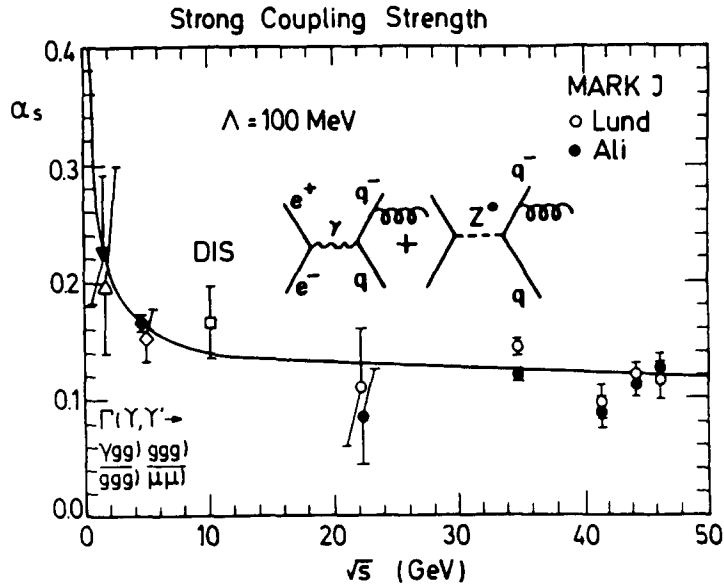
Comment from P. Langacker, DESY

I would like to comment on the determination of $sin^2\theta_W$ from the forward-backward asymmetries in e^+e^- annihilation. There has been a lot of confusion as to what processes depend on what physical parameters and I would like to clarify this. The asymmetries do not determine $sin^2\theta_W$ within the standard model. What they do determine are the axial-vector couplings of the electron, muon and tau if you allow deviations from universality and they also determine ρ if you allow that to be different from unity. They only determine $sin^2\theta_W$ if you do a simultaneous fit with other types of reaction such as directly measured Z masses. It is very important to be clear about what experiment is measuring what parameter at what time.

Answer

That is why I showed a correlation plot of $sin^2\theta_W$ and the Z mass.

Question from G.G. Ross, Oxford

When you talked about the bounds on the neutral Higgs you said they were sensitive to the branching ratio into muon pairs. Can you give any limits if the neutral Higgs does not couple to muons?

Answer

If there is no coupling to muons then the limits are much weaker. Limits via the π pair channel should improve with increasing statistics however.